A Ubiquitin-dependent Surveillance System Mediates Plasma Membrane Protein Quality Control in Yeast

A Dissertation

Presented to the Faculty of the Graduate School

Of Cornell University

In Partial Fulfillment of the Requirements for the Degree of

Doctor of Philosophy

by

Yingying Zhao

January 2013

A UBIQUITIN-DEPENDENT SURVEILLANCE SYSTEM MEDIATES PLASMA MEMBRANE PROTEIN QUALITY CONTROL IN YEAST

Yingying Zhao, Ph. D.

Cornell University 2013

A key function of the ubiquitin-proteasome system is targeting of misfolded proteins for degradation. In the cytosol, specialized E3 ligases target soluble misfolded proteins for ubiquitination and subsequent proteasomal degradation. However, the case is more complicated for integral membrane proteins. Following co-translational insertion in the ER membrane, proteins that fail to fold properly in the ER are subject to ER-assisted degradation (ERAD), which involves retrotranslocation of proteins back into the cytosol followed by ubiquitin-dependent proteasomal degradation. Properly folded PM proteins, such as signaling receptors, ion channels, and nutrient transporters, exit the ER and traffic through the Golgi to the cell surface where they mediate their specific functions. Maintenance of proper PM proteostasis, particularly with respect to ion channels and nutrient transporters, is crucial to prevent loss of PM integrity and dissipation of essential ion and chemical gradients. As such, when PM resident proteins become damaged or misfolded, they must be recognized, removed by endocytosis and delivered to the lysosome for degradation. Thus, cells maintain a “cradle to grave” quality monitoring system for integral membrane proteins, yet the mechanisms of

quality surveillance, particularly at the PM, remain poorly understood.

Here we present evidence that the E3 ubiquitin ligase Rsp5, the yeast homolog of Nedd4, is part of a critical protein quality surveillance mechanism at the PM. We show that proteotoxic stress triggers global activation of Rsp5-dependent ubiquitination, endocytosis, and vacuolar trafficking of PM proteins. Mutants defective for this protective response exhibit toxic accumulation of integral membrane proteins at the cell surface and suffer catastrophic loss of PM integrity during misfolding stress, phenotypes that can be suppressed by the presence of chemical chaperones. We present the identification of specific Rsp5 adaptors which target the ubiquitination of misfolded PM proteins during proteotoxic stress. Genetic interaction analysis reveals that this PM quality surveillance mechanism exhibits striking synthetic defects with components of both ERAD and the unfolded protein response, indicating that different quality control pathways cooperate to protect cells during misfolding stress. We propose that this ubiquitin-mediated PM quality surveillance pathway, together with other quality control pathways like ERAD, protects cells from proteotoxic stress by limiting the toxic accumulation of misfolded integral membrane proteins at the PM.

BIOGRAPHICAL SKETCH

Yingying Zhao was born in a beautiful city Changzhi in north China. In 1996, she graduated from ChangZhi Dier High School and entered Shanxi Medical University. Five years later, Yingying received her Medical degree in Clinic Medicine in 2001. Then she started her master degree study in the field of Biochemistry and Molecular Biology in Shanxi Medical University. Under the guidance of Dr. Bo Niu, Yingying worked on a project related to Hematopoiesis Protection (HP) domain of Human Platelet Factor 4. Upon completion of her Master degree in 2004, Yingying worked as a lecturer teaching molecular biology in Shanxi Medical University. In 2006 Yingying accepted an offer from graduate school of Cornell University and joined the department of Biomedical Science. The first three year, she worked with Dr. Timothy O'Brien and explored the role of Sprouty2 in mouse embryo lung development. In 2009, she joined Dr. Scott Emr lab and continued the Ph. D study in the molecular mechanism of how cell deal with toxic accumulation of misfolded plasma membrane protein.

This work is dedicated to my dear mother Wanping Cui.

此書獻給我親愛的母親崔晚萍

ACKNOWLEDGMENTS

This research project would not have been possible without the support of many people. I would like to express my gratitude to my supervisor, Dr. Scott Emr, whose expertise, understanding, and patience, added considerably to my graduate experience. I appreciate his vast knowledge and skill in many scientific areas, and his assistance in guidance and constant encouragement throughout my Ph. D. work.

I am very grateful for having an exceptional committee and would like to thank Dr. Mark Roberson, Dr. Ruth Colins, and Dr. Shu-bing Qian for their research expertise, and creative advise and the assistance they provided at all levels of the research project. Specially, I would like to thank Dr. Mark Roberson from the department of Biomedical Science for taking time out from his busy schedule to serve as my field appoint committee supporting me throughout all my six years gradate school.

A very special thank goes out to Dr. Jason MacGurn, without whose mentor, motivation and encouragement I would not have fulfilled my thesis project in three years. It was under his guidance that I developed a focus and became interested in membrane protein turn over under the stress condition. He provided me with directions, technical support and became more of a mentor and friend, than a colleague.

I must also acknowledge all the Emr lab people for our philosophical debates,

exchanges of knowledge, skills, and venting of frustration during failure of experiment. It's my great honor to work with such talented colleagues.

Six years ago, I came to graduate school at Cornell University with great support from my family. As a woman scientist, I cannot imagine even a second what my life will be without help from them. So I like to take this chance to thank my parents for the support they provided me through my entire life and in particular, I must acknowledge my husband and best friend, Le, without whose love, encouragement and editing assistance, I would not have finished this thesis. Last but not the least, a special thank goes to my dear daughter Xixi for growing up happily and healthily. From now on, I will try my best on my lifelong project: what makes a good mom.

TABLE OF CONTENTS

LIST OF FIGURES

LIST OF TABLES

Chapter I

INTRODUCTION

Protein biosynthesis, folding, maintenance and degradation requires an elaborate yet balanced network of systems that coordinate to ensure the health of a cell. Cellular protein homeostasis, called proteostasis, plays a critical role in many normal cellular functions. Cells have developed elaborate protein quality control (PQC) systems that assist nascent proteins in proper folding, help damaged proteins to refold, and target misfolded/unfolded proteins for degradation. Perturbation of proteostasis can lead to nonfunctional protein or proteotoxic aggregation. Therefore, maintenance of proteostasis is central to understanding the causes of many diseases. In this chapter, I will summarize the current understanding of proteostasis networks with a special emphasis on protein ubiquitination and degradation.

I. Protein folding, misfolding and unfolding

Protein folding is a complex process influenced by various environmental factors including temperature, solute concentration, pH, mechanical forces, and oxidation. Under unfavorable conditions, proteins can lose their tertiary or even secondary structures. In certain harsh conditions, the 3D structure of a protein can be fully abolished and reduced to a random coil. This process is called denaturation. In some cases, proteins can be refolded into their native states. However in most cases, the fully-denatured state is irreversible and thus the protein cannot refold.

Molecular mechanisms of protein folding

Three-dimensional structure is essential for protein function. Nascent proteins emerge from the ribosome as a linear polypeptide chain which folds as it reaches a low-energy state by traversing a unique free energy landscape. This process of protein folding can take place co- or post-translationally and can happen either spontaneously or with the assistance of molecules called chaperones (Hardesty and Kramer 2001). Chaperones are molecules that help unfolded/misfolded proteins navigate the free energy landscape of folding to achieve a correct low-energy conformation that corresponds to proper folding. Heat shock protein 90 (Hsp90) has the substrate binding region at its C terminus, where hydrophobic residues can attract exposed hydrophobic regions of an unfolded protein with high affinity. Upon ATP hydrolysis at Hsp90 N terminus, a large comformational change of Hsp90 will help its substrate protein gain the low energy native state. Chaperones can be small molecules or other proteins, which are often upregulated in conditions that promote protein misfolding.

Many studies have made significant progress towards understanding how nascent proteins fold into unique three-dimensional structures. One driving force is the hydrophobic effect, which minimizes hydrophobic residues exposed to solvent. Besides hydrophobic interactions, intramolecular hydrogen bond formation and van der Waals forces both play critical roles in establishing protein secondary and tertiary structures. Physiological conditions, such as solvent, temperature, and salt

concentration, also influence the outcome of protein folding. For example, all proteins unfold at high temperature. Similarly, point substitutions in a protein, such as the most common mutation of cystic fibrosis (the cystic fibrosis conductance regulator CFTR ΔF508), can influence protein folding, alter stability, and shorten half-life.

Chaperones

Often protein folding is assisted by a group of specialized proteins called chaperones. Chaperones are key players in the protein quality control system and they function to maintain the intricate balance between protein synthesis and degradation.

Chaperones are ubiquitous, highly conserved across evolution, and generally function to assist the folding and assembly of polypeptides into their correct tertiary and quaternary structures (Ellis 1987). Partially folded or misfolded proteins tend to have exposed hydrophobic sequences, which can serve as a platform for chaperone recognition. Some chaperones, such as Hsp60 and Hsp70, bind to partially folded clients to prevent them from aggregating. Some chaperones target misfolded proteins via intrinsically disordered regions, which tend to bind the exposed hydrophobic regions of clients, thereby improving client solubility. In contrast to chaperones that prevent protein aggregation, Hsp104 is a chaperone that functions to disassemble existing protein aggregates (Parsell, Kowal et al. 1994; Glover and Lindquist 1998). After several cycles of binding and releasing from

different chaperones, proteins have opportunities to fold or refold into a native state. (Garcia-Mata, Gao et al. 2002; Horwich 2004).

Because chaperones are excellent at distinguishing native from misfolded proteins, they also can be adapted to target misfolded proteins for degradation. Some chaperones can interact with the ubiquitination machinery, ensuring that proteins which cannot fold are ultimately ubiquitinated and targeted for proteasomal degradation. For example, Hsc70-Hsp70 and Hsp90 interact with the tetratricopeptide (TPR) domain of carboxyl terminus of Hsc70-*i*nteracting *p*rotein (CHIP). CHIP has an E3 ubiquitin ligase activity that ubiquitinates clients of Hsc70-Hsp70 and Hsp90. Thus, extended binding to chaperones can result in CHIP-recruitment, client ubiquitination, and proteasomal degradation (Connell, Ballinger et al. 2001; Murata, Udono et al. 2001).

Chemical chaperones are a group of low molecular weight compounds known to assist proteins in achieving their native conformation**.** Several studies have shown that cellular osmolytes, such as glycerol, arabitol, mannitol, mannose, and sorbitol, act as chemical chaperones to counteract proteotoxic environments. Probably these organic osmolytes function to protect proteins against the proteotoxic stress by raising the free energy of the unfolded/ denatured state, and in turn the equilibrium of protein folding is shifted in favor of the native state (Bolen and Baskakov 2001). Some of these chemical chaperones such as glycerol and TMAO (trimethylamine oxide) are effective in correcting folding defects associated with the maturation of

ΔF508-CFTR protein (Brown, Hong-Brown et al. 1996). One of the most commonly used chemical chaperones in scientific research is glycerol, which has been demonstrated to stabilize native protein conformations probably via the osmophobic effect (Gekko and Timasheff 1981; Meng, Hong et al. 2004; Shearer and Hampton 2004).

Chaperones and stress responses

Environmental conditions that are not favorable for protein folding may result in a broad accumulation of misfolded proteins, triggering proteotoxic stress. For example, misfolding of proteins in the ER can trigger the unfolded protein response (UPR), an evolutionarily conserved stress response. UPR triggers the upregulation of chaperones and degradation pathways in the ER while simultaneously down-regulating protein translation. When ER stress is not reversible or defects in UPR can result in cell apoptosis.

Like UPR, the heat-shock response is an evolutionarily conserved stress response that involves the upregulation of chaperones and protein folding pathways in response to high temperatures. The main mediator of the heat shock response is a transcription factor called HSF1 (Heat shock factor 1). HSF1 monomers form a complex with Hsp40/Hsp70 and Hsp90, which keeps HSF1 inactive in the cytoplasm. Following heat stress, HSF1 rapidly dissociates from the complex and traffics to the nucleus, where it is activated and binds to heat shock elements (NGAAN). This DNA binding event activates transcription of heat shock response genes (Nunes and

Calderwood 1995; Shi, Mosser et al. 1998; Hu and Mivechi 2003). Interestingly, accumulation of misfolded proteins activates mammalian target of rapamycin complex 1 (mTORC1) signaling and cellular protein synthesis is transiently increased. mTORC1 signaling can balance protein homeostasis in response to celluar molecular chaperon accessibility (such as Hsp90) (Qian, Zhang et al. 2010).

Folding of integral membrane proteins

Integral membrane proteins have domains that span lipid bilayers and are anchored in membranes. Roughly one third of proteins encoded in eukaryotic genomes is integral membrane proteins with various cellular functions including signaling receptors, nutrient transporters, and ion channels. Some transmembrane proteins have beta barrels that insert into the membrane; however, the majority of transmembrane domains are alpha-helices which are found mostly in the inner membranes of bacterial cells or the plasma membrane of eukaryotes.

Unlike soluble proteins, integral membrane proteins undergo a distinct protein folding mechanism. Most eukaryotic secretory protein transmembrane domains become inserted into the membrane of the endoplasmic reticulum (ER) through a membrane embedded protein-conducting pore, the Sec61 translocon. In this process, nascent polypeptides pass through Sec61 following “the positive-inside rule”, in which positively charged flanking regions are oriented on the cytosolic side of the membrane (Sipos and von Heijne 1993). For most transmembrane proteins,

the orientation of the first hydrophobic span determines the topology of subsequent membrane spans (Blobel 1980).

After membrane insertion, proteins achieve their tertiary and quaternary structures including assembly and reorientation of TM segments, establishment of soluble domain interactions, insertion of reentrant portions of the chain, and subunit oligomerization (Bowie 2005). All of these events are influenced by many factors including lipid composition of the bilayer, pH, and temperature. Integral membrane domain structure is critical for many transmembrane proteins, such that any perturbation of alpha helices forming the wall of an ion channel might cause the channel to lose its selectivity (leaky) or integrity. In general, transmembrane proteins, with their transmembrane domains anchoring to lipid, are relatively stable. More energy is required for them to completely unfold. However, under stress conditions, transmembrane domains and soluble portions of proteins can still misfold, and these partially folded membrane proteins can easily aggregate together within the surrounding lipids.

II. Mechanisms of Protein Degradation

The accumulation of misfolded proteins can be extremely toxic to cells. As a result, cells have developed protein quality control (PQC) mechanisms to ensure that misfolded and damaged proteins are maintained at limited levels to prevent toxic aggregation. While chaperones can help protect cells from misfolding stress, terminally misfolded or damaged proteins must be degraded in order to protect cells. This section summarizes the current understanding of the molecular mechanisms that constitute the degradation arm of protein quality control.

Eukaryotic cells mark misfolded and damaged proteins for degradation by conjugation to ubiquitin, a 76 amino acid peptide that is covalently attached to substrates by the formation of an isopeptide bond between its C terminal glycine carboxyl group and a ε-amino group (usually of a lysine side chain) of a substrate (Hochstrasser 2009). Ubiquitin has seven lysine residues (K6, K11, K27, K29, K33, K48, and K63) which can be further ubiquitinated to form polyubiquitin chains, with different linkage types conferring distinct structures and properties. The K48 linkage usually targets a substrate protein for proteasome degradation, whereas other types of linkages are associated with both proteolytic and nonproteolytic outcomes. For example, the K63 polyubiquitin chain and linear polyubiquitin chain (head to tail) have been shown to play important roles in the NF-λB pathway signaling cascade activation (Kopito 2000; Tokunaga, Sakata et al. 2009). Ubiquitin modification of damaged or misfolded proteins is highly selective. Thus, the detection of quality control substrates requires the recognition of aberrant

structural elements that allow the ubiquitination machinery to distinguish between native and misfolded or damaged proteins.

Ubiquitination requires a series of three distinct enzymatic reactions. Frist, the ubiquitin-activating enzyme E1 hydrolyzes ATP to activate ubiquitin. Second, ubiquitin is transferred to an ubiquitin-conjugating enzyme E2. In the last step, an E3 ubiquitin ligase binds specifically to both the E2 enzyme and the substrate protein, and the activated ubiquitin moiety is then covalently attached to a lysine residue on the protein substrate. There are two major families of E3 ubiquitin ligases that function by very different mechanisms. RING (really interesting new gene) domain-containing E3 ligases serve as scaffolds that can recruit both E2 ubiquitin conjugating enzymes and substrates, providing a steric orientation that promotes ubiquitin transfer to substrate. In contrast, HECT (Homology to E6AP C-Terminus) domain-containing E3 ubiquitin ligases contain a conserved cysteine residue that accepts activated ubiquitin from the E2 conjugation enzyme and subsequently transfers the ubiquitin to substrates. Humans have 616 RING E3 ligases and 28 HECT E3 ligases, while the yeast genome encodes 40 RING and 5 HECT E3 ligases (Macgurn, Hsu et al. 2012).

In this section, I summarize the current understanding of the recognition and degradation of misfolded proteins by two major protein degradation systems: Ubiquitin-Proteasome System (UPS) and lysosomal degradation

Figure 1.1

A

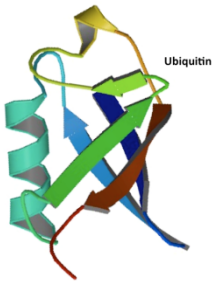

B

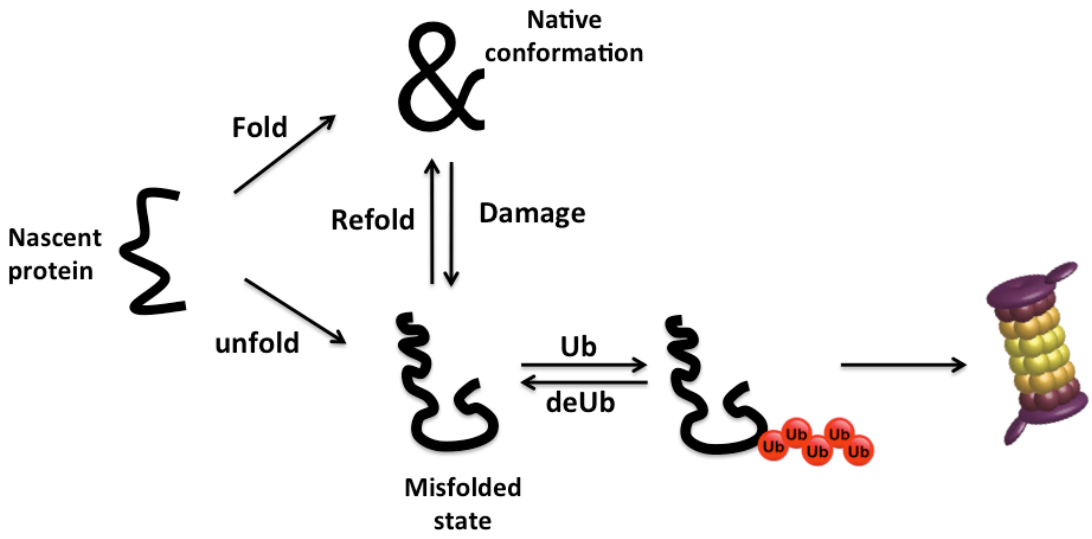

C

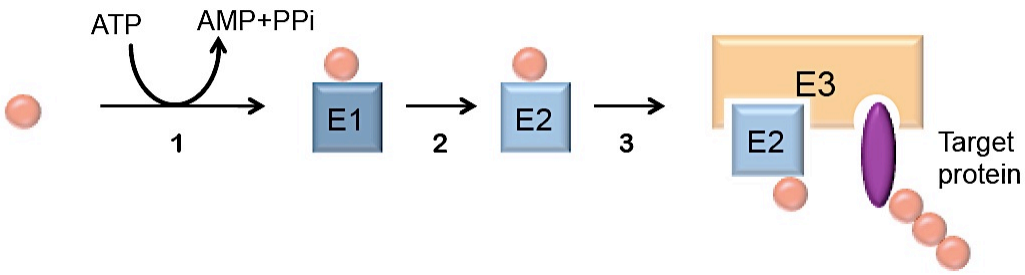

Figure 1.1 Ubiquitin and ubiquitination of target protein

(A) Structure of ubiquitin (PDB identifier 1ubq)

(B) Nascent protein folds into its native conformation with the help of a set of chaperones. Damaged and unfolded protein will undergo chaperone mediated refolding or be recognized by UPS. Deubiquitinase can reverse the ubiquitin modification and give target protein a chance to fold into its native state.

(C) Ubiquitin modification happens via a three steps process: ubiquitin is first activated by E1, and it is subsequently transferred to an ubiquitin-conjugating enzyme E2. In most cases, the E2 enzyme and the protein substrate both bind to an ubiquitin-protein ligase E3, and ubiquitin is then transferred to the target protein.

Ubiquitin-proteasome system (UPS)

The ubiquitin proteasome system (UPS) plays a critical role in protein quality control. Many cellular proteins are degraded by the proteasome, which degrades the majority of soluble proteins. The proteasome also degrades many misfolded secreted proteins that have been targeted by ER associated degradation (ERAD), which involves retrotranslocation from the ER followed by proteasomal degradation. Furthermore, several studies have suggested that a mitochondria associated degradation (MAD) pathway may target mitochondrial proteins for proteasomal degradation (Heo, Livnat-Levanon et al. 2010).

The proteasome is a large protein complex located in both the cytoplasm and nucleus. The main function of the proteasome complex is to degrade proteins. The proteasome consists of a 20S core particle and a 19S regulatory particle. The 20S core contains the proteolytic activities of the proteasome, whereas the 19S regulatory particle contains an ATP-dependent activity that unfolds ubiquitin protein conjugates. The 20S core is made up of four stacked rings around a central pore. The two inner rings consist of 7 β (β1 - β7) subunits, which have protease active sites and proteolysis activity. Seven α subunits (α1 - α7) form two outer rings, serving as docking domains for regulatory subunits and to block non-substrate proteins from getting into the interior cavity. β1, β2, and β5 have catalytic activity. β5 has chymotrypsin-like activity which can cleave protein after hydrophobic residues, while β1 (caspase-like activity) and β2 (trypsin-like activity) cleave after basic and acidic residues. The substrate protein can be first cleaved into seven to

eight amino acid long peptides, which can be further degraded into amino acids and used to synthesize new protein. The 19S regulatory particle functions to recognize the K48-linked polyubiquitinated substrates, unfold them and finally feed them into the core particle for proteolysis. Meanwhile, the19S also functions to remove the ubiquitin chain from the substrate so that the ubiquitin can be recycled back to cytoplasm.

The ER is the main organelle where secretory proteins are made. Aberrant ER proteins are degraded by the cytoplasmic UPS. This process is mediated by a well-studied pathway: endoplasmic reticulum associated protein degradation (ERAD). Terminally misfolded protein substrates are recognized and exported from ER via a channel formed by Sec61. Once exposed to the cytoplasm, lysine residues of the substrate protein are ubquitinated by ER-localized ubiquitin ligases. Cdc48/p97 complexes assist in the extraction of substrate protein from the ER membrane. Ubiquitinated substrates are then destroyed by the cytoplasmic UPS (Meusser, Hirsch et al. 2005). Defects in ERAD have been implicated in many human diseases, including Parkinson's disease and cystic fibrosis. Protein misfolding related diseases will be further discussed in a later section.

Protein degradation by lysosomal/vacuolar trafficking

The lysosome (vacuole in yeast and plants) is an organelle that contains an acidic environment (around pH4.5) and a plethora of degradative enzymes. Lysosomes maintain low pH by pumping H+ from the cytosol through vacuole membrane

proton pumps and chloride ion channels. The lumen of the lysosome/vacuole contains many acid hydrolases, which digest the proteins, lipids and other macromolecules. Specialized channels and pumps on the limiting membrane of the lysosome/vacuole are responsible for transporting macromolecules from the lumen into the cytosol for reuse. Importantly, trafficking of most proteins to the lysosome/vacuole requires ubiquitination. Whereas K48-linked polyubiquitin targets a substrate for proteasomal degradation, lysosomal trafficking often involves conjugation to mono- or K63-linked poly ubiquitin.

Degradation of integral plasma membrane proteins occurs primarily by a complicated process called endocytic downregulation, which involves endocytosis, endosomal sorting into intralumenal vesicles, and endosomal-lysosomal fusion. In yeast, ubiquitination is required and sufficient for the endocytosis of various plasma membrane proteins, including the ABC transporters Ste6 and Pdr5, alpha-factor pheromone receptor Ste2, as well as numerous ion channels and nutrient transporters (Kolling and Hollenberg 1994; Egner and Kuchler 1996; Hicke and Riezman 1996; Jenness, Li et al. 1997). In mammalian cells, there are ubiquitin-dependent as well as ubiquitin-independent pathways for endocytosis. Although many plasma membrane proteins are endocytosed in an ubiquitin independent manner, several membrane proteins, such as receptor tyrosine kinase (RTKs) and G protein-coupled receptors (GPCRs), have been shown to be turned over by ubiquitin mediated endocytosis (Haglund, Sigismund et al. 2003; Sigismund, Woelk et al. 2005; Macgurn, Hsu et al. 2012).

Ubiquitination plays a key role in several steps along the path of endocytic downregulation. At the PM, ubiquitin is recognized as a sorting determinant. Several components of the endocytic machinery, including the Ede1 and the Ent proteins (Eps15 and epsins in mammalian cells, respectively) contain ubiquitin binding domains (UBDs) thought to recognize and sort ubiquitinated proteins into budding vesicles. During endosomal sorting, several key complexes, including ESCRT-0, ESCRT-I and ESCRT-II, have been demonstrated to have UBDs that can interact with ubiquitinated cargoes. For example, TSG 101 (yeast Vps23) of ESCRT-I has a UEV (Ubiquitin E2 Variant) domain, which has been shown to bind ubiquitin (Katzmann, Babst et al. 2001). In the ESCRT-II complex, the GLUE domain of Vps36 was shown to contain a UBD domain (Slagsvold, Aasland et al. 2005; Hirano, Suzuki et al. 2006). Prior to budding into the lumen of the endosome, ubiquitin is removed from cargo that has been captured and sorted by the deubiquitinating enzyme Doa4, which serves to recycle ubiquitin.

Ubiquitination has also been shown to function as a sorting determinant at the Golgi complex. Ubiquitination of carboxyperptide S (CPS) is required for its Golgi to endosome/vacuole sorting and trafficking (Katzmann, Sarkar et al. 2004). For many integral membrane proteins that normally are delivered to the plasma membrane, including the general amino acid transporter (Gap1) and the PM localized proton pump (Pma1), ubiquitin modification at the Golgi complex results in sorting directly to endosomes without reaching the plasma membrane (Pizzirusso and Chang 2004; Rubio-Texeira and Kaiser 2006; Risinger and Kaiser 2008; Macgurn, Hsu et al. 2012).

Ubiquitination at the Golgi complex is thought to play an important role in Golgi protein quality control (GQC). GQC targets unfolded proteins, which escape from ER, for degradation in lysosome. Unfortunately, very little is known about the GQC system. One possible component of GQC is Vps10, a transmembrane protein required for CPY (Carboxypeptidase Y) sorting that may recognize misfolded proteins at the Golgi and target them for trafficking to the vacuole (Marcusson, Horazdovsky et al. 1994; Macgurn, Hsu et al. 2012). One study fused mutant lambda repressor to secreted protein and found that at high temperature the hybrid protein is transported from the Golgi to the vacuole by a Vps10 mediated pathway (E hong 1996) (Macgurn, Hsu et al. 2012). Golgi-endosome trafficking mediators GGA (Golgi-localizing,γ-adaptin ear homology domain, ARF-binding) proteins, are required for many cargoes sorting at the Golgi complex. GGAs contain a VHS domain at their N terminus, a conserved GGA homology domain (GGAH) interacting directly with ADP-ribosylation factors (ARFs), a proline-rich hinge region required for interaction with chathrin, and a C terminus adaptor γ ear homology (AGEH) domain. The VHS domain has been shown to bind ubiquitin moiety of cargo proteins and interact with lipid (Ren and Hurley ; Puertollano and Bonifacino 2004; Wang, Sun et al. 2007; Demmel, Beck et al. 2008). Cargo ubiquitination can induce GGA mediated trafficking from Golgi to endosome (Stringer and Piper). GGAs might be potential factors functioning in Golgi protein quality control. As a post ER compartment, the Golgi complex must have its own protein quality control to ensure the quality of secreted proteins, however, the detailed mechanisms of such a Golgi protein quality control system still needs to be further studied.

Misfolded protein recognition

Protein quality control requires the ability to distinguish between native and misfolded states of a protein. Ultimately, understanding how misfolded proteins are recognized involves investigating the mechanisms of E3 ligase substrate targeting. Although quality control mechanisms that distinguish native from misfolded proteins are still poorly understood, a few examples that have been described are summarized in this section.

Molecular chaperones have been predicted to contain intrinsically disordered regions which play key roles in misfolded protein recognition. Hsp10 can recognize a broad spectrum of misfolded proteins and there is no defined common domain among those substrates. Intrinsically disordered regions are predicted across the protein, especially in the C terminal lid domain of Hsp10, where substrates bind. Misfolded proteins are prone to aggregate and tightly associate with chaperones such as Hsp70 and Hsp40. The cytosolic E3 ligase CHIP does not recognize misfolded proteins directly, but instead interacts with the chaperone Hsp70. CHIP binds to Hsp70 via its TRP domain which allows it to target aberrant proteins for ubiquitination (Connell, Ballinger et al. 2001; Murata, Minami et al. 2001). Although the yeast genome does not encode a CHIP homolog, the yeast ubiquitin ligases Ubr1 and Ubr2 can target substrates by interaction with Hsp70 and Hsp110 (Heck, Cheung et al. 2010; Nillegoda, Theodoraki et al. 2010). Thus, indirect targeting via chaperone association appears to be a major mechanism of misfolded protein

recognition. In contrast, the nuclear-localized ubiquitin ligase San1 has its own intrinsically disordered domain which can bind directly to many different substrates and target them for ubiquitination (Gardner, Nelson et al. 2005). Despite these examples, recognition of misfolded proteins in the cell is still very poorly understood.

How cells deal with misfolded plasma membrane proteins

The proteasome and the lysosome are two distinct destinations where misfolded/damaged proteins are degraded. For membrane proteins, the site where misfolded proteins are degraded is determined by the location of misfolding. For example, if misfolding happens at ER, ERAD-mediated proteasomal degradation will take place, whereas if misfolding happens at a post-ER compartment, degradation is likely to occur via ubiquitin-dependent trafficking to the lysosome.

The plasma membrane separates the cell interior from the extracellular environment. Many physiological functions are associated with plasma membranes, including signal transduction, nutrient and ion uptake, energy conversion as well as osmotic homeostasis. Most PM functions are fulfilled by integral membrane proteins. Therefore, many cell surface proteins are vital for the health of an organism by determining cellular growth, differentiation, and death. Many diseases have been associated with aberrant proteins at the cell surface, leading to broad interest in understanding the proteostasis of integral membrane proteins at the PM.

Several cellular stresses are associated with protein misfolding, including heat, oxidative stress, genetic mutations and chemical stress. Because these stresses are known to induce misfolding of soluble proteins or integral membrane proteins at the ER, we reasoned that such conditions might also induce misfolding of plasma membrane proteins at a certain rate. The accumulation of misfolded membrane proteins could result in the loss of plasma membrane integrity. We reasoned that there may exist a protective PM quality maintenance system to protect the membrane from toxic protein accumulation in order to maintain membrane homeostasis. However, unlike the protein quality control system at the ER, less is known about the mechanism of plasma membrane protein degradation. Several studies support the existence of protein quality control mechanisms at the plasma membrane. Mutations in the yeast mating pheromone receptor Ste2, a GPCR, were shown to be rapidly endocytosed and degraded in the vacuole following a shift to nonpermissive temperatures (Jenness, Li et al. 1997; Macgurn, Hsu et al. 2012). Mutant alleles of the arginine transporter Can1 and the proton pump Pma1 were also found to be midfolded at nonpermissive temperature and be internalized and degraded in vacuole (Macgurn, Hsu et al. ; Li, Kane et al. 1999; Gong and Chang 2001). Furthermore, plasma membrane proteins are tightly associated with surrounding lipids, which have been shown to play an important role in regulating the folding state of membrane proteins. One study indicated that the absence of sphingolipids destabilized the general amino acid transporter Gap1, resulting in its

rapid ubiquitination, endocytosis, and vacuolar degradation (Lauwers, Grossmann et al. 2007).

Most plasma membrane proteins have transmembrane domains as well as cytoplasmic and extracellular domains. Nonetheless, little is known about the mechanism of how and where misfolded/damaged plasma membrane proteins are recognized. To test how yeast cells recognize and degrade misfolded cytoplasmic domains, one study anchored temperature-induced misfolding soluble domains to plasma membrane proteins and found it failed to trigger turnover or endocytosis (Lewis and Pelham 2009). Several recent studies have shown in mammalian cells that mutation of cytosolic portion of CFTR Δ F508 exhibits temperature instability: at low temperature CFTR Δ F508 traffics to the cell surface. However, once the temperature is raised, misfolded CFTR Δ F508 is recognized and ubiquitinated by an E3 ligase, CHIP. As we previously discussed, CHIP can interact Hsc70, Hsp90 and other chaperones with its N-terminal tetratricopeptide repeat domain. Ubiquitination of CFTR Δ F508 triggers its endocytosis and lysosome mediated degradation (Okiyoneda, Barriere et al.). Another study analyzed the temperature-induced trafficking of CD4 fused to the temperature sensitive bacteriophage λ domain, which is also recognized and ubiquitinated by CHIP (Apaja, Xu et al. ; Macgurn, Hsu et al. 2012). These studies propose that misfolded soluble domains of plasma membrane proteins are targeted for turnover by CHIP. However, these studies do not address mechanisms for detection of aberrent transmembrane

domains or damaged extracellular domains, which are also likely to be toxic to the cell (Apaja, Xu et al. ; Macgurn, Hsu et al. 2012).

Figure 1.2

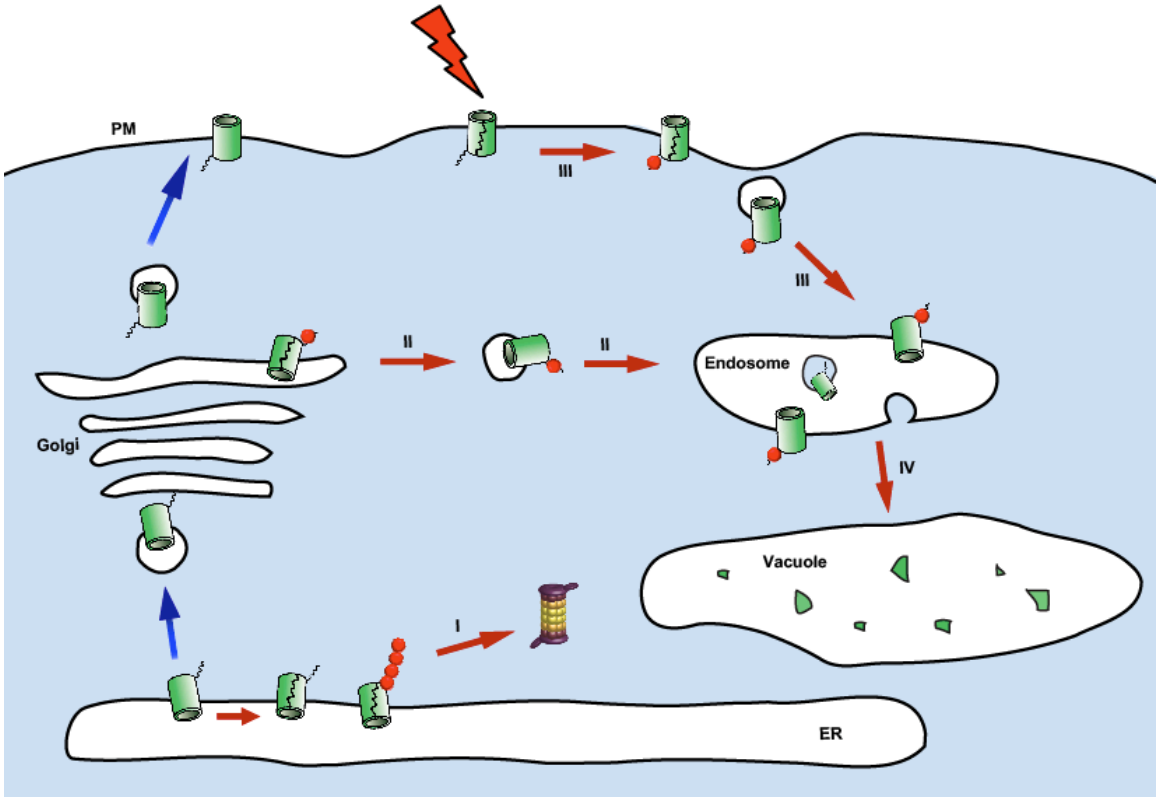
PM
III
III
II
II
Endosome
Golgi
IV
Vacuole
I
ER
Secretory pathway
I
ERAD
II
Golgi PQC
III
PMQM (PM protein quality Maintainence)
IV
lysosomal degradation

Figure 1.2 Compartmentalized quality control systems for membrane protein

The proteasome and the lysosome are two distinct destinations where membrane proteins are degraded. Where misfolded membrane proteins are degraded is determined by the location of misfolding. Misfolded ER membrane proteins will be degraded by ERAD mediated proteasome degradation. Parallel to ERAD, there are Golgi and PM protein quality control systems that maintain protein homeostasis at different compartments.

Role of DUBs in PQC

Ubiquitination is a key determinant of protein degradation, but it can also be reversed by the activity of deubiquitinating enzymes (DUBs). There are nearly 100 deubiquitinases encoded in human genome and about 20 in yeast. Compared to E3 ubiquitin ligases, DUBs remain poorly understood. However, DUBs clearly play an important role in cellular proteostasis with key functions in: rescue of proteins from proteasomal degradation; editing of the ubiquitin chain from one linkage type to another; regulation of protein function or localization; and maintenance of the level of monomeric ubiquitin in the cell.

The ubiquitin ligase CHIP has been found to be monoubiquitinaed and this modification stabilizes its interaction with the deubiquitinase Ataxin-3. Ataxin-3 antagonizes CHIP, limiting the length of polyubiquitin chains of CHIP substrates. Following CHIP-mediated ubiquitination of substrate, ataxin-3 can effectively terminate the reaction by deubiquitination of CHIP (Scaglione, Zavodszky et al. 2011). One important deubiquitinase function involves editing of polyubiquitin chains by the DUB A20. A20 is known as a negative regulator of the NF-κB pathway, which is activated in response to many stress conditions. A20 has an N-terminal ovarian tumor (OTU) domain and C-terminal zinc finger containing domain, which allows A20 to function both as a deubquitinase and as an E3 ligase. One of the important signaling molecules in the NF-κB signaling pathway is receptor interacting protein-1 (RIP1). RIP1 is ubiquitnated by the E3 ligases cIAP-1 and cIAP-2 with K63 polyubiquitin chains, which is required for its interaction with NF-

kappa-B essential modulator (NEMO). A20 can deubiquitinate RIP1 and prevent its interaction with NEMO. RIP1 can be further ubquitinated by A20 using its ubiquitin ligase domain, which modifies RIP1 with a K48 polyubquitin chain and targets it for proteasomal degradation. Other than the above functions, some DUBs such as Ubp6 and Rpn11 in yeast, (mammalian POH1/PSMD14, USP14 and UCH37) have been shown to tightly associate with the proteasome (Papa, Amerik et al. 1999; Leggett, Hanna et al. 2002; Hanna, Hathaway et al. 2006; Finley 2009). These DUBs functions in recycling ubiquitin as well as control the rate of protein degradation (Lee, Lee et al. ; Yao and Hong 2001; Jacobson, Zhang et al. 2009). DUBs will be further discussed in chapter III in the context of their role in membrane protein trafficking and degradation.

III. Protein misfolding related Diseases

Many human disease states are associated with protein misfolding. The molecular mechanism of many of these diseases is caused by misfolding that results in loss of a critical cellular function. A well-studied example is cystic fibrosis (CF), which results from misfolding and loss of function of a chloride transporter called CFTR. Diseases can also result when misfolded proteins aggregate, which is a hallmark of many neurodegenerative disorders such as Alzheimer's and Parkinson's disease. For this type of disease, there are three major hypothesizes that have been proposed to explain how protein aggregates may interfere with cellular functions: (i) the channel hypothesis, which suggests that aggregates form pores on the membrane; (ii) aggregates interact with native proteins to disrupt global cellular proteostasis; (iii) aggregates may sequester chaperones, ubiquitination machinery, and other components of protein quality control systems, siphoning them away from their normal cellular functions. (Barral, Broadley et al. 2004; Aigelsreiter, Janig et al. 2007) Some cancers, although not considered misfolding diseases, rely on chaperones to stabilize and protect aberrant oncogenes. For example, Hsp90 has been a target protein for tumor therapy. As a chaperone, Hsp90 interacts with its substrate proteins to correct their folding and protect them from degradation. However, many of those substrate proteins function in tumor progression. Several Hsp90 inhibitors have been shown efficiently block tumor growth, invasion and angiogenesis (Eccles, Massey et al. 2008; Jensen, Schoepfer et al. 2008).

Neurodegenerative diseases are a large class of human diseases, which are characterized by a wide range of clinical symptoms and distinct pathological phenotypes associated with various regions of the nervous systems. Many neurodegenerative diseases are protein deposition disorders including prion diseases, Huntington's disease, and Alzheimer's disease. At the molecular level, recent studies have indicated that these diseases share a common pathophysiologic mechanism, and represent a subset of a broader class of diseases known as the protein conformational or protein misfolding diseases. Failure of a specific protein to fold into its native functional conformation can contribute to the formation of protein aggregates, ultimately resulting in broader cellular functions including mitochondrial dysfunction, increased vulnerability to stress, neurotoxic signaling, pore formation, synaptic deficits, impairment of axonal transport and defective cellular trafficking (Winklhofer, Tatzelt et al. 2008). Ubiquitin has been found to be present in proteinaceous accumulations in various neurodegenerative disorders (Sokolov, Panyutin et al. ; Mori, Kondo et al. 1987; Lennox, Lowe et al. 1988; Lowe, Lennox et al. 1988; Paulson and Prior 1997). Therapeutic strategies for these neurodegenerative disorders have been designed to reduce protein misfolding and aggregation, as well as to up regulate the activity of the protein quality control system (Taylor, Hardy et al. 2002; Lansbury and Lashuel 2006; Roberson and Mucke 2006; Wooten and Geetha 2006). Molecular chaperone Hsp104 has a disaggregation activity and has been shown to inhibit amyloid formation in Alzheimer's disease and also reverse α-synulein fiber formation in Parkinson's disease (Vashist, Cushman et al.). Theses finding are promising for developing therapeutic strategies that target

Hsp104. Furthermore, the small molecule Tramiprostate (3- amino-1-propanesulfonic acid) was found to inhibit and sometime reverse Aβ fibrillar formation (Melnikova 2007). Further detailed studies of the underlying mechanism of the protein quality control system will provide more clues for the design of new targeted therapies for neurodegenerative diseases.

Channelopathies are a group of clinical sydromes caused by altered ion channel function. Many of these diseases are linked to point substitutions in various ion channels. Channelopathies lead to a variety of distinct symptoms, such as epilepsy, migraine headache, ataxia as well as other cardiac and neurological syndromes. Different mutations in the same ion channels might also give different symptoms (Magby, Neal et al.). One of most well studied examples is CFTR, which is mutated in cases of cystic fibrosis.

Cystic Fibrosis

Cystic fibrosis (CF) is caused by a loss of function of the cystic fibrosis transmembrane conductance regulator (CFTR), an ABC transporter that pumps chloride ions. Wildtype CFTR protein is localized at the plasma membrane of epithelial cells and functions as a cAMP-activated chloride channel. CFTR functions to maintain the anion gradient, which is important to direct water movement and maintain the normal function of epithelia. CF patients have viscous mucus that accumulates in the airways of lung and facilitates severe lung infections.

The CFTR protein is predicted to have two membrane-spanning domains (MSD), two nucleotide-binding domains (NBDs) and a regulatory (R) domain. Each MSD contains six transmembrane segments and these transmembrane segments together form the channel allowing chloride ion to pass through. The R domain resides in between the two MSDs and is a unique feature of CFTR distinct from other ABC transporters. Only when the R-domain is phosphorylated by protein kinase A (PKA) will the NBDs bind ATP, opening the channel to allow Cl- ions to pass into the cell (Sheppard and Welsh 1999). Interestingly, the regulatory R domain is where most disease causing mutations occur. 70% of all mutations of CFTR happen at F508.

Before wildtype CFTR reaches the apical membrane, it must pass through stringent PQC systems at different compartments. Within the ER lumen, the folding process of wildtype CFTR is inefficient: about 45-80% are rapidly degraded with a half-life about 0.5 hour (Lukacs, Mohamed et al. 1994; Ward and Kopito 1994; Sheppard and Welsh 1999). Furthermore, newly synthesized CFTR is found in complex with multiple molecular chaperones, including calnexin and calreticulin, which assist the folding of CFTR (Yang, Janich et al. 1993; Pind, Riordan et al. 1994; Harada, Okiyoneda et al. 2006; Rosser, Grove et al. 2008). Moreover, while trafficking from the ER to the Golgi complex and plasma membrane, CFTR is complexed with many chaperones including Hsp70, Hsc70, Hsp90 and Hdj-2 (Alberti, Bohse et al. 2004; Wang, Venable et al. 2006; Sun, Mi et al. 2008; Glozman, Okiyoneda et al. 2009). CFTR is further modified in the Golgi to a mature form by glycosylation of an extracellular loop of MSD2 (membrane spanning domain 2) (Lukacs, Mohamed et al.

1994). Mature CFTR traffics from the Golgi to plasma membrane by clathrin-coated vesicles. At the PM, 10% of CFTR is turned over consistently (Lukacs, Chang et al. 1993; Ward and Kopito 1994). Misfolded or damaged CFTR at the cell surface can be ubiquitinated by CHIP, targeting it for degradation in the lysosome (Okiyoneda, Barriere et al. ; Sharma, Pampinella et al. 2004).

The most frequent mutation of CFTR in cystic fibrosis patients (over 70%) is a deletion of a phenylalanine residue at position 508 (CFTR Δ F508). This mutant protein fails to fold into its native conformation and thereby is targeted for degradation by ERAD. However, Δ F508 is sensitive to temperature. By lowering the temperature below 30°C, a portion of mutant transporters are able to traffic to the plasma membrane, restoring chloride transport. Interestingly, previous studies have shown that some chemical chaperones can effectively stabilize Δ F508 at the cell surface (Brown, Hong-Brown et al. 1996). Sodium-4-phenylbutyrate (Buphenyl) is a candidate drug that can promote CFTRΔF508 trafficking to the apical membrane, possibly by down-regulation of Hsc70 and up-regulation of Hsp70 (Rubenstein and Zeitlin 2000; Choo-Kang and Zeitlin 2001; Rubenstein and Lyons 2001). 4-phenylbutyric acid (4-PBA) has been found to induce Hsp70 production, which leads to maturation of CFTR (Rubenstein, Egan et al. 1997). Furthermore, compounds that interfere with ER protein quality control or chaperone machinery, such as the ER Ca^{++} pump inhibitor thapsigargin, can promote CFTR Δ F508 trafficking to the plasma membrane by lowering ER Ca^{++} level (Egan, Glockner-Pagel et al. 2002).

Overview of thesis

Properly folded PM proteins, such as signaling receptors, ion channels, and nutrient transporters, exit the ER and traffic through the Golgi to the cell surface to carry out their specific functions. Maintenance of proper PM proteostasis, particularly with respect to ion channels and nutrient transporters, is crucial in preserving PM integrity and preventing the dissipation of essential ion and chemical gradients from the cell

My thesis research has focused on addressing three major questions: (1) How do cells deal with plasma membrane protein misfolding stress? (2) Does ubiquitination play central role in the turnover of misfolded/damaged PM proteins? (3) What are the key players involved in protein quality control at the plasma membrane? Ultimately, the investigation of cell surface quality control mechanisms that recognize and remove misfolded proteins at the PM will have important implications for human disease and therapeutic strategies.

Reference

Aigelsreiter, A., E. Janig, et al. (2007). "How a cell deals with abnormal proteins. Pathogenetic mechanisms in protein aggregation diseases." Pathobiology **74**(3): 145-58.

Alberti, S., K. Bohse, et al. (2004). "The cochaperone HspBP1 inhibits the CHIP ubiquitin ligase and stimulates the maturation of the cystic fibrosis transmembrane conductance regulator." Mol Biol Cell **15**(9): 4003-10.

Apaja, P. M., H. Xu, et al. "Quality control for unfolded proteins at the plasma membrane." J Cell Biol **191**(3): 553-70.

Barral, J. M., S. A. Broadley, et al. (2004). "Roles of molecular chaperones in protein misfolding diseases." Semin Cell Dev Biol **15**(1): 17-29.

Blobel, G. (1980). "Intracellular protein topogenesis." Proc Natl Acad Sci U S A **77**(3): 1496-500.

Bolen, D. W. and I. V. Baskakov (2001). "The osmophobic effect: natural selection of a thermodynamic force in protein folding." J Mol Biol **310**(5): 955-63.

Bowie, J. U. (2005). "Solving the membrane protein folding problem." Nature **438**(7068): 581-9.

Brown, C. R., L. Q. Hong-Brown, et al. (1996). "Chemical chaperones correct the mutant phenotype of the delta F508 cystic fibrosis transmembrane conductance regulator protein." Cell Stress Chaperones **1**(2): 117-25.

Choo-Kang, L. R. and P. L. Zeitlin (2001). "Induction of HSP70 promotes DeltaF508 CFTR trafficking." Am J Physiol Lung Cell Mol Physiol **281**(1): L58-68.

Connell, P., C. A. Ballinger, et al. (2001). "The co-chaperone CHIP regulates protein triage decisions mediated by heat-shock proteins." Nat Cell Biol **3**(1): 93-6.

Demmel, L., M. Beck, et al. (2008). "Nucleocytoplasmic shuttling of the Golgi phosphatidylinositol 4-kinase Pik1 is regulated by 14-3-3 proteins and coordinates Golgi function with cell growth." Mol Biol Cell **19**(3): 1046-61.

Eccles, S. A., A. Massey, et al. (2008). "NVP-AUY922: a novel heat shock protein 90 inhibitor active against xenograft tumor growth, angiogenesis, and metastasis." Cancer Res **68**(8): 2850-60.

Egan, M. E., J. Glockner-Pagel, et al. (2002). "Calcium-pump inhibitors induce functional surface expression of Delta F508-CFTR protein in cystic fibrosis epithelial cells." Nat Med **8**(5): 485-92.

Egner, R. and K. Kuchler (1996). "The yeast multidrug transporter Pdr5 of the plasma membrane is ubiquitinated prior to endocytosis and degradation in the vacuole." FEBS Lett **378**(2): 177-81.

Ellis, J. (1987). "Proteins as molecular chaperones." Nature **328**(6129): 378-9.

Finley, D. (2009). "Recognition and processing of ubiquitin-protein conjugates by the proteasome." Annu Rev Biochem **78**: 477-513.

Garcia-Mata, R., Y. S. Gao, et al. (2002). "Hassles with taking out the garbage: aggravating aggresomes." Traffic **3**(6): 388-96.

Gardner, R. G., Z. W. Nelson, et al. (2005). "Degradation-mediated protein quality control in the nucleus." Cell **120**(6): 803-15.

Gekko, K. and S. N. Timasheff (1981). "Mechanism of protein stabilization by glycerol: preferential hydration in glycerol-water mixtures." Biochemistry **20**(16): 4667-76.

Glover, J. R. and S. Lindquist (1998). "Hsp104, Hsp70, and Hsp40: a novel chaperone system that rescues previously aggregated proteins." Cell **94**(1): 73-82.

Glozman, R., T. Okiyoneda, et al. (2009). "N-glycans are direct determinants of CFTR folding and stability in secretory and endocytic membrane traffic." J Cell Biol **184**(6): 847-62.

Gong, X. and A. Chang (2001). "A mutant plasma membrane ATPase, Pma1-10, is defective in stability at the yeast cell surface." Proc Natl Acad Sci U S A **98**(16): 9104-9.

Haglund, K., S. Sigismund, et al. (2003). "Multiple monoubiquitination of RTKs is sufficient for their endocytosis and degradation." Nat Cell Biol **5**(5): 461-6.

Hanna, J., N. A. Hathaway, et al. (2006). "Deubiquitinating enzyme Ubp6 functions noncatalytically to delay proteasomal degradation." Cell **127**(1): 99-111.

Harada, K., T. Okiyoneda, et al. (2006). "Calreticulin negatively regulates the cell surface expression of cystic fibrosis transmembrane conductance regulator." J Biol Chem **281**(18): 12841-8.

Hardesty, B. and G. Kramer (2001). "Folding of a nascent peptide on the ribosome." Prog Nucleic Acid Res Mol Biol **66**: 41-66.

Heck, J. W., S. K. Cheung, et al. (2010). "Cytoplasmic protein quality control degradation mediated by parallel actions of the E3 ubiquitin ligases Ubr1 and San1." Proc Natl Acad Sci U S A **107**(3): 1106-11.

Hicke, L. and H. Riezman (1996). "Ubiquitination of a yeast plasma membrane receptor signals its ligand-stimulated endocytosis." Cell **84**(2): 277-87.

Hirano, S., N. Suzuki, et al. (2006). "Structural basis of ubiquitin recognition by mammalian Eap45 GLUE domain." Nat Struct Mol Biol **13**(11): 1031-2.

Hochstrasser, M. (2009). "Origin and function of ubiquitin-like proteins." Nature **458**(7237): 422-9.

Horwich, A. (2004). "Cell biology: sight at the end of the tunnel." Nature **431**(7008): 520-2.

Hu, Y. and N. F. Mivechi (2003). "HSF-1 interacts with Ral-binding protein 1 in a stress-responsive, multiprotein complex with HSP90 in vivo." J Biol Chem **278**(19): 17299-306.

Jacobson, A. D., N. Y. Zhang, et al. (2009). "The lysine 48 and lysine 63 ubiquitin conjugates are processed differently by the 26 s proteasome." J Biol Chem **284**(51): 35485-94.

Jenness, D. D., Y. Li, et al. (1997). "Elimination of defective alpha-factor pheromone receptors." Mol Cell Biol **17**(11): 6236-45.

Jensen, M. R., J. Schoepfer, et al. (2008). "NVP-AUY922: a small molecule HSP90 inhibitor with potent antitumor activity in preclinical breast cancer models." Breast Cancer Res **10**(2): R33.

Katzmann, D. J., M. Babst, et al. (2001). "Ubiquitin-dependent sorting into the multivesicular body pathway requires the function of a conserved endosomal protein sorting complex, ESCRT-I." Cell **106**(2): 145-55.

Katzmann, D. J., S. Sarkar, et al. (2004). "Multivesicular body sorting: ubiquitin ligase Rsp5 is required for the modification and sorting of carboxypeptidase S." Mol Biol Cell **15**(2): 468-80.

Kolling, R. and C. P. Hollenberg (1994). "The ABC-transporter Ste6 accumulates in the plasma membrane in a ubiquitinated form in endocytosis mutants." EMBO J **13**(14): 3261-71.

Kopito, R. R. (2000). "Aggresomes, inclusion bodies and protein aggregation." Trends Cell Biol **10**(12): 524-30.

Lansbury, P. T. and H. A. Lashuel (2006). "A century-old debate on protein aggregation and neurodegeneration enters the clinic." Nature **443**(7113): 774-9.

Lauwers, E., G. Grossmann, et al. (2007). "Evidence for coupled biogenesis of yeast Gap1 permease and sphingolipids: essential role in transport activity and normal control by ubiquitination." Mol Biol Cell **18**(8): 3068-80.

Lee, B. H., M. J. Lee, et al. "Enhancement of proteasome activity by a small-molecule inhibitor of USP14." Nature **467**(7312): 179-84.

Leggett, D. S., J. Hanna, et al. (2002). "Multiple associated proteins regulate proteasome structure and function." Mol Cell **10**(3): 495-507.

Lennox, G., J. Lowe, et al. (1988). "Ubiquitin is a component of neurofibrillary tangles in a variety of neurodegenerative diseases." Neurosci Lett **94**(1-2): 211-7.

Lewis, M. J. and H. R. Pelham (2009). "Inefficient quality control of thermosensitive proteins on the plasma membrane." PLoS One **4**(4): e5038.

Li, Y., T. Kane, et al. (1999). "Yeast mutants affecting possible quality control of plasma membrane proteins." Mol Cell Biol **19**(5): 3588-99.

Lowe, J., G. Lennox, et al. (1988). "A filamentous inclusion body within anterior horn neurones in motor neurone disease defined by immunocytochemical localisation of ubiquitin." Neurosci Lett **94**(1-2): 203-10.

Lukacs, G. L., X. B. Chang, et al. (1993). "The delta F508 mutation decreases the stability of cystic fibrosis transmembrane conductance regulator in the plasma membrane. Determination of functional half-lives on transfected cells." J Biol Chem **268**(29): 21592-8.

Lukacs, G. L., A. Mohamed, et al. (1994). "Conformational maturation of CFTR but not its mutant counterpart (delta F508) occurs in the endoplasmic reticulum and requires ATP." EMBO J **13**(24): 6076-86.

Macgurn, J. A., P. C. Hsu, et al. "Ubiquitin and membrane protein turnover: from cradle to grave." Annu Rev Biochem **81**: 231-59.

Macgurn, J. A., P. C. Hsu, et al. (2012). "Ubiquitin and membrane protein turnover: from cradle to grave." Annu Rev Biochem **81**: 231-59.

Magby, J. P., A. P. Neal, et al. "Channelopathies: summary of the hot topic keynotes session." Neurotoxicology **32**(5): 661-5.

Marcusson, E. G., B. F. Horazdovsky, et al. (1994). "The sorting receptor for yeast vacuolar carboxypeptidase Y is encoded by the VPS10 gene." Cell **77**(4): 579-86.

Melnikova, I. (2007). "Therapies for Alzheimer's disease." Nat Rev Drug Discov **6**(5): 341-2.

Meng, F. G., Y. K. Hong, et al. (2004). "Osmophobic effect of glycerol on irreversible thermal denaturation of rabbit creatine kinase." Biophys J **87**(4): 2247-54.

Meusser, B., C. Hirsch, et al. (2005). "ERAD: the long road to destruction." Nat Cell Biol **7**(8): 766-72.

Mori, H., J. Kondo, et al. (1987). "Ubiquitin is a component of paired helical filaments in Alzheimer's disease." Science **235**(4796): 1641-4.

Murata, S., Y. Minami, et al. (2001). "CHIP is a chaperone-dependent E3 ligase that ubiquitylates unfolded protein." EMBO Rep **2**(12): 1133-8.

Murata, S., H. Udono, et al. (2001). "Immunoproteasome assembly and antigen presentation in mice lacking both PA28alpha and PA28beta." EMBO J **20**(21): 5898-907.

Nillegoda, N. B., M. A. Theodoraki, et al. (2010). "Ubr1 and Ubr2 function in a quality control pathway for degradation of unfolded cytosolic proteins." Mol Biol Cell **21**(13): 2102-16.

Nunes, S. L. and S. K. Calderwood (1995). "Heat shock factor-1 and the heat shock cognate 70 protein associate in high molecular weight complexes in the cytoplasm of NIH-3T3 cells." Biochem Biophys Res Commun **213**(1): 1-6.

Okiyoneda, T., H. Barriere, et al. "Peripheral protein quality control removes unfolded CFTR from the plasma membrane." Science **329**(5993): 805-10.

Papa, F. R., A. Y. Amerik, et al. (1999). "Interaction of the Doa4 deubiquitinating enzyme with the yeast 26S proteasome." Mol Biol Cell **10**(3): 741-56.

Parsell, D. A., A. S. Kowal, et al. (1994). "Protein disaggregation mediated by heat-shock protein Hsp104." Nature **372**(6505): 475-8.

Paulson, G. W. and T. W. Prior (1997). "Issues related to DNA testing for Huntington's disease in symptomatic patients." Semin Neurol **17**(3): 235-8.

Pind, S., J. R. Riordan, et al. (1994). "Participation of the endoplasmic reticulum chaperone calnexin (p88, IP90) in the biogenesis of the cystic fibrosis transmembrane conductance regulator." J Biol Chem **269**(17): 12784-8.

Pizzirusso, M. and A. Chang (2004). "Ubiquitin-mediated targeting of a mutant plasma membrane ATPase, Pma1-7, to the endosomal/vacuolar system in yeast." Mol Biol Cell **15**(5): 2401-9.

Puertollano, R. and J. S. Bonifacino (2004). "Interactions of GGA3 with the ubiquitin sorting machinery." Nat Cell Biol **6**(3): 244-51.

Qian, S. B., X. Zhang, et al. (2010). "mTORC1 links protein quality and quantity control by sensing chaperone availability." J Biol Chem **285**(35): 27385-95.

Ren, X. and J. H. Hurley "VHS domains of ESCRT-0 cooperate in high-avidity binding to polyubiquitinated cargo." EMBO J **29**(6): 1045-54.

Risinger, A. L. and C. A. Kaiser (2008). "Different ubiquitin signals act at the Golgi and plasma membrane to direct GAP1 trafficking." Mol Biol Cell **19**(7): 2962-72.

Roberson, E. D. and L. Mucke (2006). "100 years and counting: prospects for defeating Alzheimer's disease." Science **314**(5800): 781-4.

Rosser, M. F., D. E. Grove, et al. (2008). "Assembly and misassembly of cystic fibrosis transmembrane conductance regulator: folding defects caused by deletion of F508 occur before and after the calnexin-dependent association of membrane spanning domain (MSD) 1 and MSD2." Mol Biol Cell **19**(11): 4570-9.

Rubenstein, R. C., M. E. Egan, et al. (1997). "In vitro pharmacologic restoration of CFTR-mediated chloride transport with sodium 4-phenylbutyrate in cystic fibrosis epithelial cells containing delta F508-CFTR." J Clin Invest **100**(10): 2457-65.

Rubenstein, R. C. and B. M. Lyons (2001). "Sodium 4-phenylbutyrate downregulates HSC70 expression by facilitating mRNA degradation." Am J Physiol Lung Cell Mol Physiol **281**(1): L43-51.

Rubenstein, R. C. and P. L. Zeitlin (2000). "Sodium 4-phenylbutyrate downregulates Hsc70: implications for intracellular trafficking of DeltaF508-CFTR." Am J Physiol Cell Physiol **278**(2): C259-67.

Rubio-Texeira, M. and C. A. Kaiser (2006). "Amino acids regulate retrieval of the yeast general amino acid permease from the vacuolar targeting pathway." Mol Biol Cell **17**(7): 3031-50.

Scaglione, K. M., E. Zavodszky, et al. (2011). "Ube2w and ataxin-3 coordinately regulate the ubiquitin ligase CHIP." Mol Cell **43**(4): 599-612.

Sharma, M., F. Pampinella, et al. (2004). "Misfolding diverts CFTR from recycling to degradation: quality control at early endosomes." J Cell Biol **164**(6): 923-33.

Shearer, A. G. and R. Y. Hampton (2004). "Structural control of endoplasmic reticulum-associated degradation: effect of chemical chaperones on 3-hydroxy-3-methylglutaryl-CoA reductase." J Biol Chem **279**(1): 188-96.

Sheppard, D. N. and M. J. Welsh (1999). "Structure and function of the CFTR chloride channel." Physiol Rev **79**(1 Suppl): S23-45.

Shi, Y., D. D. Mosser, et al. (1998). "Molecular chaperones as HSF1-specific transcriptional repressors." Genes Dev **12**(5): 654-66.

Sigismund, S., T. Woelk, et al. (2005). "Clathrin-independent endocytosis of ubiquitinated cargos." Proc Natl Acad Sci U S A **102**(8): 2760-5.

Sipos, L. and G. von Heijne (1993). "Predicting the topology of eukaryotic membrane proteins." Eur J Biochem **213**(3): 1333-40.

Slagsvold, T., R. Aasland, et al. (2005). "Eap45 in mammalian ESCRT-II binds ubiquitin via a phosphoinositide-interacting GLUE domain." J Biol Chem **280**(20): 19600-6.

Sokolov, M. V., I. V. Panyutin, et al. "Dynamics of the transcriptome response of cultured human embryonic stem cells to ionizing radiation exposure." Mutat Res **709-710**: 40-8.

Stringer, D. K. and R. C. Piper "A single ubiquitin is sufficient for cargo protein entry into MVBs in the absence of ESCRT ubiquitination." J Cell Biol **192**(2): 229-42.

Sun, F., Z. Mi, et al. (2008). "Chaperone displacement from mutant cystic fibrosis transmembrane conductance regulator restores its function in human airway epithelia." FASEB J **22**(9): 3255-63.

Taylor, J. P., J. Hardy, et al. (2002). "Toxic proteins in neurodegenerative disease." Science **296**(5575): 1991-5.

Tokunaga, F., S. Sakata, et al. (2009). "Involvement of linear polyubiquitylation of NEMO in NF-kappaB activation." Nat Cell Biol **11**(2): 123-32.

Vashist, S., M. Cushman, et al. "Applying Hsp104 to protein-misfolding disorders." Biochem Cell Biol **88**(1): 1-13.

Wang, J., H. Q. Sun, et al. (2007). "PI4P promotes the recruitment of the GGA adaptor proteins to the trans-Golgi network and regulates their recognition of the ubiquitin sorting signal." Mol Biol Cell **18**(7): 2646-55.

Wang, X., J. Venable, et al. (2006). "Hsp90 cochaperone Aha1 downregulation rescues misfolding of CFTR in cystic fibrosis." Cell **127**(4): 803-15.

Ward, C. L. and R. R. Kopito (1994). "Intracellular turnover of cystic fibrosis transmembrane conductance regulator. Inefficient processing and rapid degradation of wild-type and mutant proteins." J Biol Chem **269**(41): 25710-8.

Winklhofer, K. F., J. Tatzelt, et al. (2008). "The two faces of protein misfolding: gain- and loss-of-function in neurodegenerative diseases." EMBO J **27**(2): 336-49.

Wooten, M. W. and T. Geetha (2006). "The role of ubiquitin in neurotrophin receptor signalling and sorting." Biochem Soc Trans **34**(Pt 5): 757-60.

Yang, Y., S. Janich, et al. (1993). "The common variant of cystic fibrosis transmembrane conductance regulator is recognized by hsp70 and degraded in a pre-Golgi nonlysosomal compartment." Proc Natl Acad Sci U S A **90**(20): 9480-4.

Yao, X. L. and M. Hong (2001). "Dipolar filtered 1H-13C heteronuclear correlation spectroscopy for resonance assignment of proteins." J Biomol NMR **20**(3): 263-74.

Chapter II

The Rsp5-ART network provides a quality surveillance mechanism that targets the removal of misfolded, toxic proteins at the PM

Chapter II includes work for a manuscript that will be submitted for publication. The authors are Yingying Zhao, Jason A. MacGurn, Max Liu, and Scott D. Emr (author name with underline contributed equally to this study). Yingying's major contributions to this chapter are presented in Figure 2.2, 2.3, 2.4, 2.5, 2.7B C, 2.8, 2.9, 2.10B, 2.11, 2.12A, 2.13, 2.14, 2.15, 2.16C D, 2.17B, 2.18, 2.19 and Table 2.1.

Abstract

Secretory cargos that cannot fold properly in the ER are targeted for removal by a well-studied ER-associated degradation pathway, or ERAD. In contrast, very little is known about post-ER quality control mechanisms for integral membrane proteins. Here we describe a heat-induced endocytic response, which is mediated by the Rsp5-ART network of proteins and functions to protect plasma membrane (PM) integrity. Failure to mediate this protective response during heat stress leads to toxic accumulation of integral membrane proteins at the cell surface, which causes loss of PM integrity and cell death. Thus, the Rsp5-ART network comprises a PM quality control system that works together with parallel quality control pathways to limit accumulation of toxic proteins at the cell surface during heat stress

Introduction

Cells have evolved elaborate protein quality control mechanisms that assist proteins in achieving desired native structure and also help target the degradation of

proteins that have become misfolded, damaged, or otherwise aberrant. This system, often referred to as the cellular proteostasis network, consists of an elaborate network of proteins dedicated to preventing the toxic accumulation of unfolded or misfolded proteins. Often, the cell employs compartment-specific mechanisms that ensure protein quality control. For example, misfolded protein domains that are soluble and accessible to the cytosol can be targeted for degradation by CHIP, an E3 ligase that interacts with various chaperones to target ubiquitination of misfolded substrates (Meacham et al., 2001). Similarly, unfolded soluble protein domains in the lumen of the ER are clients of the Hsp70 family member BiP/Kar2, and extended association with BiP/Kar2 can lead to targeting for ubiquitination by the ERAD machinery and substequent proteasomal degradation (Claessen et al., 2011; Walter and Ron, 2011). In these examples, targeting of misfolded proteins for ubiquitination and subsequent degradation is mediated by prolonged interaction with chaperones, which serve as adaptors that recruit E3 ubiquitin ligases to modify misfolded substrate. In both cases, substrates are ultimately degraded by the proteasome.

Quality control of integral membrane proteins plays a critical role in many human diseases because it affects the quantity of functional proteins – ion channels, nutrient transporters, and signaling receptors – at the cell surface. In contrast to soluble proteins in the cytosol or the lumen of the ER, which are degraded by the proteasome, the degradation of most post-ER integral membrane proteins occurs via lysosomal trafficking. This process is typically ubiquitin-dependent and involves:

(i) selective recognition of cargo for ubiquitination, (ii) capture of ubiquitinated cargo for trafficking to the endosome, (iii) endosomal sorting by ESCRT complexes, which package ubiquitinated cargo into vesicles that bud into the lumen of the endosome (intralumenal vesicles, or ILVs), and (iv) fusion of these multivesicular endosomes with lysosomal/vacuolar compartments, resulting in cargo degradation (Henne et al., 2011; Hurley, 2010; Macgurn et al., 2012; Shields and Piper, 2011). While the sorting and trafficking mechanisms in this elaborate downregulation process have been studied extensively, the initial step of cargo recognition for ubiquitination, particularly with respect to the recognition of misfolded proteins in post-ER secretory and endocytic pathways, is still poorly understood.

Previously, we identified and characterized a network of Rsp5 adaptors called ARTS, or arrestin-related trafficking adaptors. The ART modular adaptor network mediates the recognition and ubiquitination of cell surface proteins, thereby directing the endocytic remodeling of PM protein composition. Thus, ART proteins serve as a key point of regulation during changes in nutrient availability and environmental stress. Here, we report that heat stress triggers extensive cell surface remodeling in yeast cells that is driven by ubiquitin-mediated endocytosis. This heat-induced endocytic response is a protective mechanism that requires the modular ART adaptor network, which targets Rsp5-mediated ubiquitination and degradation of proteins at the surface. Defects in this endocytic targeting system result in an accumulation of cell surface proteins that is toxic during heat stress. This toxicity is associated with loss of PM integrity, which we propose is caused by

conformational flux or misfolding of nutrient transporters and ion channels at the cell surface. The ART-Rsp5 quality surveillance mechanism at the PM functions in parallel with both ERAD and Golgi QC systems to control both quality and quantity of protein composition at the cell surface.

Material and Method

Yeast strains and Plasmid Construction

A list of all Saccharomyces cerevisiae strains and plasmids used in this study and their genotype can be found in Supplementary Table S1 and S2. Homologous recombination was used to tag or delete genes in yeast. All integrations were verified by PCR analysis and expression of fusion proteins was confirmed by Western Blot analysis. Gene subcloning was performed by PCR using Ex Taq (Tafara) or KOD Polymerase (Novagen) and subsequent ligation into the designated expression vector with T4 DNA ligase (Fermentas). The yeast shuttle vectors used in this study have been previously described (Sikorski, 1989). Restriction enzymes were purchased from New England Biolabs (Ipswich, MA)

Fluorescence Microscopy

Yeast cells expressing fluorescent fusion proteins were grown to mid-log in synthetic media. Microscopy was perfomed using a fluorescence microscope (DeltaVison RT; Applied Precision) equipped with FITC and rhodamine filters. Images were captured with a digital camera (Cool Snap HQ; Photometrics) and deconvolved using softWoRx 3.5.0 software (Applied Precision).

Analysis of Cellular Protein Expression Levels

Yeast cells expressing epitope tagged protein were grown to mid-log in synthetic media. OD600 equivalents of mid-log cells pretreated at the indicated temperatures were harvested by precipitation in 10% trichloroacidic acid (TCA). Precipitates

were washed in acetone, aspirated, resuspended in lysis buffer (150mM NaCl, 50mM Tris pH7.5, 1mM EDTA, 1% SDS), and mechanically lysed with glass beads. Protein sample buffer (150mM Tris pH 6.8, 6M Urea, 6% SDS, 10% beta-mercaptoethanol, 20% Glycerol) was added and extracts were analyzed by SDS-PAGE and immunoblotting with anti-FLAG (sigma) antibody.

Yeast Growth Assay

Yeast strains were grown to mid-log in synthetic media. Spin down OD600 cells and resuspend in 1mL of sterilized H2O. Serially dilute at a ratio of 1:10 using 96-well plate. Us plate frogger to plate the dilutions one the drop out plate and incubate at the appropriate temperature.

Plasma membrane integrity assay

Yeast strains were grown to early-log (around 0.2 OD600) in synthetic media, shift the culture to 40°C and grow for 3hours, spin down 1 OD 600 cells and resuspend in PBST (0.01% tween20) , add 1uL propidium iodide (sigma) and stain for 20min. Spin down the cells and wash twice with ddH2O. Vortex and run on the flow cytometry.

Results

Heat stress triggers extensive endocytic downregulation

Previously, we found that certain environmental changes elicit highly-specific surface remodeling programs, such as the methionine-induced endocytic degradation of the methionine transporter Mup1 (Lin et al., 2008b), whereas other changes can stimulate global surface remodeling programs, such as the TORC1-mediated tuning of PM protein composition by activation of the ART adaptor network (MacGurn et al., 2011). Given the affect of temperature on protein folding, stability, and overall quality (Fang et al., 2011), we hypothesized that heat-stress might activate a surface remodeling program associated with PM protein quality control. To characterize heat-induced surface remodeling in yeast, we analyzed the trafficking and degradation of various PM cargoes in cells grown at 26^0C and shifted to 38^0C for 60 minutes. Although a few cargoes appeared to be stable and/or induced during heat stress (Yor1, Figure 2.1 and 2.2, Pdr5, Figure 2.2), most cargoes were observed to undergo endocytosis followed by vacuolar trafficking (Figure 2.1) and degradation (Figure 2.2, 2.3 and Figure 2.4). This heat-induced endocytic downregulation was observed with varying kinetics and efficiency for many diverse cargoes including amino acid transporters (Mup1, Lyp1, Dip5), hexose transporters (Hxt3), and proton pumps (Pma1).

Table 1. Cargo Thermostability

Cargo	34°C	38°C	40°C
Pma1	1103	97	53
Mup1	491	100	66
Lyp1	164	51	25

Table 1: Cargo Thermostability (Half-life, in minutes, following temperature shift)

Kinetic analysis of heat-induced cargo degradation (Supplemental Figure 1, 1B, and 1C) was used to estimate half-lives of each cargo at each temperature tested. Half-lives are indicated in minutes.

Figure2.1 Heat Stress Triggers Endocytic Downregulation

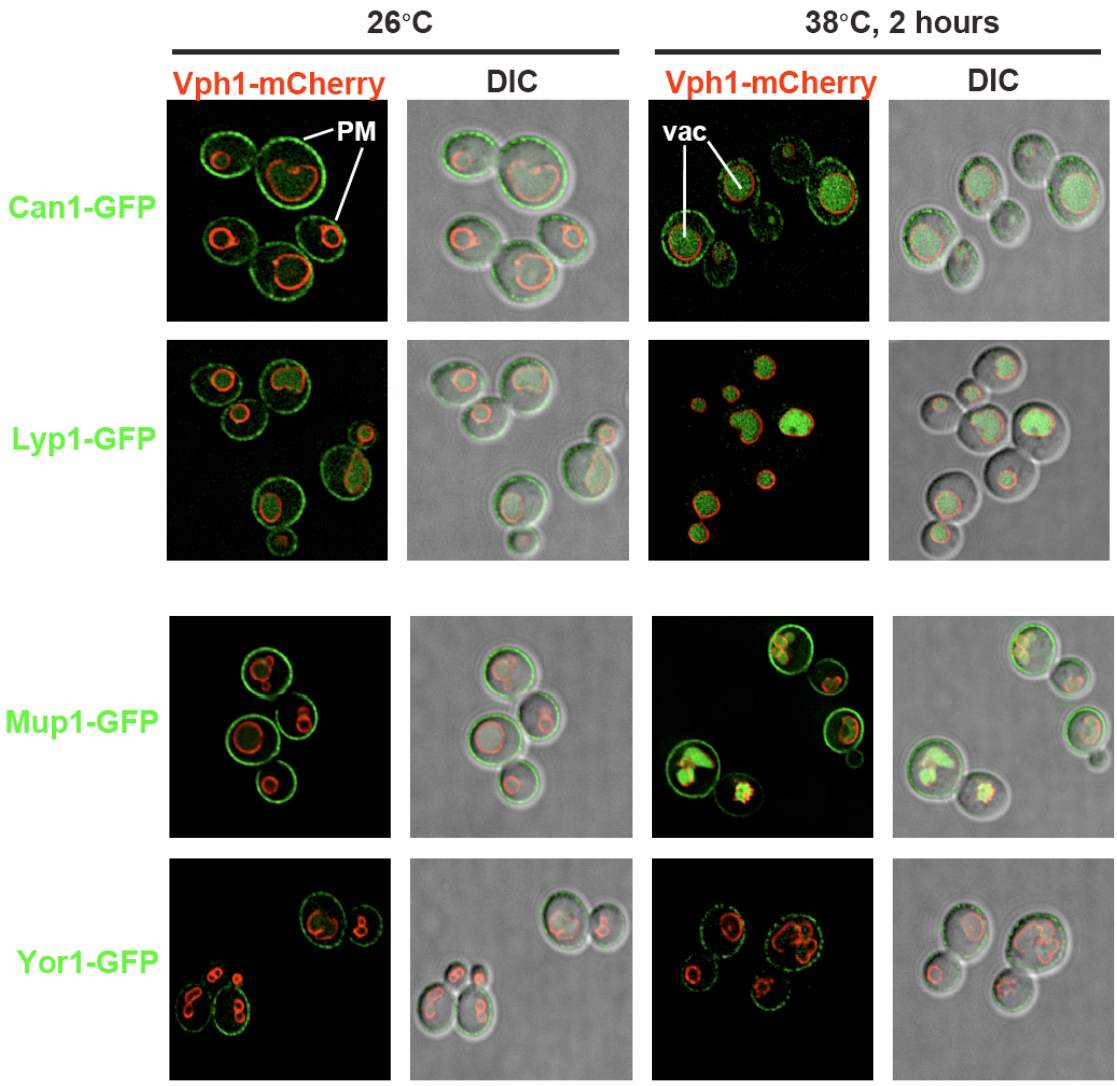

Figure 2.1. Heat Stress Triggers Endocytic Downregulation

Fluorescence distribution of GFP-tagged endocytic cargoes (green) was analyzed in wildtype yeast cells expressing the vacuolar marker Vph1-mCherry (red). Cells were grown to mid-log at 26^0C (left panels) and then shifted to 38^0C for two hours (right panels). Plasma membrane ("PM") and vacuole ("vac") localization are indicated.

Figure 2.2. Heat Stress Triggers Endocytic Downregulation

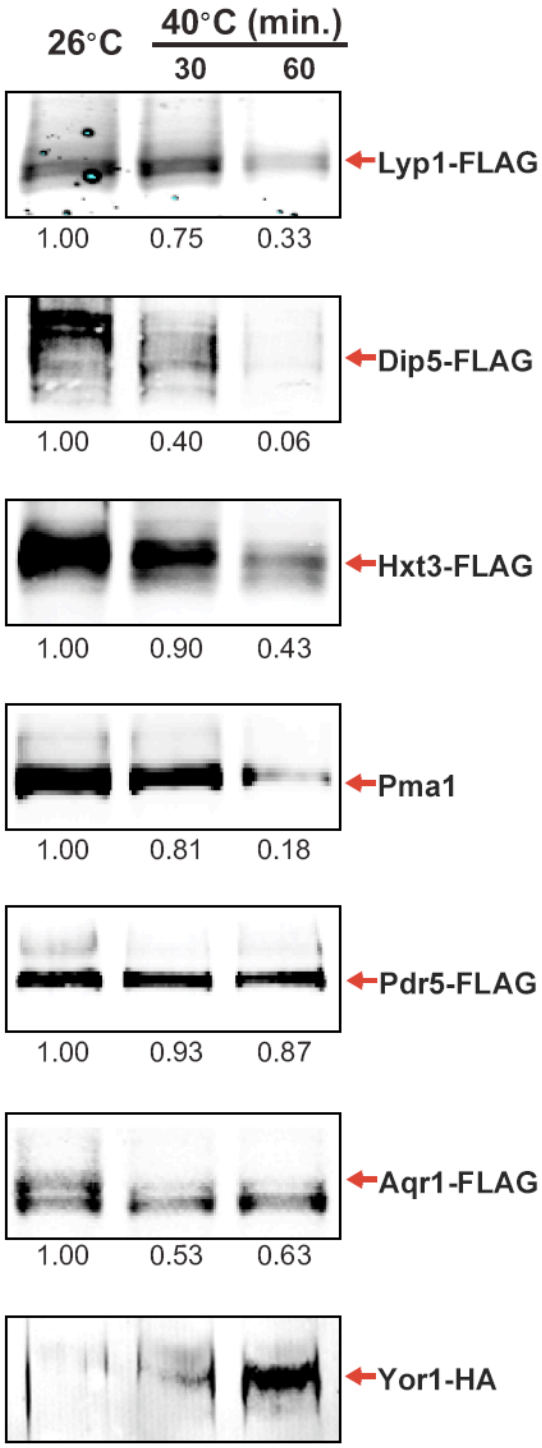

Figure 2.2. Heat Stress Triggers Endocytic Downregulation

Stability of affinity-tagged cargoes was analyzed following temperature shift from 26^0C (left lane) to 40^0C. The number beneath each lane indicates quantification of protein abundance (relative to 26^0C, t=0) determined using the Li-Cor system.

One possible explanation for the heat-induced endocytic downregulation program we observed during thermal stress could involve the general induction of bulk endocytosis. A general increase in the bulk rate of endocytosis predicts that most cargoes should display similar degradation kinetics in response to heat stress. To analyze cargo thermostability, we grew yeast cells at 26^0C and measured the kinetics of cargo degradation following shift to various temperatures. We found that different cargoes exhibited a range of thermostabilities (Figure 2.3, 2.4 and Table 1). For example, following shift to 34^0C, Lyp1 is degraded with a half-life of about 164 minutes, whereas degradation of Mup1 or Pma1 is negligible on the same timescale (Figure 2.4 and Table 1). However, following shift to 40^0C both Lyp1 and Mup1 are degraded with the half-lives of ~25 minutes and ~66 minutes, respectively (Table 1). Our observations that different cargoes exhibit different thermostabilities and that some cargoes (Yor1, Pdr5) are actually stabilized and/or induced during heat stress are not consistent with an increased rate of bulk endocytosis and instead suggest that heat stress triggers thermo-instability that is cargo-intrinsic.

Figure 2.3 Heat Stress Triggers Endocytic Downregulation

A

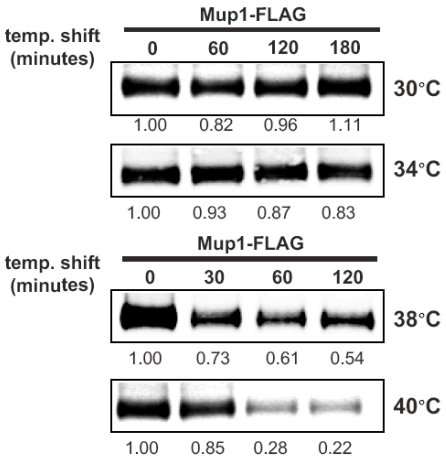

B

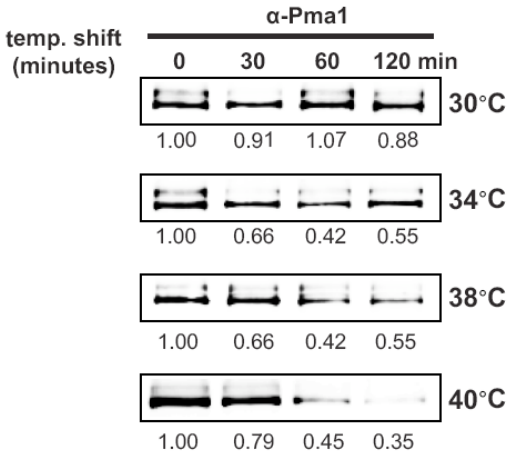

C

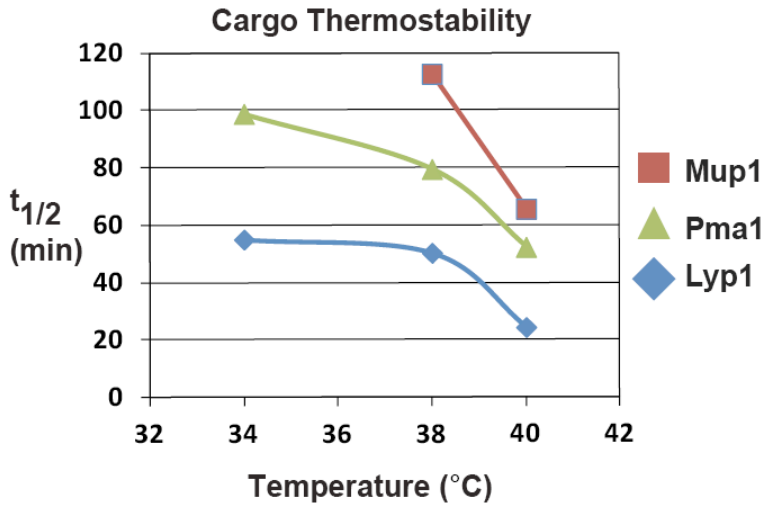

Figure 2.3 Heat Stress Triggers Endocytic Downregulation

(A) (B) Stability of affinity-tagged cargo Mup1 (A) and Pma1 (B) were analyzed following temperature shift from 26^0C to 30^0C, 34^0C, 38^0C or 40^0C. The number beneath each lane indicates quantification of protein abundance (relative to 26^0C, t=0) determined using the Li-Cor system.

(C) Half live of different cargoes (Mup, Pma1 or Lyp1) were generated based on the quantification from western blot analysis.

Figure 2.4 Heat Stress Triggers Endocytic Downregulation

A

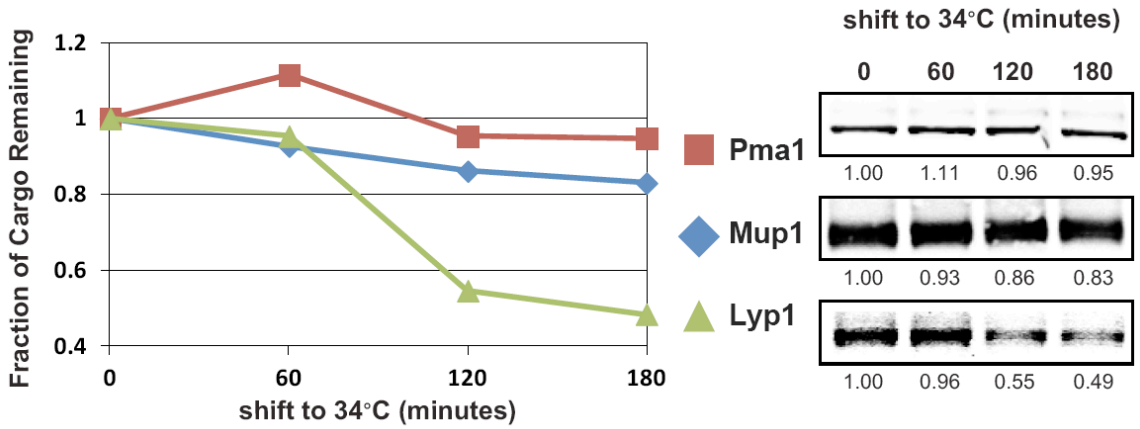

B

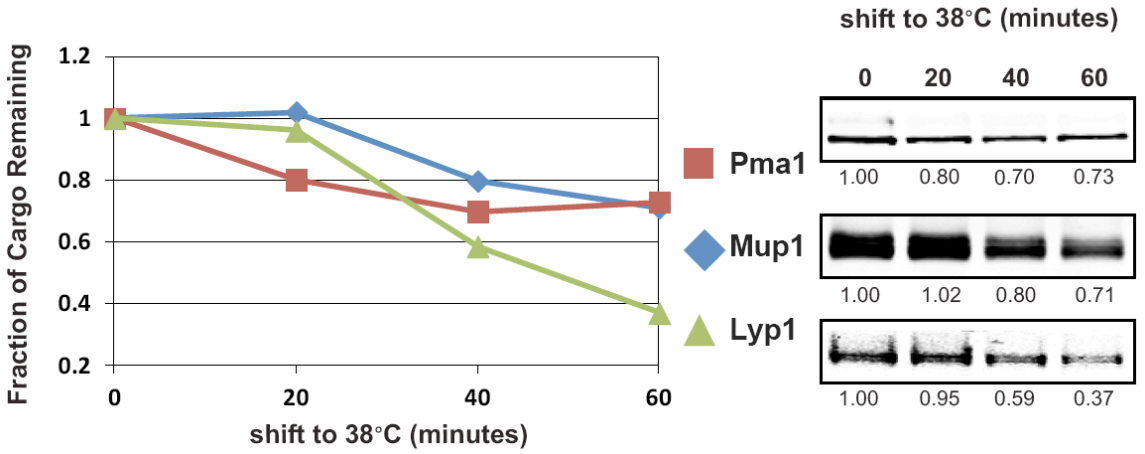

Figure 2.4. Heat Stress Triggers Endocytic Downregulation

(A) (B) Thermostability analysis of various cargo (Mup1, Lyp1, Pma1) at 34 ^{0}C (C) and 38^{0}C with corresponding western blot on the right.

Since conformational flux and protein misfolding both increase as a function of temperature, we reasoned that heat-induced endocytosis and degradation of PM cargoes may relate to misfolding or conformational instability caused by increased temperature. To test this idea, we performed thermostability analysis of the highly thermo-labile lysine transporter Lyp1 in the presence of glycerol, which is known to promote protein folding and function as a chemical chaperone (Bernier et al., 2004). Importantly, glycerol enhanced the thermostability of Lyp1 (Figure 2.5 A B and B), indicating that endocytosis and degradation of Lyp1 during heat stress is (at least partially) the result of conformational instability or misfolding. Importantly, glycerol did not stabilize the methionine triggered endocytic downregulation of the methionine transporter Mup1 (Figure 2.5 D), demonstrating that glycerol does not generally inhibit endocytosis. We believe these data are consistent with a mechanism whereby heat stress induces conformational instability or misfolding of integral PM proteins, resulting in recognition and targeting for endocytic downregulation.

Figure 2.5 Heat Stress Triggers Endocytic Downregulation

A

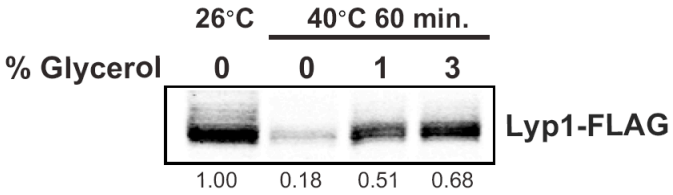

B

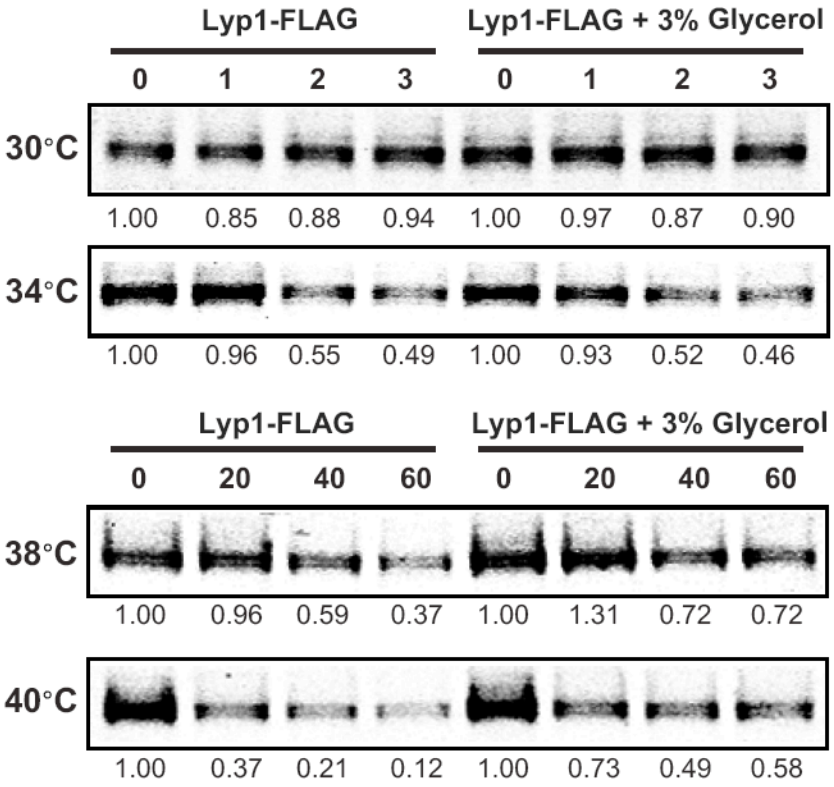

C

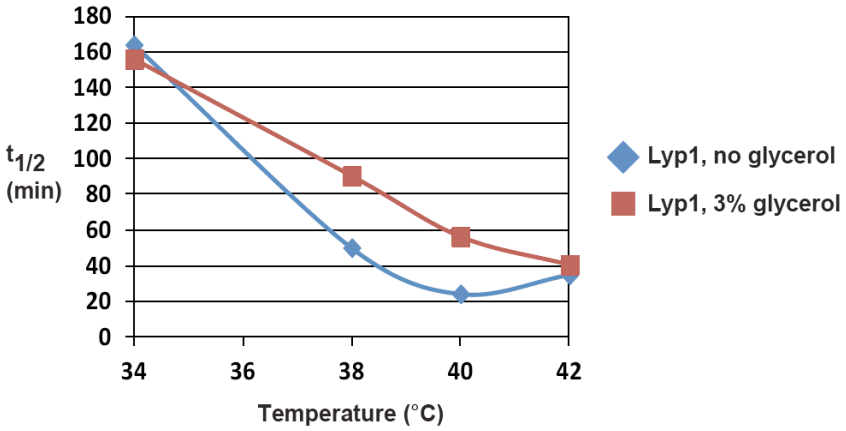
180
160
140
120
100
80
60
40
20
0
t1/2 (min)
34
36
38
40
42
Temperature (°C)
Lyp1, no glycerol
Lyp1, 3% glycerol

D

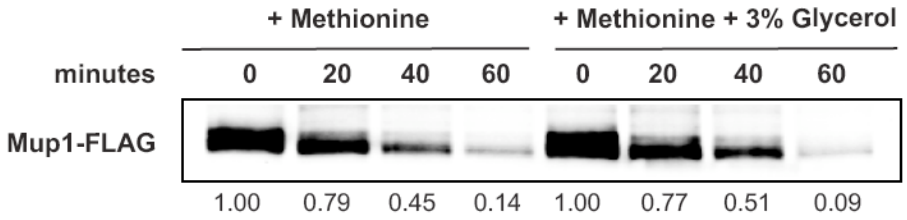
+ Methionine
+ Methionine + 3% Glycerol
minutes
0
20
40
60
0
20
40
60
Mup1-FLAG
1.00
0.79
0.45
0.14
1.00
0.77
0.51
0.09

Figure 2.4 Heat Stress Triggers Endocytic Downregulation

(A) (B) Analysis of heat-induced degradation of Lyp1 in the presence of glycerol, a chemical chaperone. See also Supplemental Figure 1.

(C) Half life of Lyp1 protein with or without 3% glycerol at different temperature.

(D) Analysis of methionine-induced degradation of Mup1 in the presence of glycerol.

The Heat-induced endocytic response is mediated by the Rsp5 ubiquitin ligase

To identify the molecular mechanism that targets thermolabile cargo for endocytosis during heat stress, we tested if this stress response requires Rsp5, a yeast Nedd4 family ubiquitin ligase that targets many cargoes for ubiquitination and endocytosis (Lauwers et al., 2010; Macgurn et al., 2012). To do this, we analyzed heat-induced cargo trafficking in yeast strains expressing various mutant alleles of Rsp5. While the WW1 domain of Rsp5 was dispensable for heat-induced cargo degradation, mutations in either WW2 or WW3 significantly abrogated the endocytic response (Figure 2.6). Since these mutations result in significant accumulation of cargo at the PM during heat stress, we tested if mutant alleles of RSP5 exhibited defects in thermotolerance. While rsp5-ww1 mutants did not exhibit any observable temperature sensitivity defect, rsp5-ww2 and rsp5-ww3 mutants were extremely temperature sensitive and failed to grow at 38 ^{0}C (Figure 2.7A).

Figure 2.6 Rsp5 Mediates the Heat-induced Endocytic Response

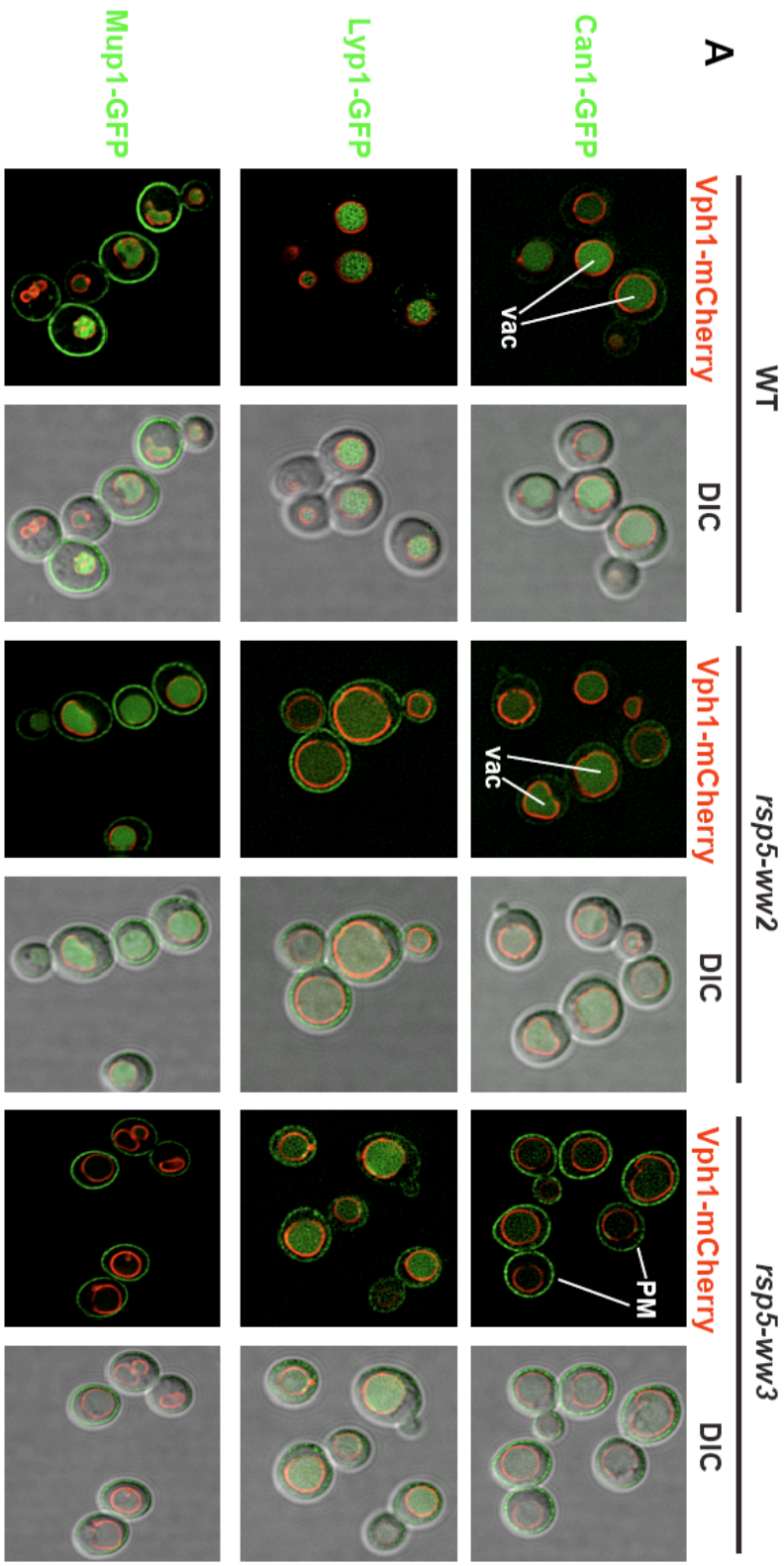

Figure 2.6 Rsp5 Mediates the Heat-induced Endocytic Response

Fluorescence distribution of GFP-tagged endocytic cargoes (green) was analyzed in wildtype (left panels), rsp5-ww2 (middle panels), or rsp5-ww3 (right panels) yeast cells expressing the vacuolar marker Vph1-mCherry (red). Cells were grown to mid-log at 26^0C and then shifted to 38^0C for two hours. Plasma membrane ("PM") and vacuole ("vac") localization are indicated.

To better understand the basis of this temperature sensitive phenotype, we utilized a 8 fluorescent vital dye, propidium iodide (PI), which binds to DNA but is membrane impermeant. Thus, PI staining can be used to score the number of cells in a population that have lost PM integrity. For example, wildtype yeast cells grown at 26^0C exhibit negligible (<1%) PI-positive cells within the population (Figure 2.7 B). However, if these same yeast cells are treated with the drug nystatin, which binds to ergosterol and forms pores in the yeast plasma membrane, all yeast cells (100%) stain positive for PI (Figure 2.7 B), demonstrating the utility of PI as a marker for PM integrity. Next, we used flow cytometry to analyze PI staining in wildtype and mutant cells following heat stress. After a three hour heat stress, wildtype and *rsp5-ww1* yeast cells did not exhibit any significant PI staining (Figure 2.8). In contrast, *rsp5-ww2* and *rsp5-ww3* mutant cells exhibited a significant fraction of the population that stained PI-positive in response to heat stress (Figure 2.7 and 2.8). Combined with previous analysis of thermotolerance (Figure 2.7 B), these results suggest that rapid loss of PM integrity during heat stress is the basis of thermosensitivity of *rsp5-ww2* and *rsp5-ww3* mutants.

Figure 2.7 Rsp5 Mediates the Heat-induced Endocytic Response

A

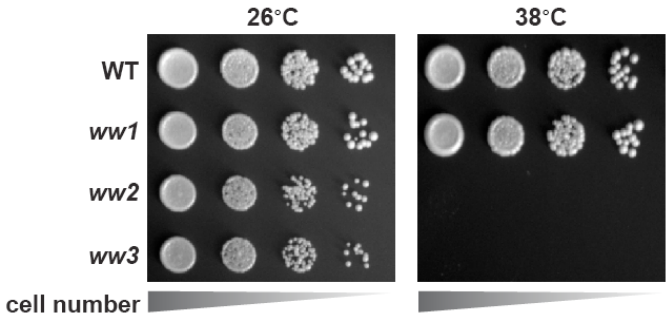

B

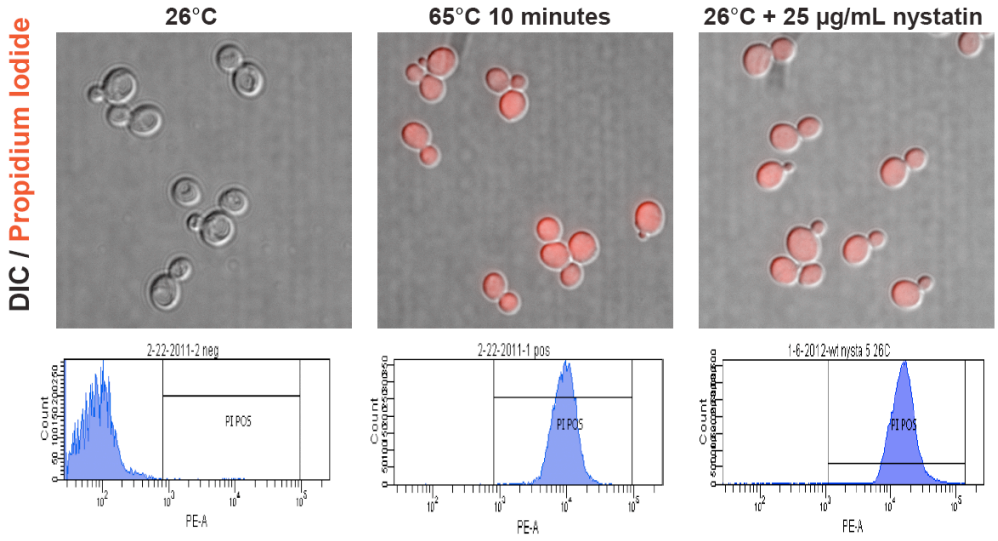

C

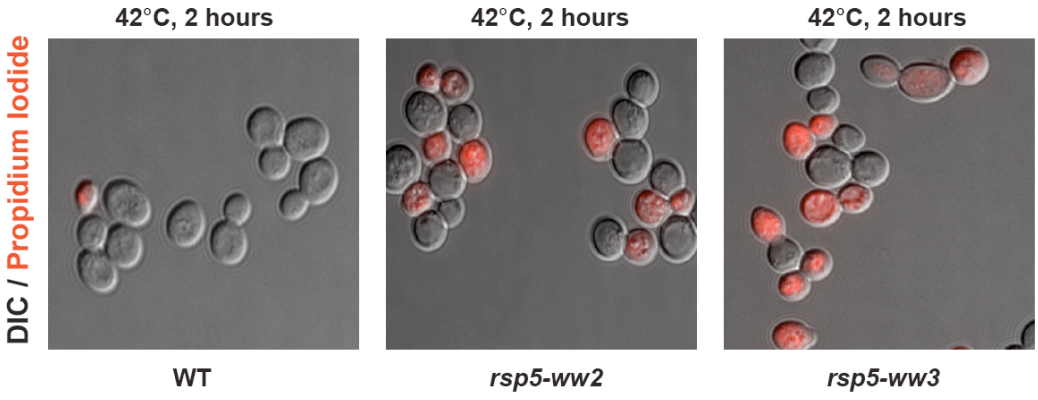

Figure 2.7 Rsp5 Mediates the Heat-induced Endocytic Response

(A) Heat-sensitivity analysis of wildtype, rsp5-ww2, or rsp5-ww3 yeast cells.

(B) Yeast cells that were either grown at 26^0C to mid-log phase (left), heated to 65^0C for 10 minutes (middle), or treated with nystatin (right) were stained with propidium iodide (PI) and analyzed by fluorescence microscopy (top) and flow cytometry (bottom).

(C) Wildtype (left), rsp5-ww2 (middle), or rsp5-ww3 (right) yeast cells were grown to mid-log at 26^0C, shifted to 42^0C for two hours, stained with PI, and analyzed by fluorescence microscopy.

We next wanted to determine if loss of PM integrity during heat stress is linked to the accumulation of cargo at the cell surface. To test this, we analyzed PI staining following heat stress for mutants that affect different stages of the endocytic pathway. While mutations that abrogate endocytosis (*Δend3*, *Δrvs167*) resulted in significant PI staining in response to heat stress, mutant cells defective for downstream trafficking events such as endosomal sorting and multivesicular body 2 biogenesis *(Δvps23*), endosomal-vacuolar fusion (*Δvam3*), and vacuolar degradation (*Δpep4*) exhibited negligible PI staining in response to heat stress (Figure 2.8). These results indicate that plasma membrane clearance is the critical event protecting cells from heat-induced loss of PM integrity, while downstream sorting and trafficking events are dispensable.

Figure 2.8 Rsp5 Mediates the Heat-induced Endocytic Response

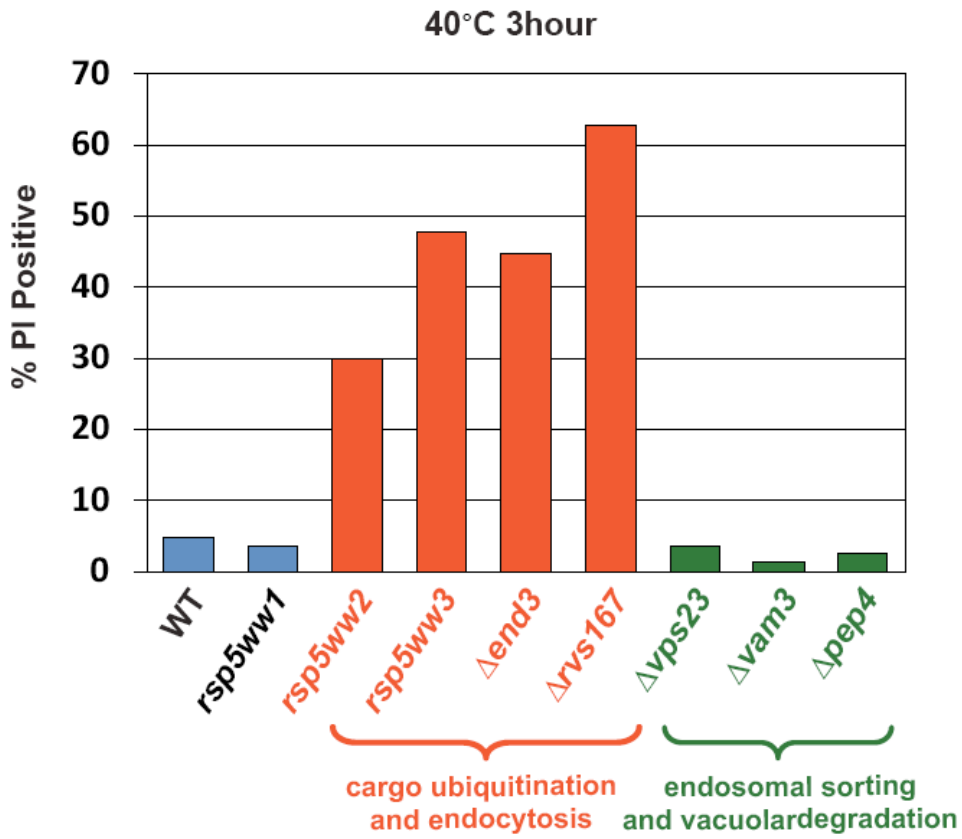

Figure 2.8 Rsp5 Mediates the Heat-induced Endocytic Response

Flow cytometry was used to analyze PI staining of the indicated strains following growth at 40^0C for three hours.

The ART adaptor network protects PM integrity during heat stress

In many cases, Rsp5 ubiquitin ligase activity is directed by adaptor proteins which target specific cargoes at the PM in response to various stimuli. To test if any Rsp5 adaptor proteins function in targeting cargoes for endocytic downregulation during heat stress, we screened a set of yeast knockout strains to identify Rsp5 adaptors required for thermotolerance. While most ART (*a*rrestin-*r*elated *t*rafficking adaptor) family proteins were found to be dispensable for growth at high temperatures, *Δart1* yeast cells were highly sensitive to heat (Figure 2.9 A B). The temperature sensitivity phenotype of *Δart1* yeast cells was not as severe as that observed for *rsp5-ww2* and *rsp5 ww3* mutant yeast strains (data not shown), indicating that loss of Art1 only partially abrogates the heat stress-induced endocytic response. Importantly, our analysis revealed that heat-induced endocytosis and vacuolar degradation of most cargoes is Art1-independent, with the exception of the lysine transporter Lyp1 (Figure 2.10 A). In contrast to other cargoes, Lyp1 endocytosis and vacuolar degradation is abrogated in the absence of Art1 (Figure 2.10), underscoring the cargo-specific role Art1 plays in the heat-induced endocytic response. Consistent with its role in the heat-induced endocytic response, we found that Art1-GFP translocates to the PM in response to heat stress (Figure 2.9C). Thus, while *rsp5* mutant strains exhibit broad defects in the heat-induced endocytic response, *Δart1* mutant cells are defective for the turnover of only a subset of PM cargoes which is consistent with a less-severe thermotolerance defect.

Figure 2.9 ARTs Protect Plasma Membrane Integrity During Heat Stress

A

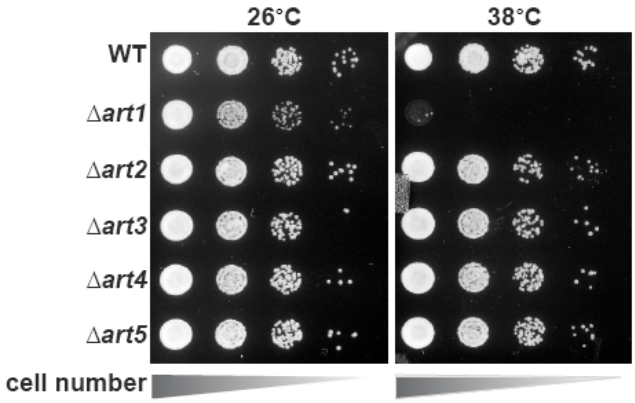

B

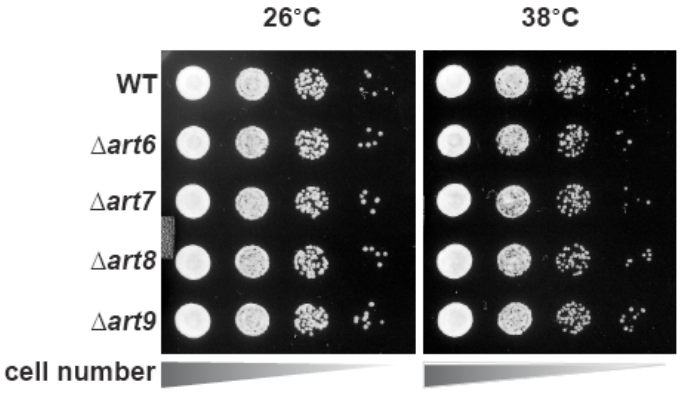

C

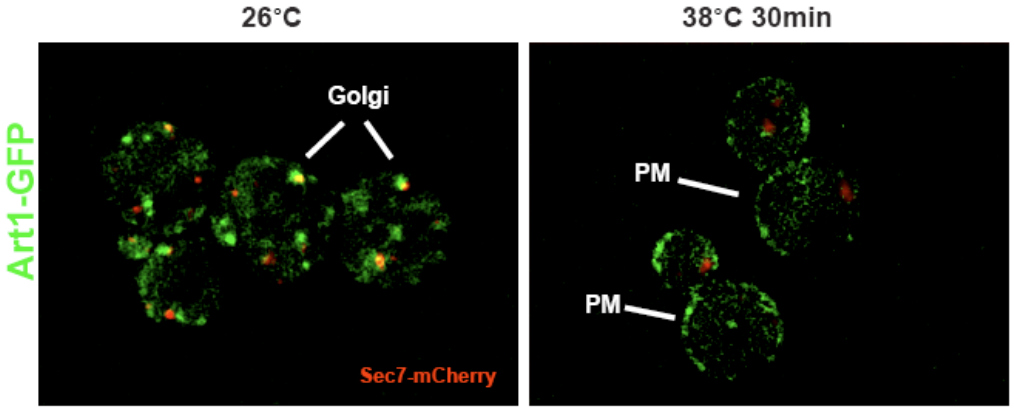

Figure 2.9 ARTs Protect Plasma Membrane Integrity During Heat Stress

(A) (B) Heat-sensitivity analysis of wildtype and art mutant yeast cells.

(C) At steady state, Art1 GFP mainly localizes in the cytosol and partially colocalizes with Golgi marker Sec7 (chromosomal tagged with mcherry); Art1 localizes to plasma membrane upon heat stress.

Figure 2.10 ARTs Protect Plasma Membrane Integrity During Heat Stress

A

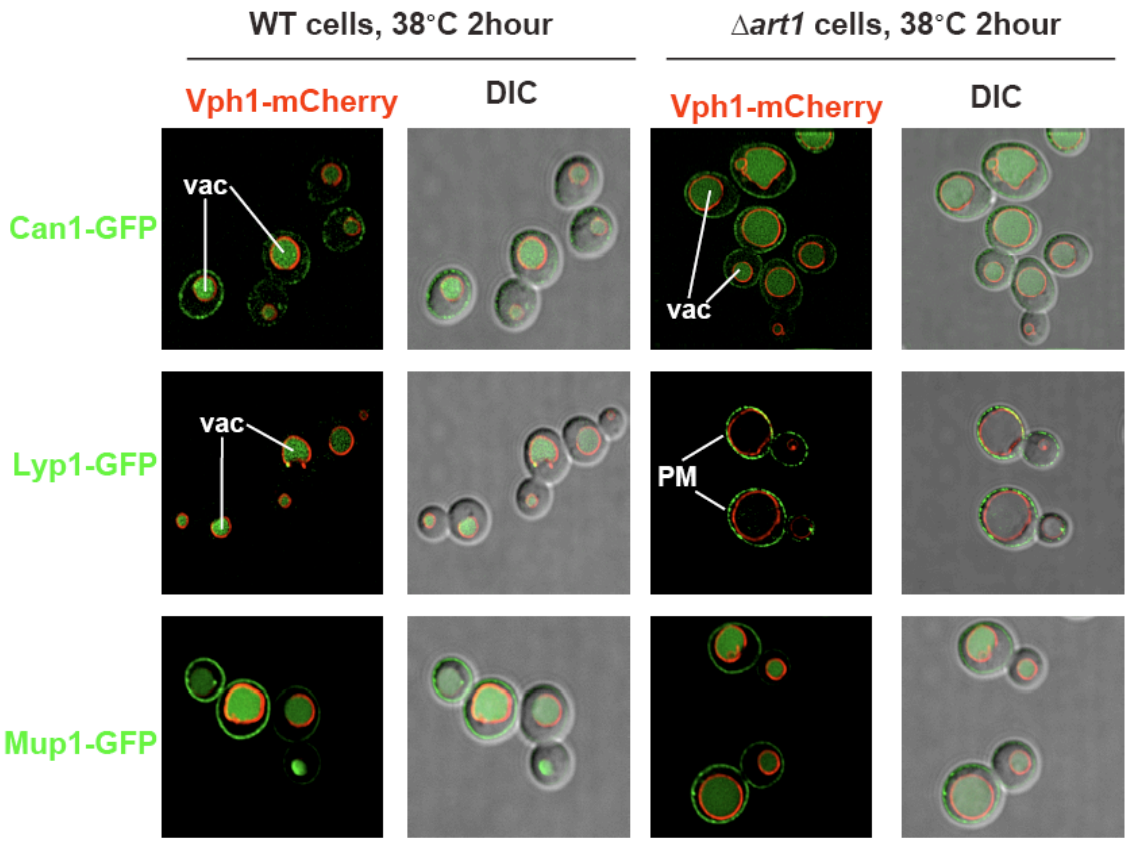

B

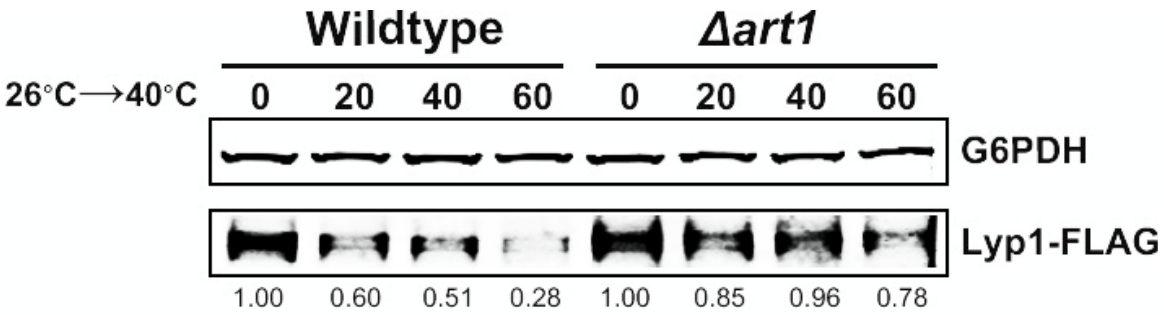

Figure 2.10 ARTs Protect Plasma Membrane Integrity During Heat Stress

(A) Fluorescence distribution of GFP-tagged endocytic cargoes (green) was analyzed in wildtype (left panels) and Δart1 (right panels) yeast cells expressing the vacuolar marker Vph1-mCherry (red). Cells were grown to mid-log at 26^0C and then shifted to 38^0C for two hours. Plasma membrane ("PM") and vacuole ("vac") localization are indicated.

(B) Stability of affinity-tagged Lyp1 was analyzed following temperature shift from 26 ^{0}C (left lane) to 40^0C. The number beneath each lane indicates quantification of protein abundance (relative to 26^0C, t=0) determined using the Li-Cor system.

To better understand the function of Art1 during heat stress, we screened for suppressors of the *Δart1* temperature sensitivity phenotype using a multicopy overexpression plasmid library. All multicopy overexpression plasmids that suppressed the *Δart1* temperature sensitivity defect were found to encode either *ART1* or *ART2* (Figure 2.11 A). The identification of *ART2* as a suppressor of the *Δart1* temperature sensitivity phenotype was surprising and indicated that (i) multiple ART family proteins may protect cells during heat stress and (ii) different ART proteins may have overlapping cargo specificities which create redundancy in the system. Although *Δart2* mutant cells did not exhibit any temperature sensitivity defects, we found that deletion of *ART2* in *Δart1* mutant cells resulted in an enhanced temperature sensitivity phenotype (Figure 2.11 B). Furthermore, we found that loss of specific combinations of ART proteins led to temperature sensitive phenotypes. One mutant deleted for seven *ART* genes (*Δart1Δ art2Δ art3Δ art4Δart5Δart6Δart9*) was highly temperature sensitive and this phenotype could be complimented by overexpression of either Art1 or Art2 (Figure 2.11 C). Furthermore, a quadruple knockout strain (*Δart4Δart5Δart7Δart9*) was found to be highly temperature sensitive, while loss of the corresponding genes individually or in pairs did not affect thermotolerance (Figure 2.12 A). Importantly, the thermosensitivity of *Δart4Δart5Δart7Δart9* cells correlated with defects in the heat-induced endocytosis of Art1-independent cargo, including the methionine transporter Mup1 (Figure 2.12 B). These results illustrate that several different ART family proteins contribute to the heat induced endocytic response, endowing this system with robust redundancy and broad cargo recognition capabilities.

Figure 2.11 ARTs Protect Plasma Membrane Integrity During Heat Stress

A

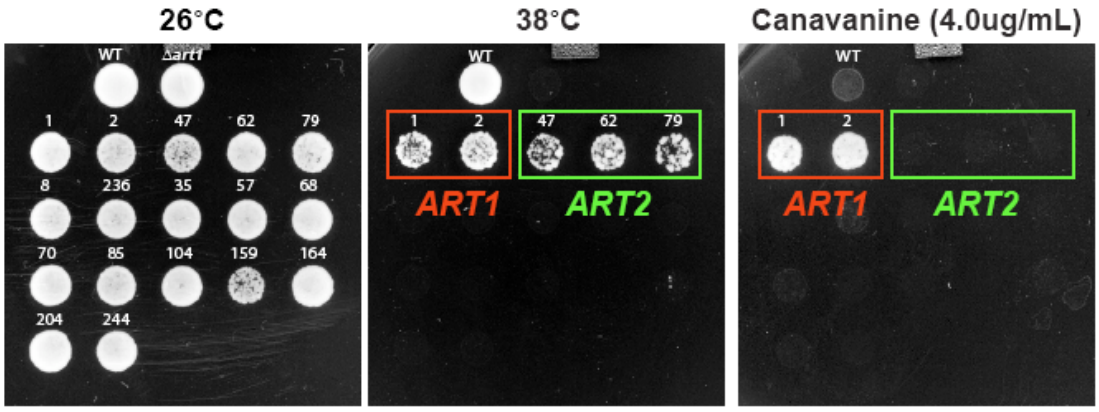

B

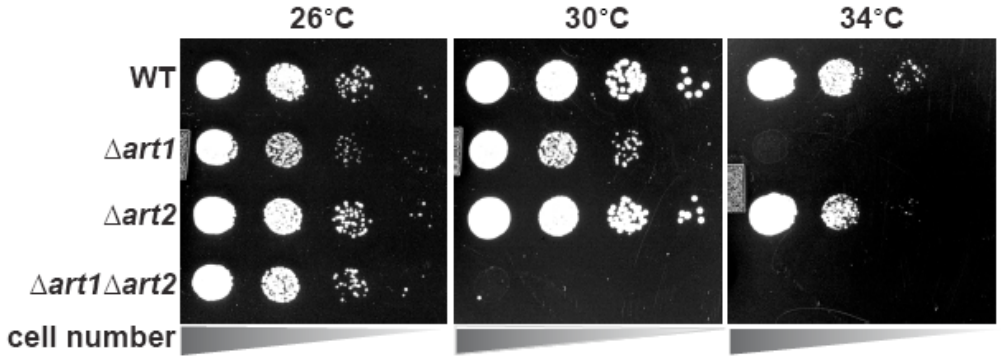

C

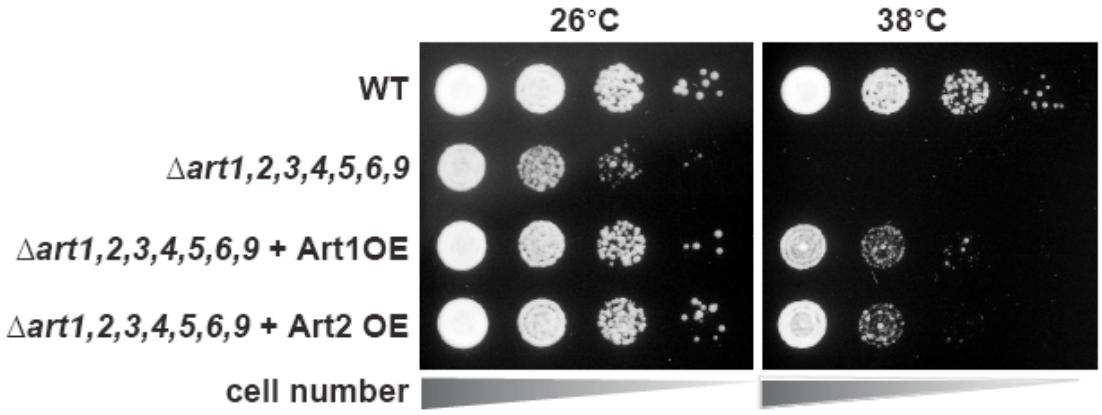

Figure 2.11 ARTs Protect Plasma Membrane Integrity During Heat Stress

(A) Multicopy suppressor screen of art1 null cell: overexpression of Art1 and Art2 protein can suppressor the temperature sensitive growth of art1null cells at 38°C

(B) Heat-sensitivity analysis of wildtype, Δart1, Δart2, and Δart1Δart2 mutant yeast cells.

(C) Heat-sensitivity of Δart1, 2, 3, 4, 5, 6,9 mutant yeast cell can be partially suppressed by overexpression of Art1 and Art2.

Figure 2.12 ARTs Protect Plasma Membrane Integrity During Heat Stress

A

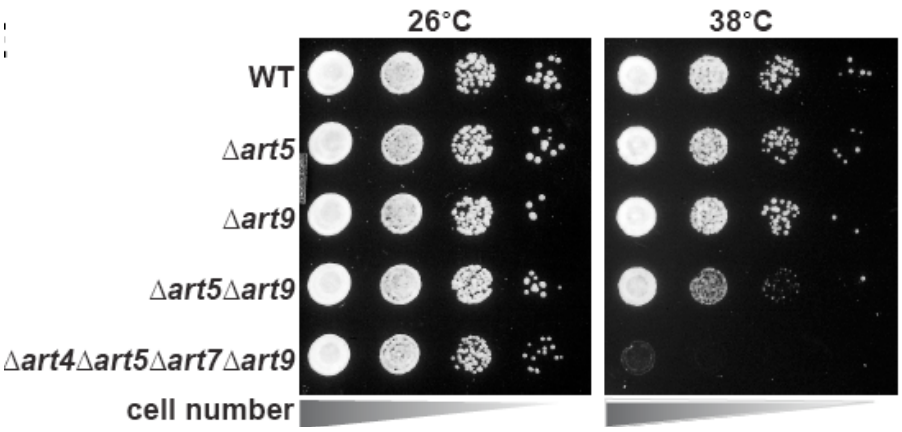

B

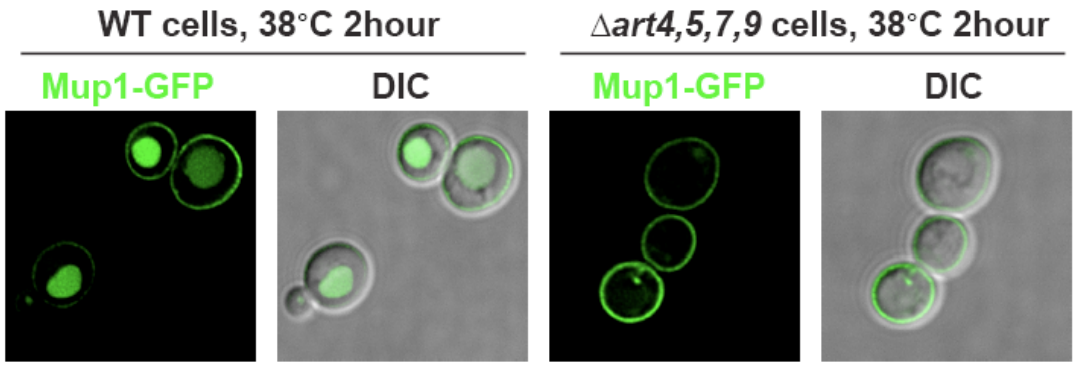

Figure 2.12 ARTs Protect Plasma Membrane Integrity During Heat Stress

(A) Heat-sensitivity analysis of wildtype, Δart5, Δart9, and Δart4Δart5Δart7Δart9 mutant yeast cells.

(B) Fluorescence distribution of GFP-tagged Mup1 (green) was analyzed in wildtype (left panels) and Δart4Δart5Δart7Δart9 (right panels) yeast cells.

To further characterize the protective role of the ART adaptor network, we used the PI staining assay to score a panel of *ART* deletion mutants for loss of PM integrity during heat stress. Although *Δart1* mutant cells exhibited a slight loss of PM integrity (~18% cells are PI-positive following 40^0C for 3 hours), the other adaptor mutants tested exhibited no defects in PM integrity in response to heat stress (Figure 2.13 A). Strikingly, yeast strains deleted for multiple ART genes exhibited significant staining with PI at high temperatures (Figure 2.13A), indicating a correlation between cargo accumulation at the cell surface and loss of PM integrity during heat stress. Furthermore, several yeast strains deleted for several *ART* genes exhibited PI staining similar to *rsp5-ww3* mutants (Figure 2,3 A and B), underscoring the critical role the ART adaptor network plays in protecting PM integrity during heat stress.

Figure 2.13 ARTs Protect Plasma Membrane Integrity During Heat Stress

A

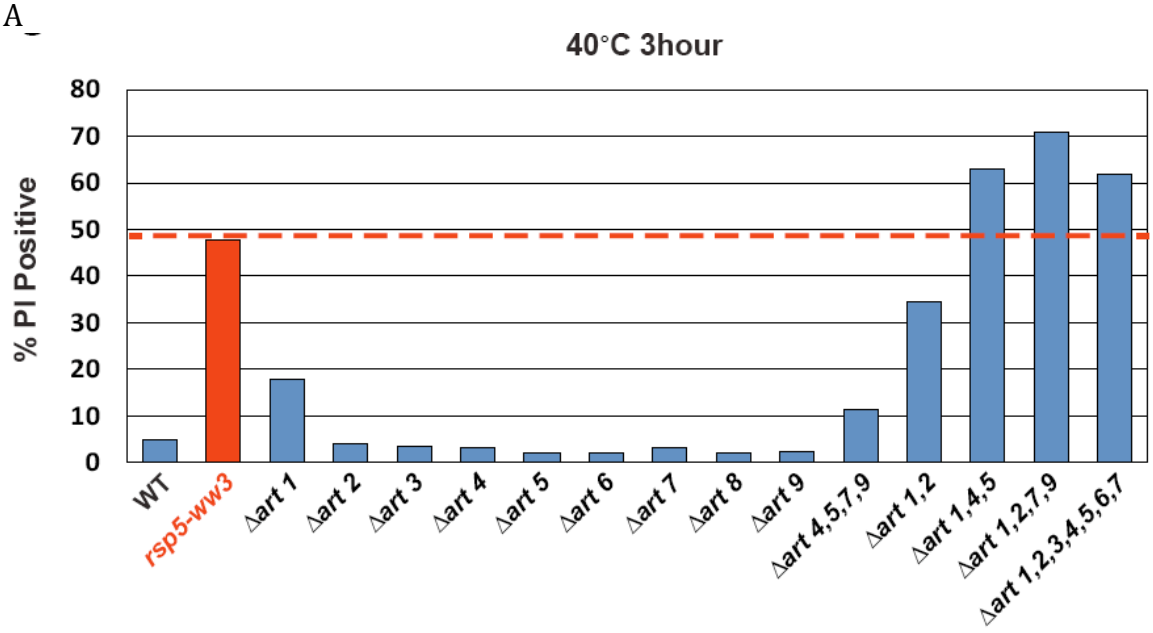

B

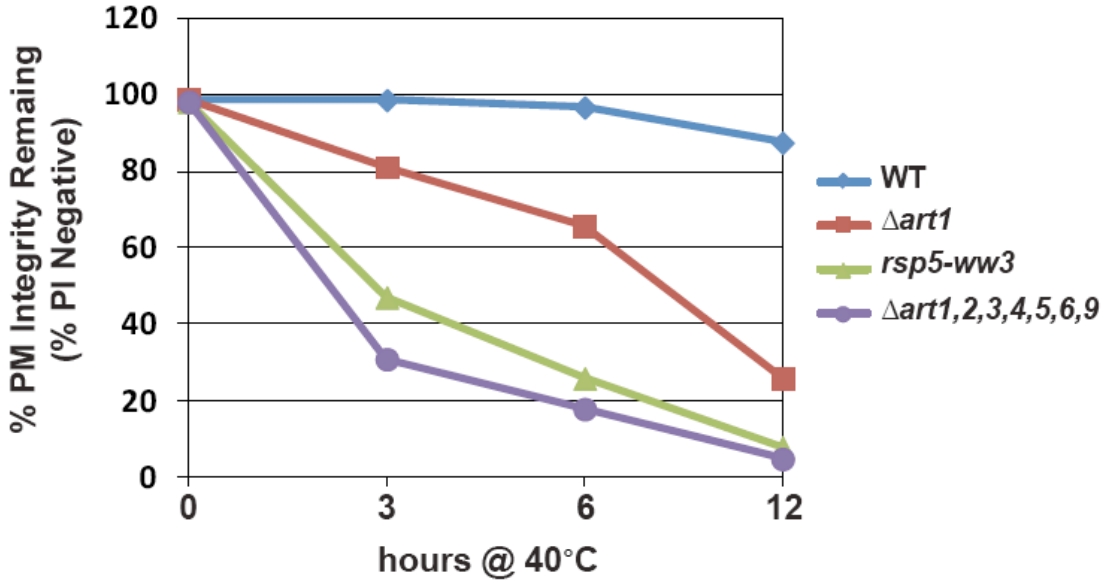

Figure 2.13 ARTs Protect Plasma Membrane Integrity During Heat Stress

(A) Flow cytometry was used to analyze PI staining of the indicated strains following growth at 40^0C for three hours.

(B) Kinetic analysis of PI staining during a 40^0C heat stress timecourse.

Cell surface protein accumulation is toxic during heat stress

Our observations that Rsp5 and the ART adaptor network are critical mediators of the heat induced endocytic response suggested that these proteins may function as a critical quality control mechanism at the PM. Given that loss of this response during heat stress results in (i) cargo accumulation at the PM, (ii) loss of PM integrity and (iii) loss cell viability, we hypothesized that heat stress may trigger conformational instability or misfolding of integral membrane proteins at the cell surface and that failure to recognize, remove and degrade these proteins threatens the integrity of the plasma membrane. Based on our observation that *Δart1* mutant cells, which are temperature sensitive, exhibit specific accumulation of the lysine transporter Lyp1 during heat stress, we decided to test if Lyp1 accumulation is toxic at high temperature. To do this, we analyzed temperature sensitivity of *Δart1Δlyp1* mutant cells and, to our surprise, found that loss of Lyp1 partially suppressed the temperature sensitivity phenotype of *Δart1* mutant cells (Figure 2.14 A). This result suggests that Lyp1 accumulation at the PM is toxic during heat stress.

Figure 2.14 Cargo Accumulation at the PM is Toxic During Heat Stress

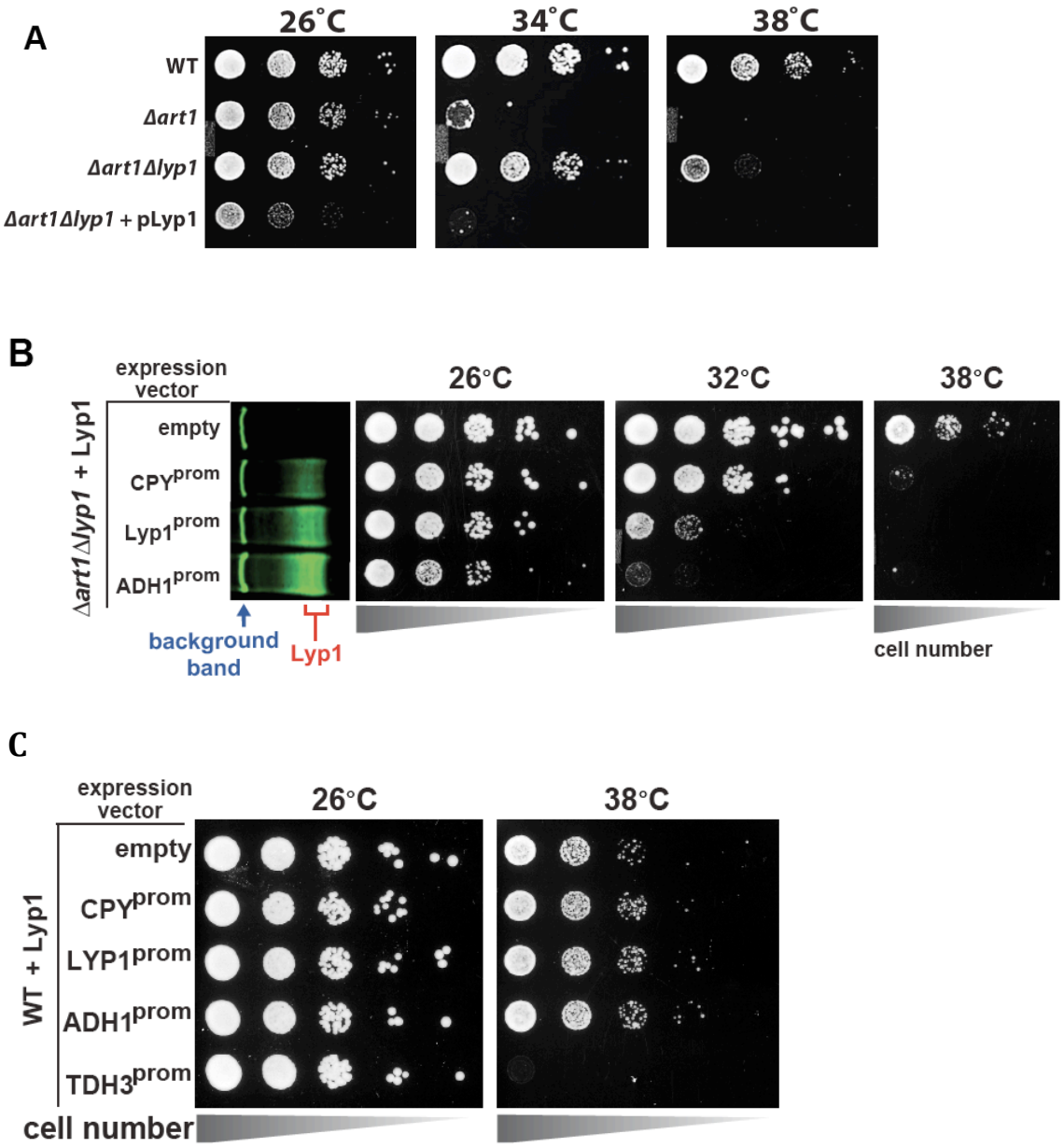

Figure 2.14 Cargo Accumulation at the PM is Toxic During Heat Stress

(A) Heat-sensitivity analysis of wildtype, Δart1, Δlyp1, and Δart1Δlyp1 mutant yeast cells.

(B) Empty vector or plasmids encoding Lyp1-FLAG expressed from different promoters (pCPY, pLYP1, pADH1) were transformed into Δart1Δlyp1 mutant yeast cells and the affect on heat tolerance was scored by growth at the indicated temperatures. Lyp1 expression level for each strain was analyzed by quantitative Western blot (Li-Cor).

(C) Empty vector or plasmids encoding Lyp1-K10XR-FLAG (which lacks N-terminal lysine residues) expressed from different promoters (pCPY, pLYP1, pADH1, pTDH3) were transformed into wildtype yeast cells and the affect on heat tolerance was scored by growth at the indicated temperatures.

To further explore this idea, we titrated Lyp1 expression using several different promoters to determine if Lyp1 accumulation in *Δart1Δlyp1* cells is toxic during heat stress. Importantly, we found that Lyp1 expression correlated with temperature sensitivity in *Δart1Δlyp1* cells, where the expressed Lyp1 could not be internalized in response to heat stress (Figure 2.14B). This same Lyp1 titration failed to cause temperature sensitivity in wildtype cells where Lyp1 undergoes heat-induced endocytosis, but higher levels of Lyp1 expression using the TDH3 promoter did confer temperature sensitivity (Figure 2.4 C). To further explore the toxicity of Lyp1 at high temperatures, we engineered a mutant of Lyp1 that cannot be internalized or degraded by the heat-induced endocytic response (Figure 2.15 A) and found that high expression levels of this mutant resulted in increased temperature sensitivity even in wildtype cells (Figure 2.15 B), demonstrating that accumulation of Lyp1 at the PM is toxic to the cell during heat stress. The temperature sensitivity conferred by Lyp1 accumulation at the cell surface was independent of its lysine transporter function, since swapping the transporter region of the Lyp1-K10XR mutant protein with the transporter region of Can1, an arginine transporter, was also toxic at high temperatures (Figure 2.16A and B). Importantly, the increased temperature sensitivity observed when Lyp1 accumulates at the PM correlates with increased PI staining during heat shock (Figure 2.16 C). However, protection against this loss of PM integrity could be conferred upon increasing expression of Art1 (Figure 2.16 D), which prevents integral membrane protein accumulation at the surface (Lin et al., 2008a). Thus, our results indicate that accumulation of Lyp1 at the cell surface during heat stress is associated with loss of PM integrity and decreased cell viability.

Under normal circumstances, heat stress triggers the recognition of Lyp1 by Art1, which targets its ubiquitination and removal from the PM, protecting the cell from toxic Lyp1 accumulation at the surface.

Figure 2.15 Cargo Accumulation at the PM is Toxic During Heat Stress

A

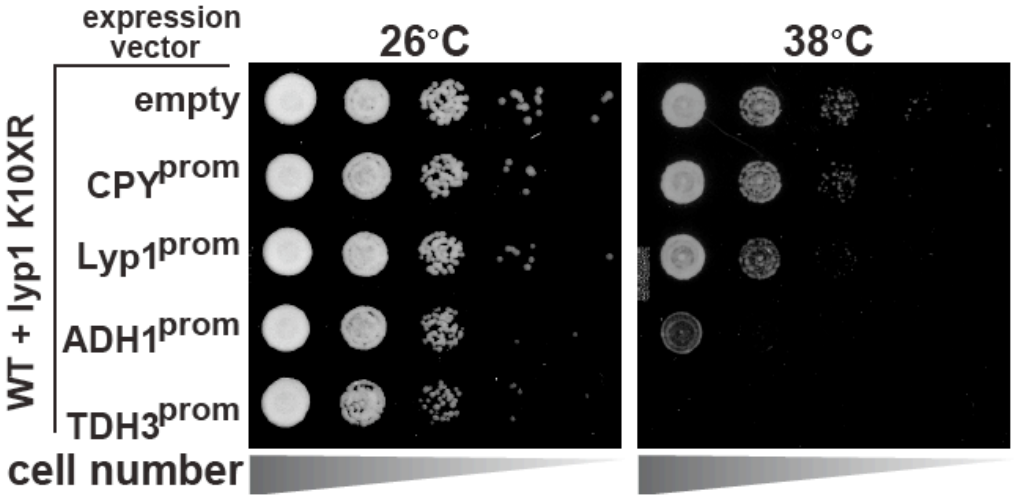

B

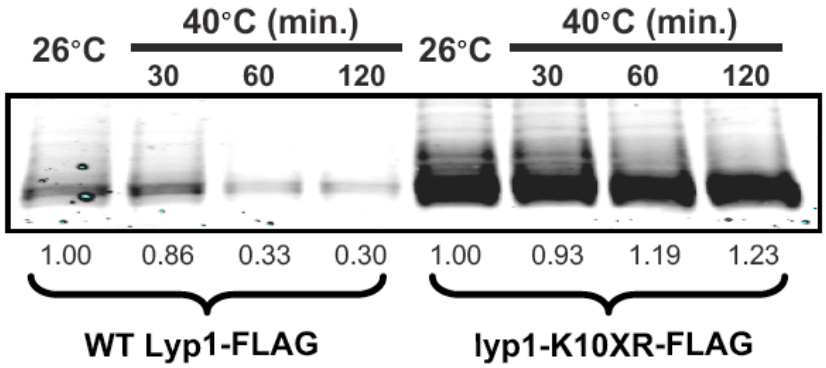

Figure 2.15 Cargo Accumulation at the PM is Toxic During Heat Stress

(A) Empty vector or plasmids encoding Lyp1-10XR mutant FLAG expressed from different promoters (pCPY, pLYP1, pADH1) were transformed into wildtype yeast cells and the affect on heat tolerance was scored by growth at the indicated temperatures

(B) Stability of affinity-tagged pLYP1-Lyp1 or pTDH3-Lyp1-10XR mutant was analyzed following temperature shift from 26 ^{0}C (left lane) to 40^{0}C. The number beneath each lane indicates quantification of protein abundance (relative to 26^{0}C, t=0) determined using the Li-Cor system.

Figure 2.16 Cargo Accumulation at the PM is Toxic During Heat Stress

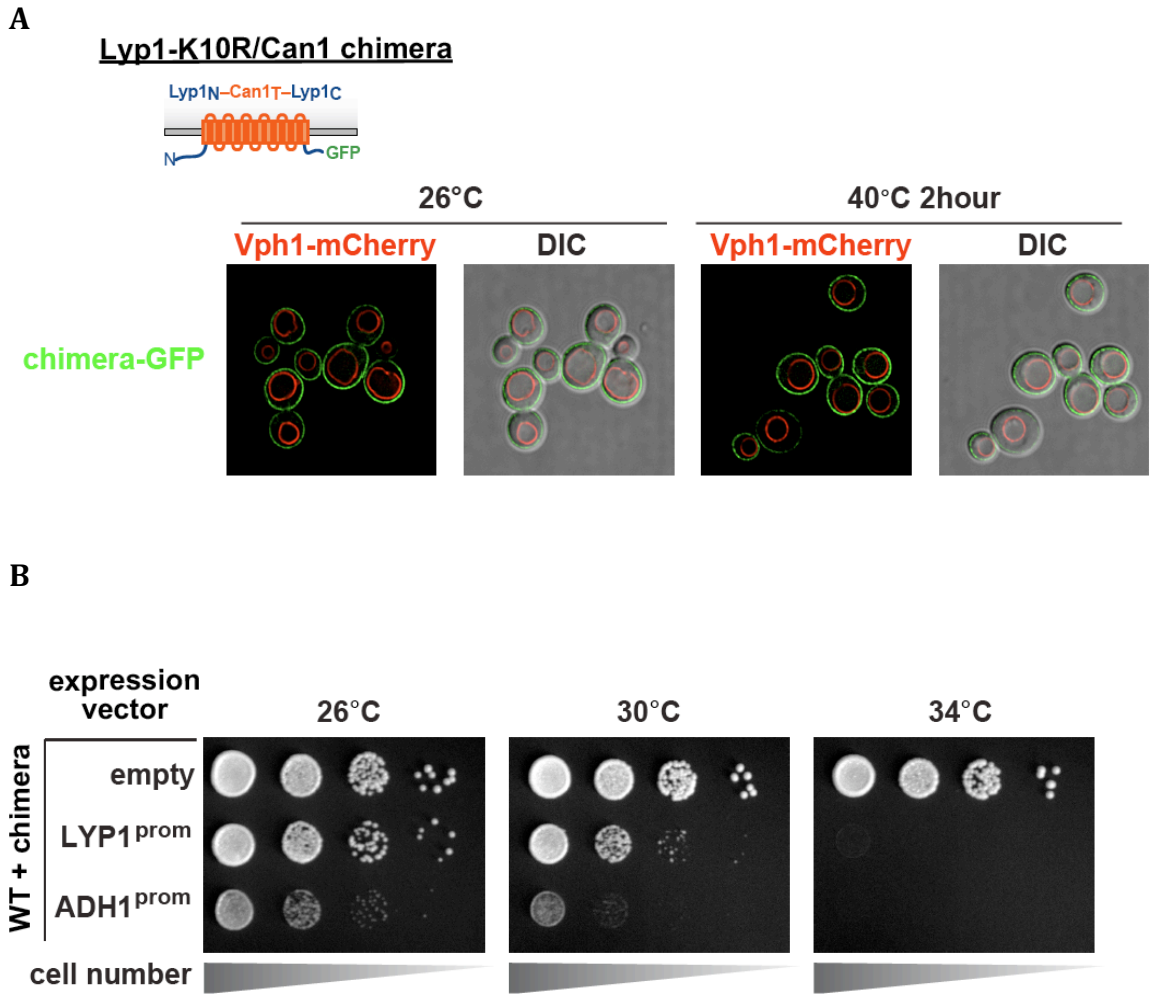

Figure 2.16 Cargo Accumulation at the PM is Toxic During Heat Stress

(A) Swapping the transporter region of the Lyp1-K10XR mutant protein with the transporter region of Can1. GFP tagged chimera protein stable at PM under the heat stress.

(B) Empty vector or plasmids encoding Lyp-K10R/Can1 chimera expressed from different promoters (pLYP1, pADH1) were transformed into wildtype yeast cells and the affect on heat tolerance was scored by growth at the indicated temperatures.

(C) Flow cytometry was used to analyze PI staining of Δart1Δlyp1 mutant yeast cells expressing Lyp1 from different promoters (pCPY, pLYP1, pADH1) following growth at 40 ^{0}C for three hours.

(D) Flow cytometry was used to analyze PI staining of wildtype yeast cells coordinately expressing Lyp1 from the TDH3 promoter and Art1 from different promoters (pART1, pCPY, pADH1, pTDH3) following growth at 40^{0}C for three hours. See also Supplemental Figure 4.

The parallel circuitry of integral membrane protein quality control

Our results indicate that Rsp5 and the ART adaptor network function as part of a PM quality surveillance system, detecting integral membrane proteins at the cell surface as they become conformationally unstable and targeting their internalization and degradation. If the Rsp5-ART system is functioning as a *bone fide* quality control pathway at the PM, we would expect to observe genetic interactions with parallel quality control systems for integral membrane proteins along the secretory pathway (Figure 2.17). To test this, we constructed a genetic array consisting of pairwise deletions known to affect protein quality control in the cytosol, nucleus, ER, Golgi complex, PM, endosome, and vacuole. We systematically scored each double deletion strain for PI staining following hours of growth at 40^0C to identify synthetic genetic interactions between parallel quality control pathways (Figure 2.17 B). In general, mutations that affected quality control of soluble cytosolic proteins did not interact genetically with mutations that affected quality control of integral membrane proteins. In contrast, we found that mutations in sequential quality control pathways for integral membrane proteins significantly enhanced the PM integrity defect observed for *Δart1* mutant cells following heat stress. For example, abrogation of either Golgi quality control (*Δvps10*, *Δgga1*, *Δtul1*) or ER quality control (*Δdoa10*, *Δhrd1*, *Δire1*) systems significantly enhanced the PM integrity defect observed for *Δart1* mutant cells during heat stress (Figure 2.18 A, B and C and Figure 2.19). Furthermore, cells with defects in all three integral membrane quality control systems (ERAD, GCQ, and PM quality control;

Δart1Δdoa10Δgga1 triple mutant cells) exhibited dramatic loss of PM integrity (~55% of total cell population) following 3 hours at 40^0C (Figure 2.19). Importantly, individual loss of either ERAD or GQC, or loss of both ERAD and GQC, does not result in significant PI positive staining of cells following heat stress, suggesting that PM quality control can compensate for defects in parallel quality control systems in the secretory pathway (Figure 2.19). However, loss of ERAD or GQC in the absence of PM quality control can exacerbate the PM integrity defect at high temperature, suggesting that loss of quality control along the secretory pathway can contribute to the accumulation of misfolded proteins at the cell surface. These interactions demonstrate how all three integral membrane quality control systems – ERAD, GQC, and PM quality control – cooperate to protect the integrity of the PM during heat stress.

Figure 2.17 Parallel Circuitry of Integral Membrane Protein Quality Control

A

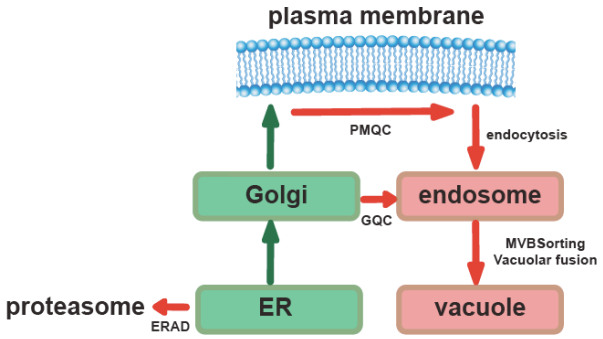

B

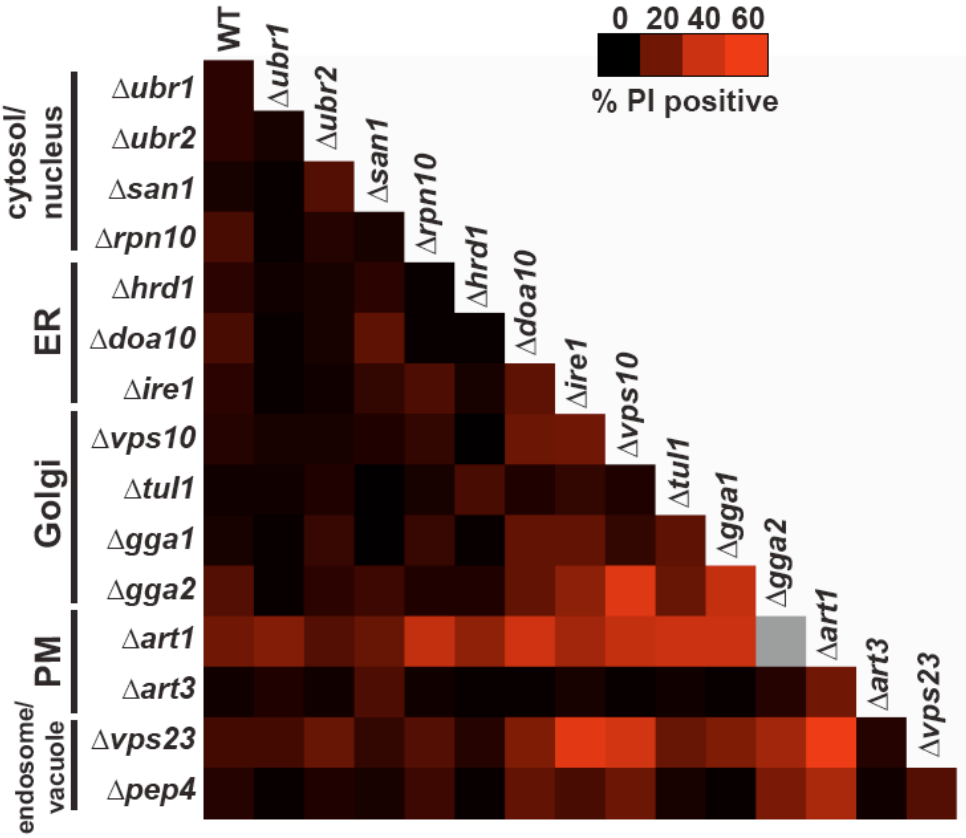

Figure 2.17 Parallel Circuitry of Integral Membrane Protein Quality Control

(A) Model illustrating the major quality control mechanisms for integral membrane proteins: ERAD (proteasomal degradation), Golgi quality control (GQC; vacuolar/lysosomal degradation), and plasma membrane quality control (PMQC; vacuolar/lysosomal degradation).

(B) Genetic array constructed for known quality control systems in the cell. Red color indicates the percentage of yeast cells staining PI positive following growth at 40^0C for three hours (see key inset). Gray box indicates a strain, which could not be obtained due to synthetic lethality in the SEY6210 background.

Figure 2.18 Parallel Circuitry of Integral Membrane Protein Quality Control

A

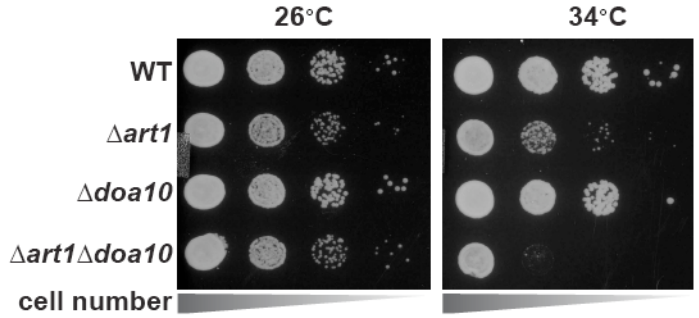

B

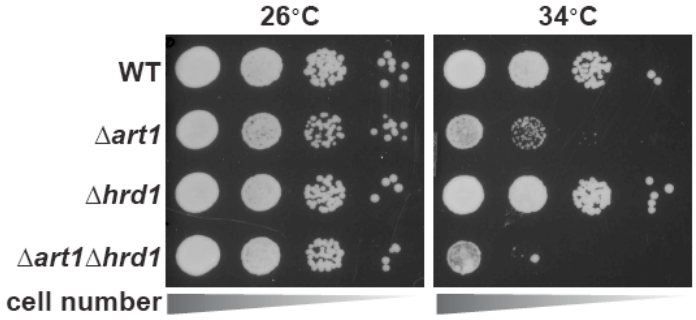

C

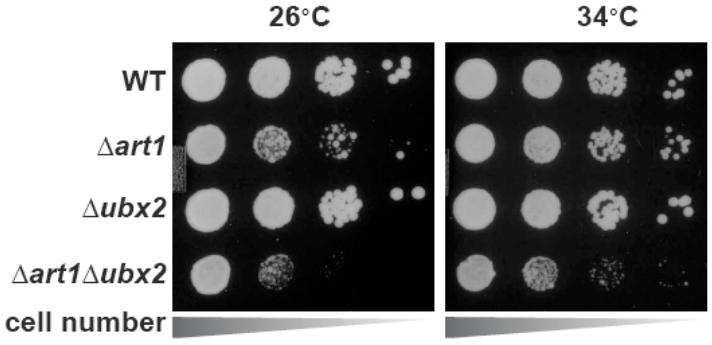

Figure 2.18 Parallel Circuitry of Integral Membrane Protein Quality Control

(A) (B) (C) Heat-sensitivity analysis of wildtype, Δart1, Δdoa10, Δart1Δdoa10, Δhrd1, Δart1Δhrd1, Δubx2, Δart1Δubx2 mutant yeast cells

Figure 2.19 Parallel Circuitry of Integral Membrane Protein Quality Control

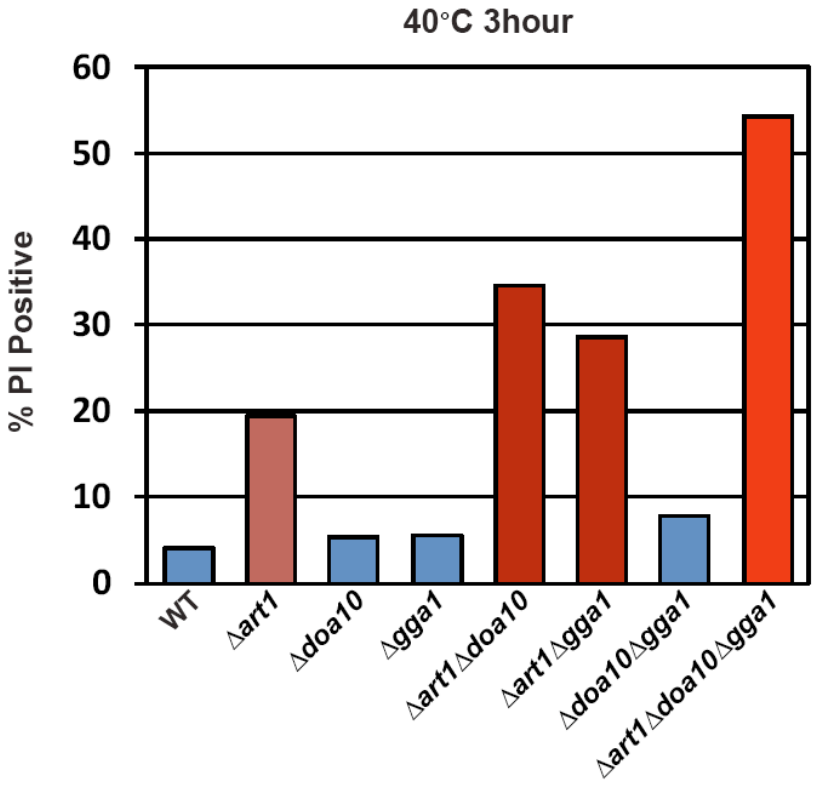

Figure 2.19 Parallel Circuitry of Integral Membrane Protein Quality Control

Flow cytometry was used to analyze PI staining of the indicated strains following growth at 40 ^{0}C for three hours.

Disscussion

Protein quality control systems share several key features that define their function as mediators of cellular proteostasis. Such quality control systems **(i)** must selectively recognize misfolded or aberrant proteins and target them either for re-folding or degradation. For example, the E3 ubiquitin ligase CHIP binds to Hsp70, which effectively targets chronically misfolded proteins for ubiquitination and subsequent proteasomal degradation (Meacham et al., 2001; Qian et al., 2006). Our data suggests that the ART-Rsp5 network may specifically recognize and target misfolded proteins since substrates are targeted in response to heat stress, which is known to induce broad misfolding of proteins in the cell (Fang et al., 2011). Furthermore, different cargo substrates targeted by the ART-Rsp5 network exhibit different turnover kinetics (Figure 1 and Supplemental Figure 1) and unique thermostability profiles (Supplemental Figure 1D and Table 1), which suggests that the heat-induce endocytic response is cargo intrinsic. Since each specific protein is expected to experience unique conformational dynamics as a function of temperature, these results are consistent with the targeting of proteins as they become conformationally aberrant or misfolded (Claessen et al., 2012; Roth and Balch, 2011). Nevertheless, future experiments will need to establish the mechanistic basis for heat-induced recognition of cargo by ARTs at the cell surface. Protein quality control systems **(ii)** must also be able to recognize a broad array of substrates. For example, the nuclear E3 ubquitin ligase San1 is capable of targeting many different unfolded protein sequences for degradation by a mechanism that

involves intrinsically disordered segments of the San1 protein (Rosenbaum et al., 2011). The ART-Rsp5 network in yeast also has a very broad substrate spectrum, capable of mediating the turnover of just about every cargo analyzed in response to heat stress (Figure 3). Typically, protein quality control systems are **(iii)** induced or activated during conditions of proteotoxic stress. For example, the unfolded protein response is induced following ER stress, resulting in the induction of ER chaperones and ERAD machinery (Walter and Ron 2011). While the ART-Rsp5 network does not appear to be induced transcriptionally, we find that it does appear to be activated in response to heat stress. Specifically, we find that heat stress triggers PM translocation of Art1 (Supplemental Figure 3A), although the molecular basis for this activation event remains to be elucidated. Finally, protein quality control systems are typically (iv) required to survive proteotoxic stress. We found in the course of our investigation that abrogation of the ART-Rsp5 mediated heat-induced endocytic response results in hypersensitivity to heat stress that is associated with accumulation of proteins at the cell surface (Figure 2A, 3C and 3F) and loss of PM integrity (Figure 8 2D, 2E, 3G and 3H). Thus, the ART-Rsp5 network plays a critical role in protecting the cell – and in particular, protecting the plasma membrane – during conditions of proteotoxic stress. Based on these four criteria, we propose that the ART-Rsp5 adaptor network comprises a protein quality control system that functions primarily in the recognition and targeted removal of misfolded integral membrane proteins at the PM.

Thermo-protective endocytosis and surface protein quality control

The earliest studies reporting the existence of post-ER quality control of integral membrane proteins provided evidence that misfolding of mutant alleles of yeast cargo proteins is triggered by either high temperature (Gong and Chang, 2001; Jenness et al., 1997; Li et al., 1999; Liu et al., 2006) or changes in PM lipid composition (Daicho et al., 2009; Lauwers et al., 2007; Wang and Chang, 2002). Importantly, it is clear that both high temperature and changes in PM lipid composition trigger endocytosis and degradation of PM proteins. This raises the possibility that heat stress may contribute to misfolding of integral membrane proteins either directly, through temperature-induced changes in protein conformation, or indirectly, by changing lipid dynamics which in turn alters the conformation of transmembrane spanning domains and triggers broad destabilization of integral membrane proteins. Like ERAD, recognition of PM integral membrane protein misfolding likely entails topology-specific mechanisms, including detection of misfolding in the extracellular space, in transmemebrane domains, and in cytosolic soluble domains. A series of elegant studies have recently provided evidence for a PM quality control system in mammalian cells that involves recognition of misfolded soluble domains on the cytosolic side of the plasma membrane. One study demonstrated that when ΔF506 CFTR is localized to the cell surface (which is achieved by growing cells at low temperature, a conditions that stabilizes ΔF506 CFTR and facilitates ER exit) it is subject to rapid ubiquitination, endocytosis, and vacuolar trafficking following a shift to higher temperature (Okiyoneda et al., 2010). In a different study, the same group engineered synthetic chimeras with soluble domains known to misfold at high temperature and

demonstrated that these proteins undergo heat-induced ubiquitination and endocytosis (Apaja et al., 2010). Both studies converged on a common mechanism that involves recognition of misfolded soluble cytosolic domains by chaperones (Hsp70/Hsc70/Hsp90) which recruit CHIP, an E3 ubiquitin ligase. Ubiquitination by CHIP triggers endocytosis, subsequent sorting by ESCRTs into multivesicular bodies, and eventual delivery to the lysosome for degradation (Okiyoneda et al., 2011). While the yeast genome does not encode a homolog of mammalian CHIP, the analogous proteins, Ubr1 and Ubr2, were not found to be required for the heat-induced endocytic response (data not shown). Instead, our results indicate that the recognition of misfolded integral membrane proteins in yeast is mediated by ART adaptor proteins, although it is not immediately clear if ART-mediated recognition is based on changes in transmembrane or cytosolic client domains. It is tempting to speculate that a similar peripheral quality control function may be mediated by the ARRDC family of proteins in mammalian cells, which encode proteins similar to ARTs with an N-terminal arrestin-domain and multiple C-terminal PY motifs.

Heat stress induces turnover of soluble and membrane proteins

The heat-shock response of eukaryotic cells has been studied extensively in terms of transcriptional regulation and the induced expression of both chaperone networks and protein degradation pathways that help compensate for broad misfolding in the cell (Morano et al., 2012). In particular, one recent study demonstrated the broad induction of both protein misfolding, ubiquitination, and targeting for degradation in response to heat stress (Fang et al., 2011). The results of our study demonstrate that clearance of integral membrane proteins from the PM by ubiquitination and endocytosis provides critical protection for the cell during heat stress. Indeed, analysis of quantitative trait loci linked to heat tolerance in yeast identified at least two loci that encode genes involved in endocytosis (Steinmetz et al., 2002), underscoring the important role endocytosis plays in heat tolerance. One clear protective function of endocytosis during heat stress involves the clearance of misfolded proteins from the PM. Accumulation of misfolded proteins at the cell surface is a liability for the cell because misfolding of some surface proteins, particularly transporters and channels, may result in aberrant conformations that disrupt the integrity of the plasma membrane. Removing conformationally aberrant integral membrane proteins is thus critical for protecting the integrity of the cell. We speculate that eukaryotic cells may respond to heat stress by coordinating the heat-induced endocytic response with degradation of soluble cytosolic proteins, although the details of these stress response mechanisms remain to be elucidated.

The Parallel Circuitry of Membrane Protein Quality Control

Our results indicate that parallel quality control systems for integral membrane proteins including ERAD, GCQ, and PMQC – cooperate to limit the accumulation of misfolded proteins at the PM. Although ERAD is the best understood quality control system for integral membrane proteins, we found that defects in ERAD did not significantly affect thermotolerance in the presence of Art1 but did exacerbate the loss of PM integrity in the absence of Art1. GQC, while still poorly understood, has also recently been shown to protect the cell from proteotoxic stress by capturing misfolded proteins at the Golgi and diverting them to the endosomal system for degradation in the lysosome (Wang and Ng, 2010; Wang et al., 2011). We propose that the ART-Rsp5 network functions in the clearance of misfolded proteins that traffic to the surface by escaping ERAD and GQC, in much the same way that CHIP has been shown to function in the detection and ubiquitination of misfolded cytosolic domains anchored to the PM (Apaja et al., 2010; Okiyoneda et al., 2011; Okiyoneda et al., 2010). Understanding the coordination of compartment-specific quality control systems along the secretory and endocytic pathways has the potential to contribute to improved therapeutic strategies for protein misfolding diseases like CFTR and other channelopathies (Kullmann, 2010; Roth and Balch, 2011; Rougier et al., 2010).

Reference

Apaja, P.M., Xu, H., and Lukacs, G.L. (2010). Quality control for unfolded proteins at the plasma membrane. J Cell Biol *191*, 553-570.

Bernier, V., Lagacé, M., Bichet, D.G., and Bouvier, M. (2004). Pharmacological chaperones: potential treatment for conformational diseases. Trends Endocrinol Metab *15*, 222-228.

Claessen, J.H., Kundrat, L., and Ploegh, H.L. (2011). Protein quality control in the ER: balancing the ubiquitin checkbook. Trends Cell Biol.

Claessen, J.H., Kundrat, L., and Ploegh, H.L. (2012). Protein quality control in the ER: balancing the ubiquitin checkbook. Trends Cell Biol *22*, 22-32.

Daicho, K., Makino, N., Hiraki, T., Ueno, M., Uritani, M., Abe, F., and Ushimaru, T. (2009). Sorting defects of the tryptophan permease Tat2 in an erg2 yeast mutant. FEMS Microbiol Lett *298*, 218-227.

Fang, N.N., Ng, A.H., Measday, V., and Mayor, T. (2011). Hul5 HECT ubiquitin ligase plays a major role in the ubiquitylation and turnover of cytosolic misfolded proteins. Nat Cell Biol *13*, 1344-1352.

Gong, X., and Chang, A. (2001). A mutant plasma membrane ATPase, Pma1-10, is defective in stability at the yeast cell surface. Proc Natl Acad Sci U S A *98*, 9104-9109.

Henne, W.M., Buchkovich, N.J., and Emr, S.D. (2011). The ESCRT Pathway. Dev Cell *21*, 77-91. Hurley, J.H. (2010). The ESCRT complexes. Crit Rev Biochem Mol Biol *45*, 463-487.

Jenness, D.D., Li, Y., Tipper, C., and Spatrick, P. (1997). Elimination of defective alpha-factor pheromone receptors. Mol Cell Biol *17*, 6236-6245.

Kullmann, D.M. (2010). Neurological channelopathies. Annu Rev Neurosci *33*, 151-172.

Lauwers, E., Erpapazoglou, Z., Haguenauer-Tsapis, R., and André, B. (2010). The ubiquitin code of yeast permease trafficking. Trends Cell Biol *20*, 196-204.

Lauwers, E., Grossmann, G., and André, B. (2007). Evidence for coupled biogenesis of yeast Gap1 permease and sphingolipids: essential role in transport activity and normal control by ubiquitination. Mol Biol Cell *18*, 3068-3080.

Li, Y., Kane, T., Tipper, C., Spatrick, P., and Jenness, D.D. (1999). Yeast mutants affecting possible quality control of plasma membrane proteins. Mol Cell Biol *19*,

3588-3599.

Lin, C., MacGurn, J., Chu, T., Stefan, C., and Emr, S. (2008a). Arrestin-related ubiquitin-ligase adaptors regulate endocytosis and protein turnover at the cell surface. Cell *135*, 714-725.

Lin, C.H., MacGurn, J.A., Chu, T., Stefan, C.J., and Emr, S.D. (2008b). Arrestin-related ubiquitin-ligase adaptors regulate endocytosis and protein turnover at the cell surface. Cell *135*, 714-725.

Liu, Y., Sitaraman, S., and Chang, A. (2006). Multiple degradation pathways for misfolded mutants of the yeast plasma membrane ATPase, Pma1. J Biol Chem *281*, 31457-31466.

Macgurn, J.A., Hsu, P.C., and Emr, S.D. (2012). Ubiquitin and membrane protein turnover: from cradle to grave. Annu Rev Biochem *81*, 231-259.

MacGurn, J.A., Hsu, P.C., Smolka, M.B., and Emr, S.D. (2011). TORC1 regulates endocytosis via Npr137 mediated phosphoinhibition of a ubiquitin ligase adaptor. Cell *147*, 1104-1117.

Meacham, G.C., Patterson, C., Zhang, W., Younger, J.M., and Cyr, D.M. (2001). The Hsc70 co-chaperone CHIP targets immature CFTR for proteasomal degradation. Nat Cell Biol *3*, 100-105.

Morano, K.A., Grant, C.M., and Moye-Rowley, W.S. (2012). The response to heat shock and oxidative stress in Saccharomyces cerevisiae. Genetics *190*, 1157-1195.

Okiyoneda, T., Apaja, P.M., and Lukacs, G.L. (2011). Protein quality control at the plasma membrane. Curr Opin Cell Biol *23*, 483-491.

Okiyoneda, T., Barrière, H., Bagdány, M., Rabeh, W., Du, K., Höhfeld, J., Young, J., and Lukacs, G. (2010). Peripheral Protein Quality Control Removes Unfolded CFTR from the Plasma Membrane. Science *329*, 46 805-810.

Qian, S.B., McDonough, H., Boellmann, F., Cyr, D.M., and Patterson, C. (2006). CHIP-mediated stress recovery by sequential ubiquitination of substrates and Hsp70. Nature *440*, 551-555.

Rosenbaum, J.C., Fredrickson, E.K., Oeser, M.L., Garrett-Engele, C.M., Locke, M.N., Richardson, L.A., Nelson, Z.W., Hetrick, E.D., Milac, T.I., Gottschling, D.E*., et al.* (2011). Disorder targets misorder in nuclear quality control degradation: a disordered ubiquitin ligase directly recognizes its misfolded substrates. Mol Cell *41*, 93-106.

Roth, D.M., and Balch, W.E. (2011). Modeling general proteostasis: proteome balance in health and 8 disease. Curr Opin Cell Biol *23*, 126-134.

Rougier, J.S., Albesa, M., and Abriel, H. (2010). Ubiquitylation and SUMOylation of cardiac ion channels. J Cardiovasc Pharmacol *56*, 22-28.

Shields, S.B., and Piper, R.C. (2011). HOW UBIQUITIN FUNCTIONS WITH ESCRTS. Traffic. Steinmetz, L.M., Sinha, H., Richards, D.R., Spiegelman, J.I., Oefner, P.J., McCusker, J.H., and Davis, R.W. (2002). Dissecting the architecture of a quantitative trait locus in yeast. Nature *416*, 326-330.

Walter, P., and Ron, D. (2011). The unfolded protein response: from stress pathway to homeostatic regulation. Science *334*, 1081-1086.

Wang, Q., and Chang, A. (2002). Sphingoid base synthesis is required for oligomerization and cell surface stability of the yeast plasma membrane ATPase, Pma1. Proc Natl Acad Sci U S A *99*, 12853-12858.

Wang, S., and Ng, D.T. (2010). Evasion of endoplasmic reticulum surveillance makes Wsc1p an obligate substrate of Golgi quality control. Mol Biol Cell *21*, 1153-1165.

Wang, S., Thibault, G., and Ng, D.T. (2011). Routing misfolded proteins through the MVB pathway protects against proteotoxicity. J Biol Chem.

Chapter III

Regulation of Art1 by a Ubiquitination/Deubiquitination Cycle

Chapter III contains work on a side project that currently is not planned for publication. Yingying's major contribution to this chapter is presented in Figure 3.3B C, 3.4, 3.5 B C D, 3.6 and Figure 3.7A

Introduction

Ubiquitination modification affects the properties of a substrate protein. It is well-established that ubiquitination can mark proteins for degradation by the proteasome. However, ubiquitin modification also contributes to the regulation of endocytic trafficking and signal transduction. Ubiquitin has 7 lysines which can form polyubiquitin chains of distinct linkages. Different linkages have different effects on protein function. For example, modification with K48-polyubiquitin targets a protein for degradation by the proteasome. In contrast, modification with K63- polyubiquitin plays an important role in signal propagation of the nuclear factor kappa B (NF-κB) pathway through the recruitment of adaptors and signaling kinases (Iwai and Tokunaga 2009). It is well-established that monoubquitination or multi-monoubquitination function in endocytosis, membrane trafficking, protein localization, histone function, transcription regulation, DNA repair and DNA replication (Hicke 2001, Sigismund S 2004). Comparatively less is known about linear ubiquitination (head to tail) modification, formed by C-terminal Gly to amino-terminal Met residue (Kirisako T 2006). Recently, this type modification has been demonstrated to function in NF-κB signaling (Tokunaga 2011).

Ubiquitination is a reversible modification and it can be edited by specialized isopeptidases called deubiquitinating enzymes, or DUBs. DUBs can edit or disassemble the polyubiquitin chains or monoubiquitination of a target protein. Deubiquitination can rescue a substrate protein from degradation (Rumph 2006), recycle ubiquitin (Swaminathan 1999 ; Ryu, K. Y. 2007) or control protein trafficking and localization (Nikko 2007; Yaron Mosesson 2009). Free ubiquitin in the cell exists in both a monomeric form and free polyubiquitin chains. The monomeric ubiquitin pool level is maintained from three sources: (1) synthesis of new ubiquitin from the chromosome; (2) release from ubiquitinated protein; (3) release from free polyubiquitin chains. In yeast, the deubiquitinase Doa4 has been implicated in the regulation of cellular ubiquitin homeostasis through the interaction with the Doa4 inhibitor Rfu1 (Amerik 2000; Swaminathan 1999; Kimura 2009). A human deubiquitinase called USP44 (ubiquitin specific protease 44) has been shown to control anaphase entry by deubiquitinating cell cycle regulatory protein Cdc20 (Stegmeier, F. 2007). DUBs can also act as oncoproteins or tumor supressors in neoplastic disease (Nicholson 2007; Brooks 2006; Stevenson 2007; Graner 2004; Trompouki 2003; Brummelkamp 2003; Kovalenko 2003). Ubiquitin is present in protein aggregates associated with various neurodegenerative diseases including amyloid deposition of Alzheimer's disease, Lewy bodies in Parkinson's disease, as well as intranuclear inclusions in hereditary polyglutamine disorders (Sokol V. Todi 2011; Lennox 1988; Paulson 1997; Lowe 1988; Lowe 1988; Mori 1987). Indeed, recent findings suggest that DUBs may function in determining neuronal fate, helping the axonal path connection as well as affecting synaptic

communication and plasticity (Sokol V. Todi 2011).

Figure 3.1

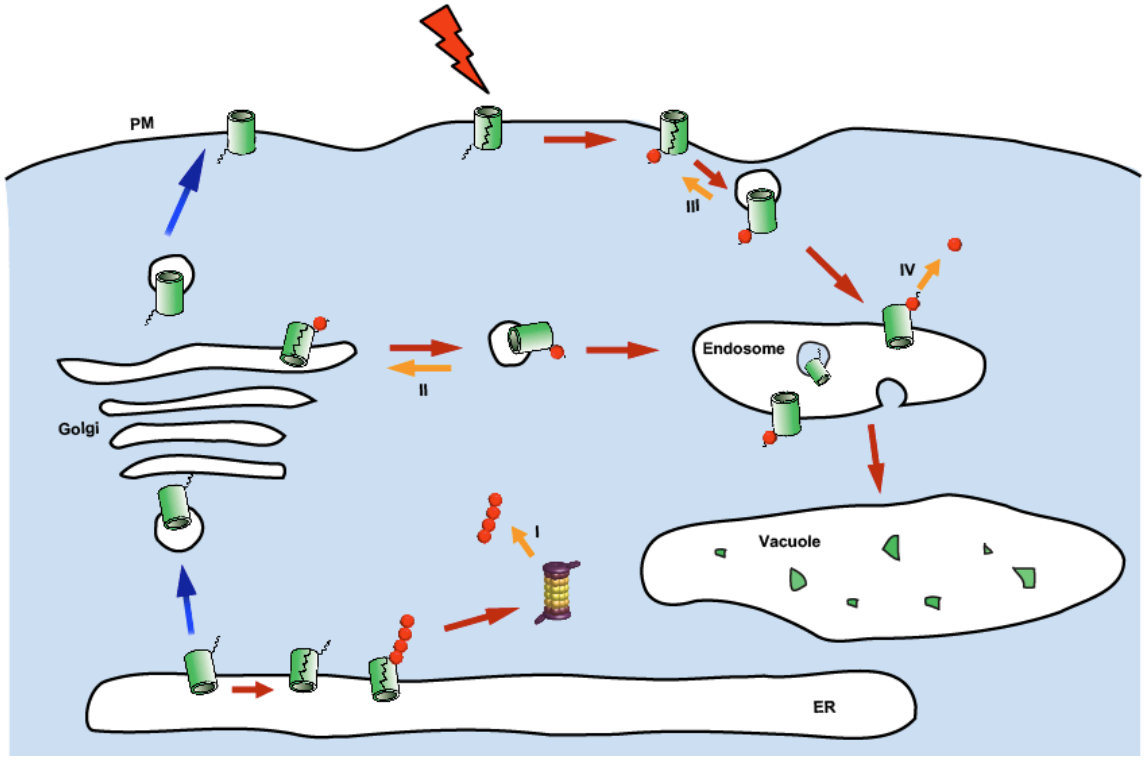

I → Recycle ubiquitin

II → Send membrane protein back to Golgi

III → Recycling back to PM

IV → Recycle ubiquitin

Figure 3.1 DUBs play critical roles in regulating protein homeostasis

DUBs can regulate membrane proteins in many different ways. DUBs tightly associate with the proteasome to recycle ubiquitin chains from substrate proteins before being degraded. DUBs reverse ubiquitin modification of substrate proteins at the Golgi complex or endosome, effectively altering cargo sorting and traicking. DUBs recycle ubiquitin to balance the cellular monomeric ubiquitin pool before membrane protein sorting into multivesicular bodies (MVBs) and degradation in the lysosome.

In mammalian cells, it is known that β-arrestin ubiquitination contributes to the stability of the GPCR-β-arrestin interaction (Shenoy, McDonald et al. 2001). Previously, the Emr lab identified a family of proteins called *a*rrestin *r*elated *t*rafficking adaptors, or ARTs, which contain PY motifs for interacting with the WW domain of Rsp5, thus targeting ubiquitin ligase activity to specific proteins at the plasma membrane (Figure 4.1 A). Modification of integral plasma membrane proteins by ubiquitin results in their removal from the PM by endocytosis. In addition, ubiquitin also plays an important role in regulating Art1 function. Our preliminary results indicate that the predominant form of Art1 in vivo is ubiquitin modified (Figure 4.1 B). Preliminary results indicate that the predominant form of Art1 is ubiquitinated at K486 by Rsp5. Mutations in either the acceptor lysine (K486R) or the PY motifs (PAIA/PACA) of Art1 prevent ubiquitin modification and abrogate function in endocytic downregulation (Figure 4.2) (Lin, MacGurn et al. 2008). Furthermore, ubiquitination of Art1 at K486 is required for function as an ubiquitin-ligase adaptor.

My research goal in this chapter is to understand how ubiquitin modification regulates Art1 function. We hypothesize that an ubiquitination/deubiquitination cycle may regulate Art1 activity (Figure 4.1 C). Ubiquitin modification may regulate Art1 stability, subcellular localization, or Art1-protein interaction (including interaction with cargo and Rsp5). Furthermore, we speculate that Art1 may be regulated by a specific deubiquitinase, which could inactivate Art1 as part of an ubiquitination/deubiquitination cycle. To better understand how ubiquitination

regulates Art1 function, in this chapter, I focus on our current understanding of the functional significance of Art1 monoubiquitination and the progress we have made to characterize the Art1 Ub-Deub cycle.

Figure 3.2 Art1regulation by a ubiquitination cycle

A

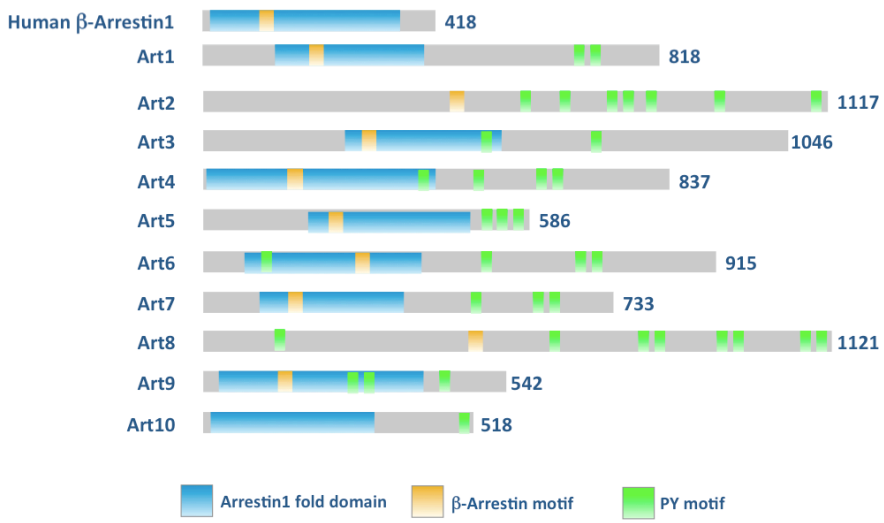

B

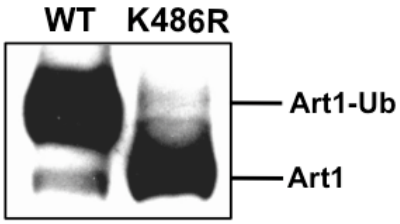

C

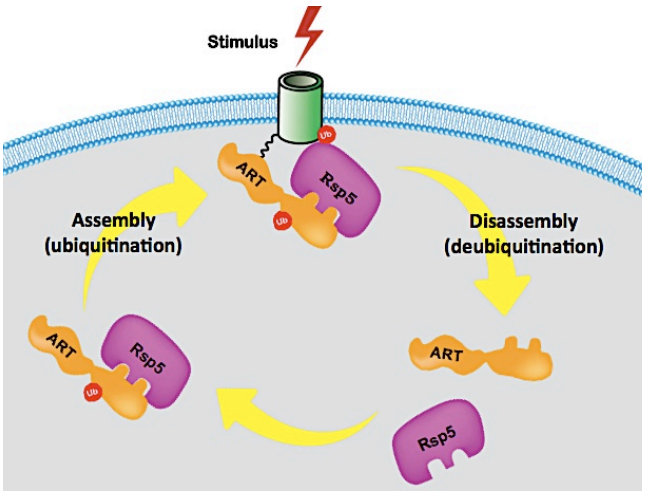

Figure 3.2 Art1regulation by a ubiquitination cycle

(A) Members of the ART protein family contain the predicted N-termianl arrestin fold domain (blue box) and C terminal PY motif (green box). PY motif can interact with WW domain of Rsp5, allowing ARTs to serve as Rsp5 adaptors that facilitate the ubiquitination of specific proteins at the plasma membrane (Lin, MacGurn et al. 2008)

(B) Previous results indicate that the predominant form of Art1 is ubiquitinated at K486 by Rsp5 (Jason MacGurn).

(C) Hypothetic model: Art1 is regualted by an ubiquitination and deuibiquitination cycle. Ubiquitinated In the shown model, Art1 is active form and deubiquitinaed Art1 is the inactive form. At steady state, the majority of Art1 is ubiquitinated. After membrane protein has been ubiquitinated, Art1 could be inactivated by deubiquitination and/or dissociated from plasma membrane.

Materials and Methods

Yeast strains and Plasmid Construction

A list of all Saccharomyces cerevisiae strains and plasmids used in this study and their genotype can be found in Supplementary Table S1 and S2. Homologous recombination was used to tag or delete genes in yeast. All integrations were verified by PCR analysis and expression of fusion proteins was confirmed by Western Blot analysis. Gene subcloning was performed by PCR using Ex Taq (Tafara) or KOD Polymerase (Novagen) and subsequent ligation into the designated expression vector with T4 DNA ligase (Fermentas). The yeast shuttle vectors used in this study have been previously described (Sikorski, 1989). Restriction enzymes were purchased from New England Biolabs (Ipswich, MA)

Fluorescence Microscopy

Yeast cells expressing fluorescent fusion proteins were grown to mid-log in synthetic media. Microscopy was performed using a fluorescence microscope (DeltaVison RT; Applied Precision) equipped with FITC and rhodamine filters. Images were captured with a digital camera (Cool Snap HQ; Photometrics) and deconvolved using softWoRx 3.5.0 software (Applied Precision).

Analysis of Cellular Protein Expression Levels

Yeast cells expressing epitope tagged protein were grown to mid-log phase in synthetic media. 5 OD600 equivalents of mid-log cells pretreated at the indicated temperatures were harvested by precipitation in 10% trichloroacidic acid (TCA). Precipitates were washed in acetone, aspirated, resuspended in lysis buffer (150mM NaCl, 50mM Tris pH7.5, 1mM EDTA, 1% SDS), and mechanically lysed with glass

beads. Protein sample buffer (150mM Tris pH 6.8, 6M Urea, 6% SDS, 10% beta-mercaptoethanol, 20% Glycerol) was added and extracts were analyzed by SDS-PAGE and immunoblotting with anti-FLAG (sigma) antibody.

Yeast Growth Assay

Yeast strains were grown to mid-log phase in synthetic media. 1 OD600 of yeast cells was pelleted, resuspend in 1mL of sterilized H_2O, serially diluted at a ratio of 1:10 using 96-well plate, and plated using a frogger.

Whole Cell S^{35} Labeling and immunoprecipitation of Yeast Protein

Yeast cells expressing epitope tagged protein were grown to mid-log phase in synthetic media. Ten OD600 equivalents of mid-log cells were washed with 2mL synthetic media (without amino acids and glucose added). Cells were pelleted and resuspended at 10 OD600/ mL and incubated for 15minutes. Add 1.25uL/OD600 of Tran S35 methionine, incubate with shaking for 20min at 30°C. At the desired chase periods, add 10Xchase solution to 1X to stop the incorporation and mix well. Transfer each labeled sample into ice-cold tubes containing 120uL 100% TCA (Trichloroacetic Acid). Incubate all samples on ice for 30min, then spin down and wash pellets twice with 1mL cold acetone. Resuspend dried TCA pellets with 100ul cracking buffer (50mM Tris PH7.5, 1mM EDTA, 1% SDS, 8M Urea), Sonication, add 100ul beads, votex 5min, boiling at 65°C for 5min. Repeat votex and boil and add 1ml Lysis buffer (1M NEM, 0.5M EDTA, 20% NP40, 1M Tris, 5N NaCl, with protease inhibitor added), spin at top speed for 10min, transfer 1ml the supernant to a new tube and repeat spin, transfer 950ul to a new tube. IPs were done by using affinity beads (Sigma-Aldrich) to the supernatant and incubated for 1h at 4°C. Spin to pellet

the beads, take out the supernant and wash the beads with Tween-20 urea buffer (100mM Tris PH7.5, 200mM NaCl, 2M Urea, 0.5% Tween20) twice; Lysis buffer once and TBS twice. Speed vac to dry the beads and add 50ul Elution buffer, boil 5min at 95°C. Run 8% SDS gel and fix the gel with Fix I solution (10% MeOH, 10%HOAC) for 30min and Fix II solution (10% MeOH, 10% HOAC, 10% Glycerol) for 30min. Dry the Gel for 2hours. Place on film in dark room and keep at -80°C until the time of development (3-4days for Art1)

Results

Monoubiquitination of Art1 is required for efficient cargo turnover

In order to test if ubiquitination of Art1 regulate Art1-cargo interactions, we analyzed cargo ubiquitination in cells expressing wildtype or K486R Art1. Mup1 ubiquitination, which can be scored as an ubiquitin ladder by Western blot, is dependent upon the presence of Art1 (Figure 4.2 A). By this approach, loss of monoubiquitination at K486 results in a decrease in cargo ubiquitination. Next we tested the Art1 non-ubiquitination mutants including K486R and two PY motif mutants (PAIA/PACA, PAIA/PPCY) for their endocytic activity. Clearly, nonubiquitination mutants show both canavanine hypersensitive and temperature sensitive phenotypes (Figure 4.2B, C) similar to art1 null cells. Thus, loss of monoubiquitination in the art1K486R mutant results in a significant loss of activity compared to wildtype Art1.

Figure 3.3 Ubiquitination of Art1 is required for its endocytic function

A

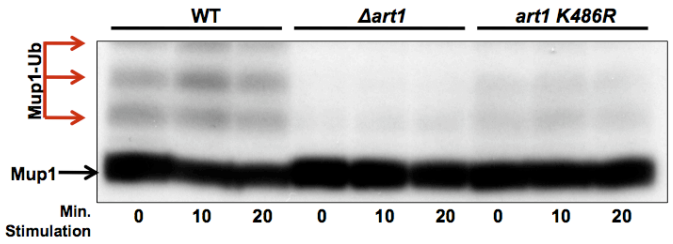

B

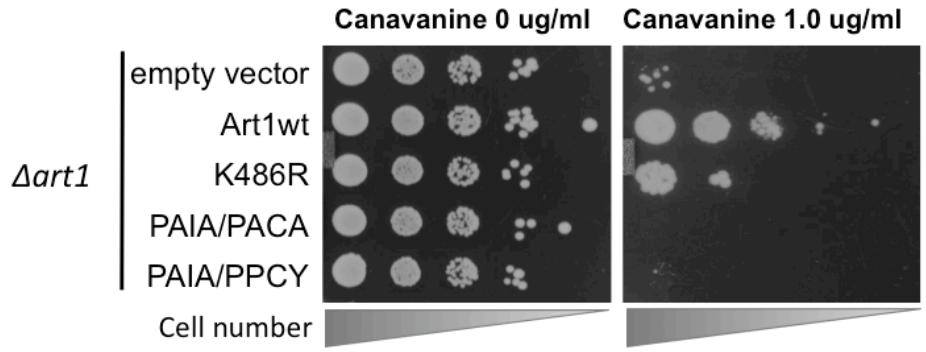

C

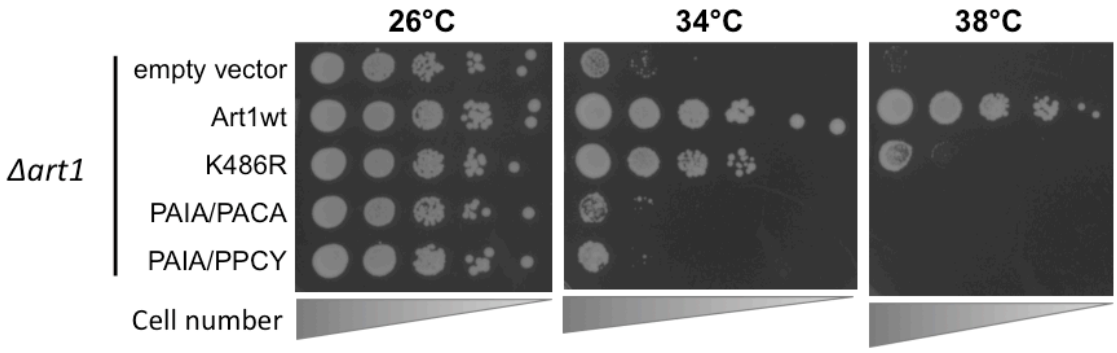

Figure 3.3 Ubiquitination of Art1 is required for its endocytic function

(A) Disappearance of ubiquitinated Mup1 in *Δart1* and art1-K486R cells. Anti-FLAG immunoblot analysis was performed using wildtype, *Δart1* and art1-K486R cells (done by Jason MacGurn)

(B) Growth of art null cells containing empty vector, Art1 wildtype, art1K486R and art1 PY motif mutants was compared on YPD or YPD plate containing 1.0ug/ml canavanine. Both K486R and PY motif mutants show canavanine sensitivity phenotype.

(C) Growth of wildtype, art null cells containing empty vector, Art1 wildtype, art1K486R and art1 PY motif mutants was compared. Both K486R and PY motif mutants show temperature sensitivity phenotype.

Monoubiquitination is required for Art1 Golgi localization

Next I tested if ubiquitination affects Art1 localization in the cell. In mammalian cells, β-arrestin is uniformly distributed in the cytoplasm at steady state. Following stimulation, ubiquitination at two sites (K11 and K12) is required for the endosomal localization of β-arrestin (Shenoy and Lefkowitz 2005). Previously, we showed that Art1 localizes to the cytosol, plasma membrane and Golgi punctae but ubiquitination mutants of Art1 (K486R, PY motif mutant) fail to localize to the Golgi (Figure 4.3). These results not only demonstrate that ubiquitination of Art1 is required for Golgi localization but also suggest that Golgi localization is important for Art1 function. However, these results do not address a possible role for Art1 monoubiquitination in plasma membrane localization, which is the primary localization of Art1 following stimulation.

Figure 3.4 Art1 localization in different mutants

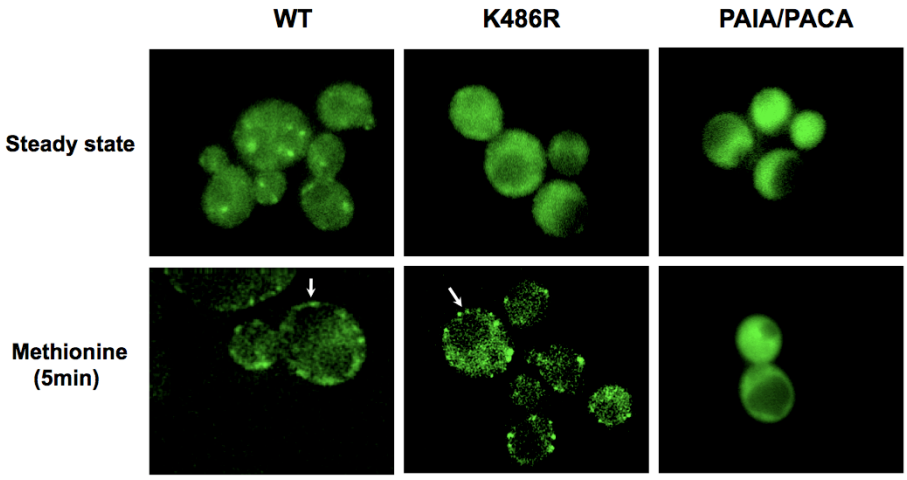

Figure 3.4 Art1 localization in different mutants

Localization of Art1 and its mutant alleles were analyzed after methionine treatment for 5min. art1 null cells were transformed with plasmids containing wildtype or mutant GFP alleles of Art1 driven by Art1 native promoter.

Art1 is regulated by a ubiquitination-deubiquitination cycle

We have shown that Art1 interacts with Rsp5 via two C-terminal PY motifs and this interaction is required for ubiquitination at K486. Using an Rsp5 temperature sensitive allele (*rsp5-1*), we observed that loss of Rsp5 ubiquitin ligase activity at the nonpermissive temperature destabilizes Art1-Ub (Figure 4.4). This loss of ubiquitinated Art1 appears to be enhanced by stimulation with methionine, which is known to activate Art1 (figure 4.4). In contrast, when the cells are pretreated with 5mM N-ethylmaleimide (NEM), a known inhibitor of deubiquitinating enzymes (DUBs), the ubiquitinated Art1 is stabilized (Figure 4.4). This result suggests that Art1 is subjected to a deubiquitinase (DUB) activity that may increase following stimulation.

There are 17 known DUBs in yeast and each one is non-essential. Although little is known about how DUBs function in yeast, some exhibit canavanine hypersensitive phenotypes suggesting that they may have a role in regulating PM protein homeostasis. These DUBs are excellent candidate regulators of Art1. To test this model, I investigated the kinetics of Art1 ubiquitination and deubiquitination using an S35 pulse chase experiment both at steady state and after stimulation. These experiments were designed to estimate the half-life of unmodified and monoubiquitinated Art1 with different stimulation conditions and mutant alleles. Initial 35S pulse-chase experiments suggested that Art1 ubiquitination does not change dramatically in response to stimulation (Figure 3.5 A B). However, one challenge in our initial experiments is that unmodified Art1 has been very difficult

to detect (figure 3.5A B), suggesting that Art1 undergoes very rapid ubiquitination following synthesis and/or deubiquitination. The inability to detect unmodified Art1 represents a significant limitation of this assay. Interestingly, we observed that the amount of unmodified Art1 is dramatically increased in a different yeast background strain (BY4741) (figure 4.5 C), suggesting that this background either has an increased DUB activity or a decreased Art1 ubiquitination activity. For future pulse-chase experiments, it is better to use this background strain, which will improve our ability to detect and quantify unmodified Art1.

Figure 3.5 Art1 is regulated by deubiquitination.

A

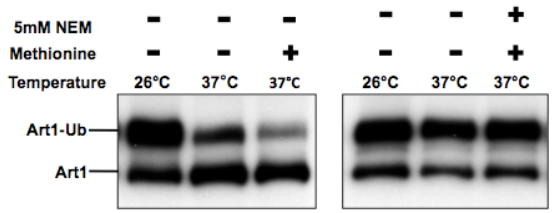

B

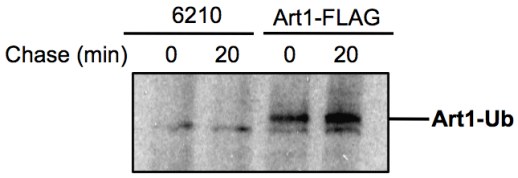

C

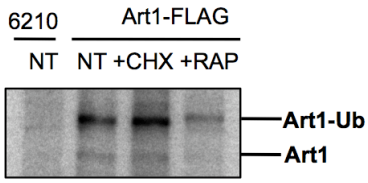

D

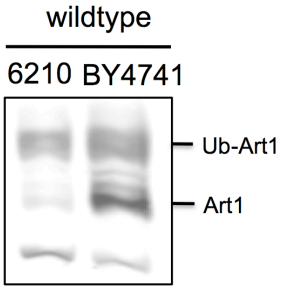

Figure 3.5 Art1 is regulated by deubiquitination.

(A) Yeast cells containing the *rsp5-1* temperature sensitive allele, which contains a mutation in HECT domain and will loss its function at 37°C. Ubiquitination of Art1 were analyzed in this strain background after shifting temperature to 37°C or methionine treatment for 5min (done by Jason MacGurn)

(B) Art1 was affinity purified from cell has been 35S pulse for 20 minute pulse and chase for 0 or 20min; Wildtype or chromosomal FLAG tagged Art1 strains are used in this experiment

(C) Art1 was affinity purified from cells following 35S pulse chase: pulse for 20min and chase for 10 minutes with different activation stimuli; chromosomal FLAG tagged Art1 strains are used in this experiment.

(D) Western blot comparing Art1 ubiquitin modification in SEY6210 and BY4741 with Art1 chromosomally tagged with FLAG.

Identification of deubiquitinases that affect Art1 ubiquitination

Our preliminary experiments suggest there is a deubiquitinase activity that reverses Art1 ubiquitination, which increases upon stimulation. In an initial attempt to identify DUBs that regulate Art1 activity, we knocked out each DUB in yeast and found that no single knockout affected the Art1 ubiquitination ratio (data not shown). However, it is likely that DUBs function in a highly redundant manner. To bypass the potential redundancy and determine if DUBs function to cycle Art1 between ubiquitinated and non-ubiquitinated forms, I designed two strategies. First, to analyze the effect of DUB loss of function, I have designed and expressed catalytic-dead mutant proteins that function as dominant negative DUBs in yeast. Second, to analyze the effect of DUB gain of function, I have overexpressed each DUB in yeast to identify candidates that affect Art1 ubiquitination.

We aligned 17 yeast DUBs protein sequences and found the catalytic center is highly conserved (Figure 4.5A) and especially the catalytic cysteine. Based on the alignment result we mutated the catalytic cysteine of several DUB candidates to valine and tested for dominant negative effects. Unfortunately, our strategy for the design of dominant negative DUB proteins did not work in most cases except doa4C571V, which functions as a dominant negative mutant (Figure 4.5 B). We found that many of the "catalytic dead" mutants were actually able to complement the phenotypes of knockout strains, suggesting that these proteins may retain catalytic activity. Because we targeted conserved cysteine residues known to function in catalysis, it is unclear why our mutants would retain function. It is

possible that other conserved cysteine residues might also function to remove ubiquitin peptides from substrates. Interestingly, the catalytic dead Doa4 did function as a dominant negative and did alter Art1 ubiquitination levels (Figure 4.4C), but this is likely an indirect effect due to depleted free ubiquitin in the cell (Figure4.4 D). Although the affect of Doa4 on Art1 ubiquitination is likely indirect, this experiment provides an important proof of concept that dominant negative DUBs can be used to probe for DUB functions and may actually lead to phenotypes stronger than those observed for null alleles (Figure 3.6D), which is important given the likelihood of redundancy in the DUB network.

Figure 3.6 Identify DUB of Art1 by Dominant negative DUB mutant

A

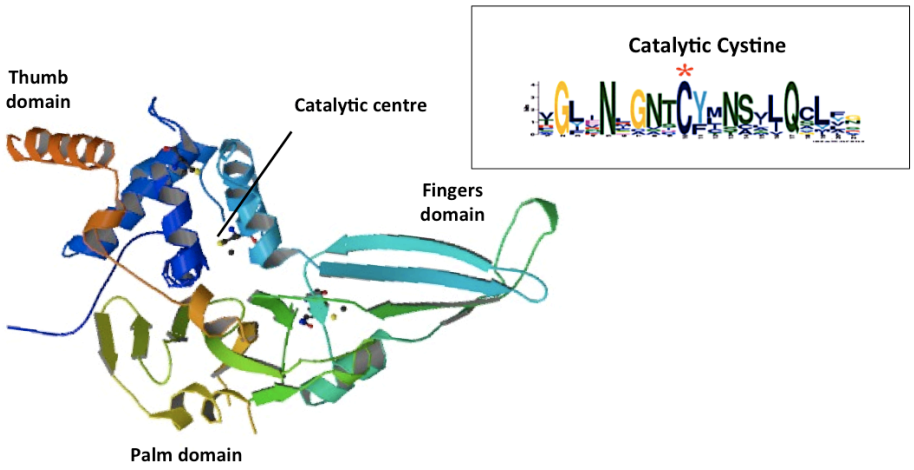

B

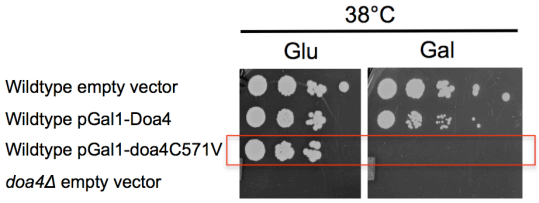

C

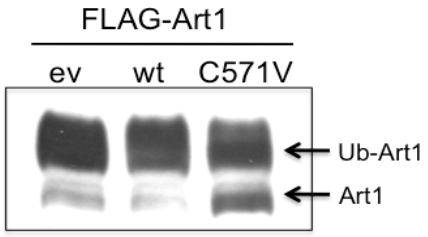

D

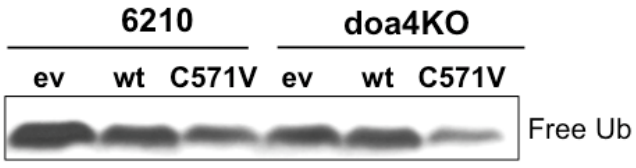

Figure 3.6 Identify DUB of Art1 by Dominant negative DUB mutant

(A) Crystal structure of mammalian USP7 (PDB identifier 1nb8). USP domains consist of three subdomains: palm, thumb and fingers domains. The catalytic center lies at the interface between the Palm and Thumb subdomains, and the fingers subdomain grips the distal ubiquitin from ubqituitin chain to deubiquitinate substrate. Conserved catalytic center with cysteine among 17 yeast DUBs is depidcted in the black box.

(B) doa4-C571V is a dominant negative mutant. Expression of the mutant is driven by the Gal1 promoter. Wildtype cells containing the plasmid exhibit temperature sensitivity similar to doa4Δ cells

(C) Accumulation of low-molecular-weight deubiquitinated form Art1 in wildtype cells expressing mutant Doa4 (C571V) driven by the pGal4 and induction in galactose media overnight. Anti-FLAG immunoblot analyses were performed using wild-type cell.

(D) Decreased level of free ubiquitin pool in *Δdoa4* cell with Doa4 C571V mutant form driven by the pGal4 promoter and induction in galactose media overnight.

Unfortunately, my analysis of DUB overexpression revealed no obvious candidates that affect Art1 ubiquitination through gain-of-function (Figure 4.5A). However, it is worth noting that overexpression may not result in gain-of-function activity, especially since several DUBs are known to use adaptor proteins to function (Cohen, Stutz et al. 2003; Lam, Urban-Grimal et al. 2009). In cases where adaptors are known (Ubp2/Rup1, Ubp3/Bre5 for example), future strategies should aim to maintain the adaptor stoichiometry by overexpressing both DUB and adaptor proteins. However, this approach is not generally suitable since adaptor proteins for many DUBs have not been identified.

Our preliminary experiments suggest there is an Art1 deubiquitinase activity, which increases upon stimulation. DUBs function in a highly redundant manner, therefore, it is possible that a group of DUBs instead of a specific DUB that regulate Art1.

Since redundancy may make it difficult to identify a specific DUB that regulates Art1, an alternative strategy is to examine candidate DUBs that may regulate the function of other Art family members. For example, it is known that Art2 (ECM21) and Art8 (CSR2) are deubiquitinated by Ubp2 in vitro (Kee, Munoz et al. 2006). Art2 is a trafficking adaptor required for stress-induced internalization of the lysine permease Lyp1. Art8 is known to turnover Smf1 upon cadmium stimulation, which is a divalent metal ion transporter at the plasma membrane. We observed that loss of Ubp2 causes Art2-GFP to relocate from the cytosol to the plasma membrane (figure 4.6 B), suggesting that Art2 may be hyperactive in a Δ ubp2 strain.

Furthermore, we also observed that disappearance of low molecular weight Art2 in Ubp2 mutant in western analysis, consistent with an accumulation of the ubiquitinated form of Art2 in the absence of Ubp2. To further explore the relationship between Ubp2 and Art2, future experiments will need to explore how Ubp2 affects cargo trafficking, cargo ubiquitination, and Art2 ubiquitination in vivo.

Figure 3.7 Identify DUB of Art1 by overexpression DUBs

A

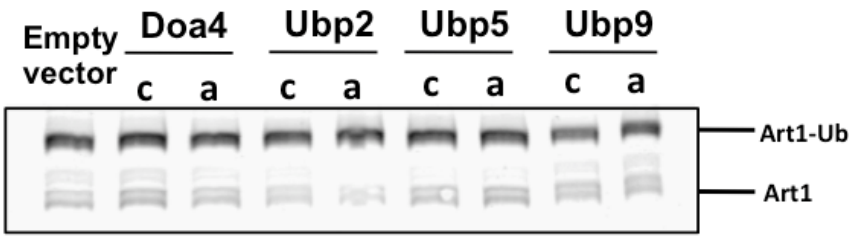

B

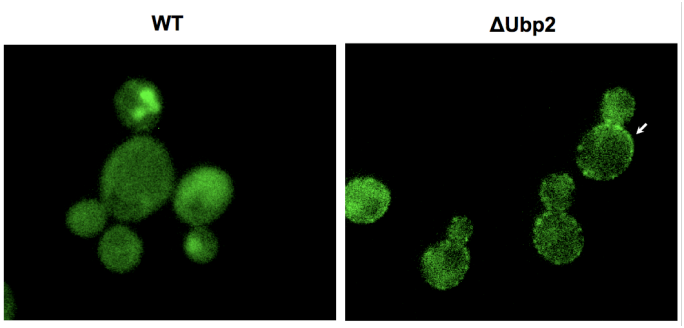

C

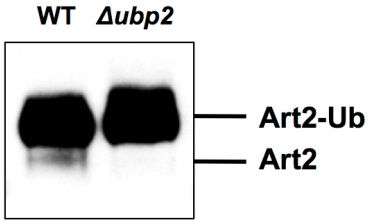

Figure 3.7 Identify DUB of Art1 by overexpression DUBs

(A) Art1 ubiquitination status was analyzed in wildtype cells contain different DUBs overexpression. Expression of Doa4, Ubp2, Ubp5 and Ubp9 are driven by either pCPY promoter (c) or pADH1 promoter (a). Western blot is done in Art1 chromosomal FLAG tagged strains using anti-FLAG antibody.

(B) Localization of Art2 in wildtype and Δubp2 cells. Art2, which is normally localized to the cytosol, is enriched at the PM in the absence of Ubp2 (done by Yi Liu).

(C) Disappearance of low molecular weight Art2 in Ubp2 mutant. Anti-FLAG immunoblot analyses were performed using wild-type, and *Δubp2* cells (done by Yi Liu).

Disscussion

It is clear that ubiquitination is a key regulator of membrane trafficking in the cell. Membrane protein ubiquitin modification is essential for its recognition by the endocytic machinery, endosome trafficking, and ESCRT sorting machinery which ensures efficient lysosomal degradation. Ubiquitination of Art1 by the E3 ligase Rsp5 has been shown to be required for its endocytic function. Ubiquitination might regulate Art1-protein interactions (including interaction with cargo, Rsp5), and also Art1 localization. Our results suggest that the Art1-Mup1 interaction may be disrupted in the absence of Art1 monoubiquitination. To expand upon these results, quantitative analysis of Mup1 ubiquitination levels in wildtype and K486R mutant cells is needed to measure the impact of Art1 ubiquitination on cargo ubiquitination. Although the coimmunoprecipitation experiments of Art1 with cargo are more direct and definitive, they are technically challenging for a variety of reasons. For example, we know that the Art1-cargo interactions are both regulated and transient, making them difficult to capture. Additionally, the cargoes that we study contain 12-13 transmembrane domains, making them difficult to isolate in a native state. Given these limitations, coimmunoprecipitation experiments in the presence of crosslinkers is better to capture transient interactions and use denaturing conditions to extract transmembrane proteins. Other technical challenges include the rapid deubiquitination of Art1 in native yeast extracts (which can be blocked by the addition of NEM to the lysis buffer) and using optimal stimulation conditions for the activation of Art1. It will also be important to test whether ubiquitination of Art1 can enhance its interaction with Rsp5. Even if loss of Art1 ubiquitination does not

affect the interaction of Art1 with Rsp5, it is still possible that ubiquitination may regulate the interaction of Art1 with some other protein. To address this possibility, future studies could use quantitative mass spectrometry to identify any Art1-protein interactions that are dependent on Art1 monoubiquitination.

Our results indicate that ubiquitination is not strictly required for Art1 recruitment to the plasma membrane, since K486R mutants localize to the PM following stimulation (figure 4.3 A). However, these still images do not address potential differences in the kinetics of Art1 localization. Art1 PM localization is very dynamic, with peripheral punctae appearing and disappearing on the order of seconds. Time-lapse imaging of wildtype and mutant Art1-GFP is needed in order to determine if ubiquitination affects Art1 residence time on the PM. Furthermore, the peripheral punctae observed in Art1 ubiquitination mutants appear to be larger than peripheral punctae observed with wildtype Art1. Co-localization analysis of wildtype and mutant Art1 with other plasma membrane patch structures, including Pil patches and sites of endocytosis to further characterize the question. Although we do not usually observe Art1 co-localization with these patches, it is possible that the ubiquitin mutants may exhibit increased association with such sites on the PM. This might indicate a defect in the recycling of Art1 following cargo ubiquitination.

Although we are able to analyze the localization of Art1-GFP using fluorescence microscopy, the low expression of Art1 (>300 molecules per cell) makes it difficult to image with high spatial or temporal resolution. To improve our ability to image

Art1, in the future to construct and characterize a vector for the expression of Art1-3xGFP will help improve the analysis. Additionally, to confirm any localization differences observed in the ubiquitination mutants of Art1, subcellular fractionation, using methods that can separate Golgi, cytosolic, and PM fractions, will be an important approach for future studies.

Our preliminary experiments suggest there is an Art1 deubiquitinase activity which increases upon stimulation. To identify the deubquitinase, we used two strategies: 1) analyze the effect of DUB loss of function by expressing catalytic-dead mutant proteins that function as dominant negative DUBs in yeast and 2) analyze the effect of DUB gain of function by overexpression. Since DUBs function in a highly redundant manner, for most DUBs there is not straightforward phenotype to test dominant negative effect. Although the affect of Doa4 on Art1 ubiquitination is likely indirect, this experiment provides an important proof of concept that dominant negative DUBs can be used to probe for DUB functions.

Blondel, M. O., J. Morvan, et al. (2004). "Direct sorting of the yeast uracil permease to the endosomal system is controlled by uracil binding and Rsp5p-dependent ubiquitylation." Mol Biol Cell 15(2): 883-95.

Bonifacino, J. S. and A. M. Weissman (1998). "Ubiquitin and the control of protein fate in the secretory and endocytic pathways." Annu Rev Cell Dev Biol 14: 19-57.

Cohen, M., F. Stutz, et al. (2003). "Ubp3 requires a cofactor, Bre5, to specifically de-ubiquitinate the COPII protein, Sec23." Nat Cell Biol 5(7): 661-7.

Gaidarov, I., J. G. Krupnick, et al. (1999). "Arrestin function in G protein-coupled receptor endocytosis requires phosphoinositide binding." EMBO J 18(4): 871-81.

Goodman, O. B., Jr., J. G. Krupnick, et al. (1996). "Beta-arrestin acts as a clathrin adaptor in endocytosis of the beta2-adrenergic receptor." Nature 383(6599): 447-50.

Gurevich, V. V. and E. V. Gurevich (2006). "The structural basis of arrestin-mediated regulation of G-protein-coupled receptors." Pharmacol Ther 110(3): 465-502.

Hicke, L. (2001). "Protein regulation by monoubiquitin." Nat Rev Mol Cell Biol 2(3): 195-201.

Hicke, L. and R. Dunn (2003). "Regulation of membrane protein transport by ubiquitin and ubiquitin-binding proteins." Annu Rev Cell Dev Biol 19: 141-72.

Iwai, K. and F. Tokunaga (2009). "Linear polyubiquitination: a new regulator of NF-kappaB activation." EMBO Rep 10(7): 706-13.

Katzmann, D. J., S. Sarkar, et al. (2004). "Multivesicular body sorting: ubiquitin ligase Rsp5 is required for the modification and sorting of carboxypeptidase S." Mol Biol Cell 15(2): 468-80.

Kee, Y., W. Munoz, et al. (2006). "The deubiquitinating enzyme Ubp2 modulates Rsp5-dependent Lys63-linked polyubiquitin conjugates in Saccharomyces cerevisiae." J Biol Chem 281(48): 36724-31.

Kim, Y. M. and J. L. Benovic (2002). "Differential roles of arrestin-2 interaction with clathrin and adaptor protein 2 in G protein-coupled receptor trafficking." J Biol Chem 277(34): 30760-8.

Lam, M. H., D. Urban-Grimal, et al. (2009). "Interaction of the deubiquitinating enzyme Ubp2 and the e3 ligase Rsp5 is required for transporter/receptor sorting in the multivesicular body pathway." PLoS One 4(1): e4259.

Laporte, S. A., R. H. Oakley, et al. (1999). "The beta2-adrenergic receptor/betaarrestin complex recruits the clathrin adaptor AP-2 during endocytosis." Proc Natl Acad Sci U S A 96(7): 3712-7.

Lefkowitz, R. J., K. Rajagopal, et al. (2006). "New roles for beta-arrestins in cell signaling: not just for seven-transmembrane receptors." Mol Cell 24(5): 643-52.

Lin, C. H., J. A. MacGurn, et al. (2008). "Arrestin-related ubiquitin-ligase adaptors regulate endocytosis and protein turnover at the cell surface." Cell 135(4): 714-25.

Lu, C., S. Pribanic, et al. (2007). "The PY motif of ENaC, mutated in Liddle syndrome, regulates channel internalization, sorting and mobilization from subapical pool." Traffic 8(9): 1246-64.

Malik, B., S. R. Price, et al. (2006). "Regulation of epithelial sodium channels by the ubiquitin-proteasome proteolytic pathway." Am J Physiol Renal Physiol 290(6): F1285-94.

Naga Prasad, S. V., A. Jayatilleke, et al. (2005). "Protein kinase activity of phosphoinositide 3-kinase regulates beta-adrenergic receptor endocytosis." Nat Cell Biol 7(8): 785-96.

Nikko, E. and H. R. Pelham (2009). "Arrestin-mediated endocytosis of yeast plasma membrane transporters." Traffic 10(12): 1856-67.

Nikko, E., J. A. Sullivan, et al. (2008). "Arrestin-like proteins mediate ubiquitination and endocytosis of the yeast metal transporter Smf1." EMBO Rep 9(12): 1216-21.

Pizzirusso, M. and A. Chang (2004). "Ubiquitin-mediated targeting of a mutant plasma membrane ATPase, Pma1-7, to the endosomal/vacuolar system in yeast." Mol Biol Cell 15(5): 2401-9.

Puthenveedu, M. A. and M. von Zastrow (2006). "Cargo regulates clathrin-coated pit dynamics." Cell 127(1): 113-24.

Rotin, D., O. Staub, et al. (2000). "Ubiquitination and endocytosis of plasma membrane proteins: role of Nedd4/Rsp5p family of ubiquitin-protein ligases." J Membr Biol 176(1): 1-17.

Shenoy, S. K. and R. J. Lefkowitz (2005). "Receptor-specific ubiquitination of beta-arrestin directs assembly and targeting of seven-transmembrane receptor signalosomes." J Biol Chem 280(15): 15315-24.

Shenoy, S. K., P. H. McDonald, et al. (2001). "Regulation of receptor fate by ubiquitination of activated beta 2-adrenergic receptor and beta-arrestin." Science 294(5545): 1307-13.

Soetens, O., J. O. De Craene, et al. (2001). "Ubiquitin is required for sorting to the vacuole of the yeast general amino acid permease, Gap1." J Biol Chem 276(47): 43949-57.

Staub, O., S. Dho, et al. (1996). "WW domains of Nedd4 bind to the proline-rich PY motifs in the epithelial Na+ channel deleted in Liddle's syndrome." EMBO J 15(10): 2371-80.

Wess, J., J. Liu, et al. (1997). "Structural basis of receptor/G protein coupling selectivity studied with muscarinic receptors as model systems." Life Sci 60(13-14): 1007-14.

Chapter IV

Conclusions and Future Directions

Conclusions

Cells have developed elaborate protein quality control systems to maintain cellular proteostasis. Secretory cargoes that cannot fold properly in the ER are targeted for removal by ERAD. Little is known about post-ER quality control mechanisms for integral membrane proteins. In my thesis, we present evidence that the E3 ubiquitin ligase Rsp5 and its adaptor network are part of a critical protein quality surveillance mechanism at the PM. Shifting cells to high temperature, a known proteotoxic stress, triggers global activation of Rsp5-dependent ubiquitination, endocytosis, and vacuolar trafficking of PM proteins. Mutants defective for this protective response exhibit toxic accumulation of integral membrane proteins at the cell surface and suffer catastrophic loss of PM integrity during misfolding stress, phenotypes that can be suppressed by the presence of chemical chaperones. We present the identification of specific Rsp5 adaptors, which target the ubiquitination of misfolded PM proteins during proteotoxic stress. Genetic interaction analysis reveals that this PM quality surveillance mechanism exhibits striking synthetic defects with components of both ERAD and the unfolded protein response, indicating that different quality control pathways cooperate to protect cells during misfolding stress. We propose that this ubiquitin-mediated PM quality surveillance pathway, together with other quality control pathways like ERAD, protects cells from

proteotoxic stress by limiting the toxic accumulation of misfolded integral membrane proteins at the PM.

Future Directions

Investigate the mechanism of recognition of misfolded membrane proteins

Protein quality control requires the ability to distinguish between native and misfolded states of a protein. Ultimately, understanding how misfolded proteins are recognized involves investigating the mechanisms of E3 ligase substrate targeting. Although quality control mechanisms that distinguish native from misfolded proteins are still poorly understood, there are a few examples that give us some clue about substrate recognition. Molecular chaperones have been predicted to contain intrinsically disordered regions, which play key roles in misfolded protein recognition. Hsp10 can recognize a broad spectrum of misfolded proteins and there is no defined common domain among those substrates. Intrinsically disordered regions are predicted across the protein, especially in the C terminal lid domain of Hsp10, where substrates bind. Misfolded proteins are prone to aggregate and tightly associate with chaperones such as Hsp70 and Hsp40. The cytosolic E3 ligase CHIP does not recognize misfolded proteins directly, but instead interacts with the chaperone Hsp70. CHIP binds to Hsp70 via its TRP domain which allows it to target aberrant proteins for ubiquitination (Connell, Ballinger et al. 2001; Murata, Minami et al. 2001). Although the yeast genome does not encode a CHIP homolog, the yeast ubiquitin ligases Ubr1 and Ubr2 can target substrates by interaction with Hsp70 and Hsp110 (Heck, Cheung et al. 2010; Nillegoda, Theodoraki et al. 2010). Thus, indirect targeting via chaperone association appears to be a major mechanism of misfolded protein recognition. In contrast, the nuclear-localized ubiquitin ligase San1 has its own intrinsically disordered domain which can bind directly to many different

substrates and target them for ubiquitination (Gardner, Nelson et al. 2005). Despite these examples, recognition of misfolded proteins in the cell is still very poorly understood. Based on our results, the E3 ligase Rsp5 also does not recognize midfolded substrates directly, but instead is targeted to misfolded proteins indirectly by ART family proteins. However, the mechanism of ART-mediated recognition of misfolded PM substrates is still unclear. From previous mammalian arrestin-receptor interaction studies and our observation in yeast, it seems likely that the arrestin fold is the substrate interaction domain of ART proteins (Vishnivetskiy, Hosey et al. 2004). Arrestin fold mutants exhibit temperature sensitive phenotypes similar to art1 null cells (Figure 4.1B). Future experiments should address: (1) how misfolded plasma membrane proteins are recognized by ARTs during proteotoxic stress, and (2) the substrate recognition code of ART proteins.

Figure 4.1

A

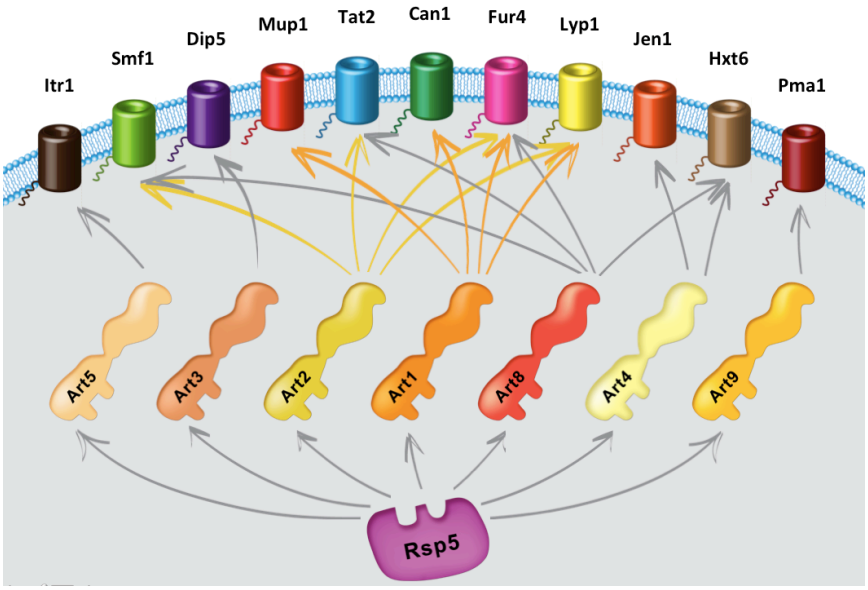
Itr1
Smf1
Dip5
Mup1
Tat2
Can1
Fur4
Lyp1
Jen1
Hxt6
Pma1
Art5
Art3
Art2
Art1
Art8
Art4
Art9
Rsp5

B

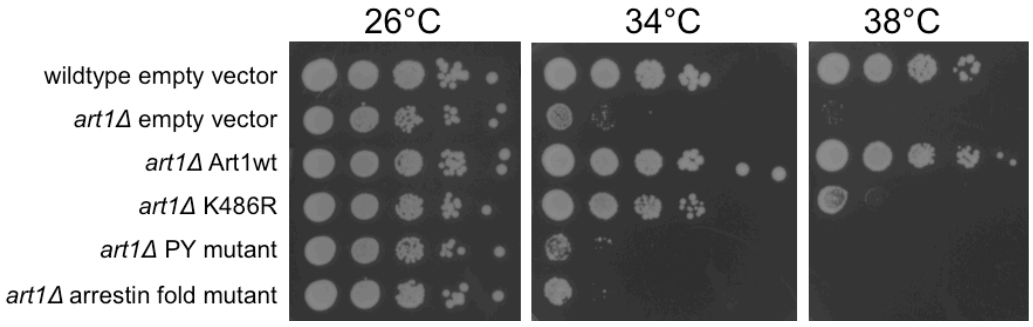
26°C
34°C
38°C
wildtype empty vector
art1Δ empty vector
art1Δ Art1wt
art1Δ K486R
art1Δ PY mutant
art1Δ arrestin fold mutant

Figure 4.1

(A) Under different stimulation condition, different Art family proteins are activated to recruit Rsp5 to ubiquitinate various distinct membrane proteins.
(Becuwe, Vieira et al. ; Hatakeyama, Kamiya et al. ; Lin, MacGurn et al. 2008; Nikko and Pelham 2009) (Kane P, unpublished results)

(B) Similar to art1 null cells, arrestin fold mutant exhibits temperature sensitive growth phenotype.

Detection of membrane protein misfolding under the heat stress

Integral membrane proteins have domains that span lipid bilayers and are anchored in membranes. Transmembrane spanning segments typically have alpha helical secondary structure and are relatively stable. However, under stress conditions, transmembrane domains and soluble portions of proteins can transit through aberrant conformations or misfold, and these partially misfolded membrane proteins could be toxic and threaten the integrity of the plasma membrane lipid bilayer. However, we do not have direct evidence that membrane proteins misfolded at high temperature. Demosntrating misfolding of a transmembrane spanning protein is technically challenging for a variety of reasons. For example, the cargoes we study are often members of the major facilitator family of transporters which contain 12-13 transmembrane domains, making them difficult to isolate in a native state. Additionally, aberrant conformations of transmembrane domains might cause severe leakage and lose of membrane integrity without resulting in gross misfolding of the protein. It may be hard to detect subtle conformational changes. Given these limitations, I observed that mutant Lyp1 K10XR tended to form patch structure in the cells, which are absent in wildtype Lyp1 cells (Figure 4.2 A). We have tested immunoprecipitation experiments in the presence of crosslinkers to capture aggregation and use denaturing conditions to extract transmembrane proteins. We haven't been able to capture these aggregates (data not shown).

Although it is challenging to demonstrate that ART substrates are misfolded at high temperature, there are some indirect ways to test the hypothesis. We tried the yeast

homolog of CFTR (Apaja et al., 2010), Yor1. The Yor1 mutation equivalent to the ΔF508 CFTR was mainly observed in the ER even at low temperature and in the presence of glycerol. Another strategy involves the use of mutant cargo alleles which exhibit decreased stability at the PM, presumably caused by misfolding. For example, Pma1 is turned over during thermal stress (40°C), however, the mutant protein pma1-10 is misfolded and turned over at 34°C (Gong and Chang, 2001). Similar mutant alleles of Ste2 also exhibit shorter half lives compared with wildtype Ste2 (Jenness et al., 1997). We will test if these unstable mutant proteins are substrates of ARTs and the Rsp5 pathway.

Misfolded proteins lose their native structure and function. Based on this, we can test the function of PM proteins at steady state and high temperature. To prevent endocytosis of PM proteins at high temperature, we will measure the lysine uptake of Lyp1-10XR mutant, which we know cannot be ubiquitinated and will stay at the PM at high temperature. Differences in lysine uptake activity at high temperature would therefore indicate protein misfolding or aberrant transporter conformations.

Identification of molecular chaperones that promote folding of plasma membrane proteins

In Chapter II, I have shown that under thermal stress accumulation of protein at the PM is toxic to cells. In the ER, there are refolding chaperones and also ubiquitin mediated ERAD to deal with protein misfolding stress. Similar chaperone refolding systems are also present in the cytosol. Under proteotoxic stress conditions, both chaperones and ubiquitin-mediated degradation mechanisms will be activated to protect cells from toxic aggregation. In Chapter II, we showed that the ART-Rsp5 network is part of a critical protein quality surveillance mechanism at the PM. We reasoned that upstream to ARTs-Rsp5 mediated ubiquitinaiton there may be a mechanism to refold the misfolded/damaged proteins and prevent toxic accumulation of misfolded proteins. We have tested several chaperone knock out mutants but at present we have not identified any single chaperone mutant with a temperature sensitive phenotype.

Overexpression of the Lyp1 K10XR mutant protein leads to a temperature sensitivity phenotype. Taking advantage of this phenotype, a multicopy suppressor screen for growth at restrictive temperature could identify potential membrane protein chaperones. However, our previous overexpression of lyp1 10XR mutant is on a plasmid, and protein levels might vary from cell-to-cell. By this method, we hope to determine if any chaperones or any heat shock proteins can suppress the toxic accumulation of nonubiquitinated lyp1. Such genetic approaches could reveal

factors that help to stabilize the native folded state of integral membrane proteins at the PM. Such factors could include chaperones or regulators of PM lipid composition.

Figure 4.2

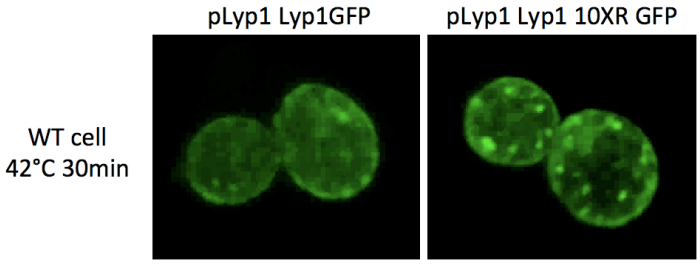

Figure 4.2

Three dimensional projection of cells expressing wildtype Lyp1GFP or lyp1 N terminal lysine mutant (10XR) under the heat stress condition.

Reference:

Apaja, P.M., Xu, H., and Lukacs, G.L. (2010). Quality control for unfolded proteins at the plasma membrane. J Cell Biol *191*, 553-570.

Connell, P., C. A. Ballinger, et al. (2001). "The co-chaperone CHIP regulates protein triage decisions mediated by heat-shock proteins." Nat Cell Biol **3**(1): 93-6.

Gong, X., and Chang, A. (2001). A mutant plasma membrane ATPase, Pma1-10, is defective in stability at the yeast cell surface. Proc Natl Acad Sci U S A *98*, 9104-9109.

Gardner, R. G., Z. W. Nelson, et al. (2005). "Degradation-mediated protein quality control in the nucleus." Cell **120**(6): 803-15.

Jenness, D.D., Li, Y., Tipper, C., and Spatrick, P. (1997). Elimination of defective alpha-factor pheromone receptors. Mol Cell Biol *17*, 6236-6245.

Heck, J. W., S. K. Cheung, et al. (2010). "Cytoplasmic protein quality control degradation mediated by parallel actions of the E3 ubiquitin ligases Ubr1 and San1." Proc Natl Acad Sci U S A **107**(3): 1106-11.

Murata, S., Y. Minami, et al. (2001). "CHIP is a chaperone-dependent E3 ligase that ubiquitylates unfolded protein." EMBO Rep **2**(12): 1133-8.

Murata, S., H. Udono, et al. (2001). "Immunoproteasome assembly and antigen presentation in mice lacking both PA28alpha and PA28beta." EMBO J **20**(21): 5898-907.

Nillegoda, N. B., M. A. Theodoraki, et al. (2010). "Ubr1 and Ubr2 function in a quality control pathway for degradation of unfolded cytosolic proteins." Mol Biol Cell **21**(13): 2102-16.

Becuwe, M., N. Vieira, et al. "A molecular switch on an arrestin-like protein relays glucose signaling to transporter endocytosis." J Cell Biol 196(2): 247-59.

Connell, P., C. A. Ballinger, et al. (2001). "The co-chaperone CHIP regulates protein triage decisions mediated by heat-shock proteins." Nat Cell Biol 3(1): 93-6.

Gardner, R. G., Z. W. Nelson, et al. (2005). "Degradation-mediated protein quality control in the nucleus." Cell 120(6): 803-15.

Hatakeyama, R., M. Kamiya, et al. "Endocytosis of the aspartic acid/glutamic acid transporter Dip5 is triggered by substrate-dependent recruitment of the Rsp5 ubiquitin ligase via the arrestin-like protein Aly2." Mol Cell Biol 30(24): 5598-607.

Heck, J. W., S. K. Cheung, et al. (2010). "Cytoplasmic protein quality control degradation mediated by parallel actions of the E3 ubiquitin ligases Ubr1 and San1." Proc Natl Acad Sci U S A 107(3): 1106-11.

Lin, C. H., J. A. MacGurn, et al. (2008). "Arrestin-related ubiquitin-ligase adaptors regulate endocytosis and protein turnover at the cell surface." Cell 135(4): 714-25.

Murata, S., Y. Minami, et al. (2001). "CHIP is a chaperone-dependent E3 ligase that ubiquitylates unfolded protein." EMBO Rep 2(12): 1133-8.

Nikko, E. and H. R. Pelham (2009). "Arrestin-mediated endocytosis of yeast plasma membrane transporters." Traffic 10(12): 1856-67.

Nillegoda, N. B., M. A. Theodoraki, et al. (2010). "Ubr1 and Ubr2 function in a quality control pathway for degradation of unfolded cytosolic proteins." Mol Biol Cell 21(13): 2102-16.

Vishnivetskiy, S. A., M. M. Hosey, et al. (2004). "Mapping the arrestin-receptor interface. Structural elements responsible for receptor specificity of arrestin proteins." J Biol Chem 279(2): 1262-8.

Chapter V

The endosomal sorting complex ESCRT-II mediates the assembly and architecture of ESCRT-III helices

Chapter V is the paper currently in press in *Cell*. The endosomal sorting complex ESCRT-II mediates the assembly and architecture of ESCRT-III helices. William Mike Henne, Nicholas J. Buchkovich, Yingying Zhao, and Scott D. Emr (author name with underline contributed equally to this study). Yingying's contribution to this chapter is helping development of novel flow cytometry assay to quantify vacuole protein sorting in yeast. Her work is presented in Figure 4L and Figure S4B C.

Introduction

The endosomal sorting complexes required for transport (ESCRTs) constitute the sorting machinery that delivers ubiquitinated transmembrane cargoes from the endosomal surface into its interior and ultimately into the vacuole lumen (lysosome in mammals). To ensure vacuole delivery, cell surface cargoes are ubiquitinated, endocytosed, and trafficked to endosomes. There, the ESCRT machinery recognizes their ubiquitin moiety and mediates their deubiquitination before packaging them into intraluminal vesicles (ILVs) that bud into the interior of late endosomes, creating multivesicular bodies (MVBs). MVB biogenesis is achieved by the coordinated action of five distinct ESCRT complexes (ESCRTs-0, -I, -II, -III, and the Vps4-Vta1 complex) (Babst 2011; Henne, Buchkovich et al. 2011). The failure of ESCRTs to properly sort cargoes is associated with numerous pathologies including cancer and various neurodegenerative diseases (Saksena and Emr 2009). Furthermore, many viruses including HIV-1 rely on ESCRT machinery to exit

infected cells, highlighting the central role of the ESCRT pathway in the study of human disease.

The ESCRT pathway executes MVB biogenesis through an exquisite division of labor. ESCRTs-0, -I, and –II are soluble hetero-oligomers that are recruited to cargo-laden endosomes by binding both the compartment-specific lipid phosphatidylinositol-3-phosphate (PtdIns(3)P) and ubiquitin-modified cargo. In addition, the ESCRT-II complex also initiates the assembly of ESCRT-III. This hetero-oligomeric complex is composed of four core subunits (Vps20, Snf7/Vps32, Vps24, and Vps2; CHMPs in mammals) and has recently been highlighted as the minimal machinery necessary to form ILVs in vitro (Hanson, Roth et al. 2008; Saksena, Wahlman et al. 2009; Wollert and Hurley 2010).

Previous studies indicate that ESCRT-III does not assemble into a stable complex. Rather, its subunits cycle between an inactive monomeric state in the cytoplasm and an assembled polymer at endosomes (Babst, Katzmann et al. 2002). ESCRT-III assembly is thus both temporally ordered and transient. ESCRT-II engages Vps20 and triggers Snf7 homo-oligomerization. Snf7 then recruits Vps24 and Vps2 which contain high affinity MIT-interacting motifs (MIMs) necessary to recruit the AAA ATPase Vps4 to immediately disassemble the complex (Teis, Saksena et al. 2008; Saksena, Wahlman et al. 2009).

Intraluminal vesicle formation is directly coupled to the ordered assembly of ESCRT-III. This is a biologically unique form of vesicle budding that is topologically inverted from "classical" vesicle formation (e.g.: clathrin and COP-coated) (Doherty and McMahon 2009). As such, the mechanism for ILV formation is unclear. Furthermore, the molecular architecture ESCRT-III adopts to drive ILV formation remains a key question in the field. Previous studies indicate that ESCRT-III assembly is initiated by conformational changes in each of its subunits that promote their association with each other and the endosome. These conformational changes involve the disruption of intramolecular interactions between the basic N-terminus with the acidic C-terminal region (Zamborlini, Usami et al. 2006; Shim, Kimpler et al. 2007). In agreement with this, recent X-ray crystal structures show that soluble ESCRT-III subunits exist in "closed" conformations with numerous intramolecular interactions between the highly structured N-terminal "core domain" and the more flexible C-terminus (Muziol, Pineda-Molina et al. 2006; Bajorek, Schubert et al. 2009) (Figure 1A). Subunit truncations, which remove these auto-inhibitory C-terminal regions, result in subunit auto-activation and the spontaneous assembly of ESCRT-III polymers in vivo and in vitro (Hanson, Roth et al. 2008; Lata, Roessle et al. 2008). However, past studies display one or more limitations: 1) they rely on the extensive manipulation of ESCRT-III subunits, often deleting up to ~48% of subunits to drive polymer assembly, 2) polymers are very heterogeneous and form linear protofilaments, rings, domes, cylinders, and sheet-like lattices, making their physiological relevance unclear, 3) they are not comprehensive and focus on only

one or a few ESCRT subunits, or 4) microscopic visualization of ESCRT-III on lipid membranes is generally limited to the resolution of light microscopy.

Here, we elucidate the molecular architecture of the ESCRT-III complexes that assemble on lipid monolayers. Furthermore, by reconstituting and visualizing distinct sub-reactions of ESCRT-III assembly, we present a comprehensive structural explanation elucidating how transmembrane cargoes are first sequestered and ultimately sorted into ILVs.

Experimental Procedures:

Negative stain transmission electron microscopy

Samples were incubated for 30 minutes at room temperature, then added to carbon-coated Formvar grids (EMS). Droplets were incubated for 10 minutes, then negative stained. All samples were examined on a FEI Morgnani Transmission Electron Microscope at 80-100kV. Digital images were taken using an AMT camera. Micrographs are representative of results from multiple experimental sessions. Distance quantitation was conducted using ImageJ (NIH). For additional information, see Supplemental Data.

Liposome flotation assays

1mg/mL of 60%phosphatidylcholine (PC):30% phosphatidylserine (PS):10% phosphatidylinositol 3-phosphate (PtdIns(3)P) (Avanti) liposomes were generated by classical dehydration in a chloroform:methanol mix, then resuspended in 500μL Buffer A. Liposomes were sonciated for 1 minute, then mixed with 14μM protein and incubated for 30 minutes. Samples were resuspended in 30% sucrose buffer layered with a 20% and 0% cushion and centrifuged in a TLS-55 ultracentrifuge rotor (Beckman Coulter) for 1 hour at 55k rpm. The top "float" fraction was separated from the bottom "unbound" fraction, TCA precipitated, run on SDS-PAGE gels, and Coomassie stained.

Mup1-pHluorin ESCRT cargo sorting assay and flow cytometry

A yeast strain (NBY44) stably expressing Mup1-pHluorin and ectopically expressing various Snf7 constructs was incubated to early log growth. Mup1-pHuorin endocytic uptake was induced by addition of methionine as previously described (Lin, MacGurn et al. 2008). Yeast were reconstituted into PBS and analyzed using a BD Bioscience LSRII cytometer. Approximately ~100,000 yeast per expt. were evaluated in at least three independent experiments for each mutant. Sorting profiles were obtained by overlaying the composite wildtype trace on composite mutant traces.

Cloning, bacterial expression, and in vitro *purification of ESCRT subunits*

Saccharomyces cerevisiae Vps20, Snf7, Vps24, and Vps2 were cloned into the pET23d bacterial expression vector (Novagen) with a homemade N-terminal His6-tag, expressed from either BL21 or C41(DE3) *E.coli* cells, and purified by TALON® (Clontech) metal bead affinity purification. GST-Vps25 was cloned into pGEX6P1 vector and purified on GSH-sepharose beads (GE Healthcare). All constructs were verified by DNA sequencing. All expression preps were grown initially at 37°C until a cell OD_{600} of ~0.6-0.8, then induced with IPTG as described below. Optimal expression conditions varied for each protein and are denoted in Supplemental Table 1. During purification, proteins were reconstituted in 500mM NaCl, 20mM HEPES pH7.4, 5mM imidazole buffer. Protein-bound TALON® beads were washed in 500mM NaCl, 20mM HEPES pH7.4, 20mM imidazole, and eluted in 150mM NaCl, 20mM HEPES pH7.4, 400mM imidazole. Samples were dialyzed overnight to remove excess imidazole. GST-Vps25 was

eluted by addition of 10mM reduced glutathione (Sigma-Aldrich), and underwent two-rounds of dialysis to ensure removal of glutathione. Proteins were reconstituted into a final buffer of 150mM NaCl, 20mM HEPES pH7.4. All reconstituted proteins used in this study were routinely run on SDS-PAGE gels and Commassie-stained to access the protein integrity and purity (e.g.: Figures S5C and S7G).

Generation of S. cerevisiae Snf7 model using Modeller software

Using the crystal structure of human Vps24 (pdb: 3FRT), a three-dimensional model of *Saccharomyces cerevisiae* Snf7 (resdues 1-183) was generated using the comparative protein structure modeling program Modeller (Eswar, Webb et al. 2007). The model was visualized using the molecular graphics program CCP4mg (McNicholas, Potterton et al. 2011).

Negative stain transmission electron microscopy studies

Samples were incubated for 30 minutes at room temperature, then added dropwise to carbon-coated Formvar grids (EMS). Droplets were incubated for 10 minutes unless specified, then desiccated and negative stained. For negative staining, 4% uranyl acetate or 2% ammonium molybdate were added for 30 seconds, then samples were desiccated and briefly air-dried. For samples using Ni^{2+} NTA-coated 5nm nano-gold beads (Nanoprobes), protein samples were first incubated with a 1:25 dilution of nano-gold beads, then added to the experimental mixture before being added to TEM grids. For order-of-addition experiments, samples were allowed to incubate on grids for 3 minutes, followed

by a gentle dehydration by wicking away the liquid and a quick addition of a buffer droplet for washing. Subsequent protein was then added for 3 more minutes, followed by dehydration and negative staining. Note: being gentle was *essential*, as early attempts to do this sequential addition led to breaks in the Formvar® coating.

For lipid monolayer experiments, monolayers of defined lipid composition [20% phophatidylethanolamine (PE), 40% phosphatidylcholine (PC), 30% phosphatidylserine (PS),10% phophatidylinositol 3-phosphate (PtdIns(3)P), unless otherwise indicated] (Avanti) were generated in a monolayer apparatus by dissolving lipids in 95:5 chloroform:methanol and pipetting 1.5μL onto the surface of the reaction well containing Buffer A (150mM NaCl, 20mM HEPES pH7.4). After 1 hour to allow the evaporation of the chloroform:methanol, monolayers spontaneously formed and were adhered to Formvar® carbon-coated TEM grids by placing them over the monolayer. Proteins were then added via the injection well, and given 20 minutes to assemble on monolayers before negative staining.

All samples were examined on a FEI Morgnani Transmission Electron Microscope at 80-100kV. Digital images were taken using an AMT camera. Micrographs are representative of results from multiple independent experimental sessions. Image analysis and distance quantitation were conducted using ImageJ software (NIH).

The table below summarizes the proteins, their concentrations, and negative stains used for the TEM micrographs in each Figure. For negative

stains, 4% uranyl acetate is denoted as “UA” and 2% ammonium molybdate as “AM”. Monolayer is also abbreviated “ML”.

Fluorescence light microscopy and imaging of yeast

Living yeast were imaged using a DeltaVision RT system (Applied Precision), consisting of a Photometrics CoolSNAP HQ Camera, an Olympus IX71 Microscope and a DeltaVision RT Standard Filter (FITC for GFP/pHluorin samples, and RD-TR-Cy3 for FM-464). Image acquisition, deconvolution, and analysis were performed in the program Softworx.

Yeast fractionation and co-immunoprecipitation assays

A total of 15 OD_{600} of living yeast were, centrifuged, resuspended in spheroplasting media containing zymolase to remove the cell wall, washed, and ruptured on ice in a pre-chilled cell douncer. Yeast lysate was resuspended in 1mL of lysis buffer (50mM Tris pH7.4, 10mM EDTA, 200mM sorbitol, and protease inhibitor cocktail). For subcellular fractionation assays, lysate was centrifuged for 5 minutes at 500xg at 10°C as a general “clearance spin” to pellet cell debris. The supernatant was then collected into a fresh ependorf and a 10 minute 13,000xg P13 spin was done at 10°C. The supernatant (S13) was separated from the pellet (P13) fraction and both samples were precipitated in 10% trichloroacetic acid (TCA). Samples were boiled in sample buffer, run on 10% SDS-PAGE gels, transferred to PVDF membrane, and Western blotted using an in house anti-rabbit Snf7 antibody (Babst, Wendland et al. 1998).

Western blots were developed on film using SuperSignal West Pico ECL (Thermo Scientific).

For co-immunoprecipitation assays, 15-25 OD_{600} of yeast were grown and lysed in a douncer as described above. A 1% final concentration Triton X-100 buffer was added to the supernatant and samples were left on ice for 15 minutes. Samples were then given one 13,000xg 10 minute "clearance spin" at 10°C. A 10% input aliquot was removed. 25μL of EZ View™ anti-FLAG M2 affinity gel beads (Sigma Aldrich) was added to the remaining ~900μL of supernatant, and samples were incubated for 1 hour at 10°C on a rotator. Samples were then sequentially centrifuged and washed 3 times in lysis buffer, then TCA precipitated, run on SDS-PAGE gels, and Western blotted.

Snf7^{redox} conformational monitoring assay

Reconstituted Snf7^{redox} was purified and resuspended in Buffer A. Initial purifications in Buffer A indicated that Snf7^{redox} existed in mixed oxidized/reduced populations, so a low concentration (~500μM) of DTT was added to generate a uniformly "open" Snf7^{redox} that could undergo conformational changes. This Snf7^{redox} was then incubated at 15μM final concentration with 0.5mg/mL liposomes (SUVs) and/or Vps20 and GST-Vps25 for 30 minutes at room temperature in 100μL volumes. Experiments which tested the ability of R52E or L67E to open Snf7^{redox} were conducted in Buffer A.

The oxidizing chemical Copper(II) phenathroline (Cu(1,10-phenathroline)$_2SO_4$) (Cu^{2+}Phen) was freshly prepared by separately preparing 200mM of 1,10-phenanthroline (Phen) in ethanol and 50mM of copper (II) sulfate

($CuSO_4$) in Ionic Buffer (150mM potassium acetate, 5mM magnesium acetate, 250mM sorbitol, 20mM HEPES pH7.0). Equal volumes of Phen and $CuSO_4$ were then mixed creating a brilliant aqua-colored Cu^{2+}Phen solution with a white precipitate. To oxidize proteins, 100μL of the Cu^{2+}Phen supernatant was added, instantly crosslinking $Snf7^{redox}$ in its current conformational state. Cu^{2+}Phen solution undergoes a color change when reduced from a brilliant green to a dark brown, so confirmation of the sample's oxidation is instantaneous. Samples were then TCA precipitated, run on SDS-PAGE gels, and Coomassie stained to evaluate the conformation of $Snf7^{redox}$.

For experiments conducted in Figure 2C, protein concentrations were-- $Snf7^{redox}$: 15μM in all lanes; Vps20: 75nM (1:200), 750nM (1:20), 3μM (1:5). GST-Vps25: 50nM (1:200), 400nM (1:20), 1.5μM (1:5).

Mup1-pHluorin ESCRT cargo sorting assay and flow cytometry

A *SNF7::His3*, *MUP1-pHluorin::kan* yeast strain (NBY44) was created by mating a *SNF7::His3* (MBY24) strain to a *MUP1-pHlourin::kan* strain (NBY39), which was generated using the integrating plasmid pBW1571, a kind gift from Beverly Wendlend (Prosser, Whitworth et al. 2010). Wildtype and mutant Snf7 proteins were expressed ectopically in NBY44 using the pRS416 plasmid containing the endogenous Snf7 promoter. For both microscopy and flow cytometry analysis, early log cultures were grown to mid-log in the presence of methionine to induce the delivery of MUP1-pHluorin to the vacuole. Microscopic analysis was performed as described the Experimental Procedures. For flow cytometry analysis, mid-log cultures were pelleted and resuspended in PBS for

analysis on a BD Bioscience LSRII cytometer. For each sample, ~100,000 cells were counted from three cultures originating from three distinct yeast colonies and combined for a total analysis of ~300,000 cells. The sorting profiles were obtained by overlaying the composite wildtype trace on the composite mutant traces. For statistical analysis, each of the three WT samples was subtracted as background from each of the individual mutant samples. The cells remaining after background subtraction were counted as those eliciting a sorting defect distinct from the wildtype population, and were used to calculate the sorting score and standard deviation for each composite mutant population. For sample comparisons, the wildtype and vector samples were set at 100 and 0, respectively, and the mutants were normalized to these values.

GUV-based light microscopy experiments

GUVs of composition 35%phosphatidylcholine(PC): 30%phosphatidylserine(PS):25%cholesterol:10%phosphatidylinositol 3-phosphate(PtdIns(3)P) were made fluorescent by adding 0.05% of the lipophilic dye DiI (Invitrogen), and were created by dehydration:rehydration of lipid films on glass coverslips. GUVs were resuspended in 150mM NaCl, 20mM HEPES pH7.4 buffer. To fluorescently label Snf7^{R52E}, we introduced a cysteine at residue 187 (along a region of the protein unaffected upon manipulation/deletion (Figure S4J)), creating Snf7$^{R52E+V187C}$. We purified this protein from *E.coli* and covalently attached a maleimide-conjugatable Alexa488 fluorophore (Invitrogen) to C187. Excess fluorophore was removed by dialysis and the protein was evaluated on

SDS-PAGE gels. For experiments, GUVs and protein were mixed in eppendorf tubes for 10 minutes, then pipetted onto glass-bottom coverslip dishes (MatTek) coated with 1mg/mL BSA to prevent the collapse of GUVs onto the glass. Protein concentrations were: $Vps20^{core}$: 600nM, $Snf7^{R52E}$-A488: 3μM, Vps24: 1.5μM, Vps2: 1.5μM.

All GUV experiments were conducted using a 100x magnification lens on a spinning disc confocal microscopy system (3I Corp) using a DMI 6000B microscope (Leica) and digital camera (QuantEM; Photometrics). Images were analyzed and processed using Slidebook 5. Movies were compiled from images captured at half-second intervals using ImageJ (NIH).

Results

Experimental Rationale

To investigate the molecular mechanism governing ESCRT-III assembly, we designed a three-stage research strategy. In the first stage, we investigated the conformational changes that convert ESCRT-III subunits from inactive monomers into an assembled complex. We began by mapping regions shared by all four ESCRT-III core subunits which are necessary for assembly into a complex, and then focused on Snf7, the most abundant subunit within ESCRT-III, as a model to indentify conformational changes that promote its activation. In the second stage, we reconstituted Snf7 assembly on lipid monolayers and addressed the molecular mechanism governing Snf7 homo-oligomerization. In our final stage, we visualized the co-assembly of ESCRTs-II and -III and propose a model describing how ESCRT-III is transformed from a cargo-capturing ring into a membrane sculpting helix to achieve cargo sorting into MVBs.

ESCRT-III "core" domains mediate ESCRT-III assembly

Previous studies demonstrate that ESCRT-III subunits are sequentially recruited by ESCRT-II to the surface of endosomes (Teis, Saksena et al. 2008). ESCRT-II directly binds Vps20, which promotes the sequential recruitment of Snf7, Vps24, and Vps2 to form the hetero-tetrameric ESCRT-III complex (Figure 1A)(Teis, Saksena et al. 2008). All four of these ESCRT-III subunits are predicted to share a common domain architecture of four alpha helices bundled into an N-terminal core domain, followed by an unstructured C-terminal region (Figure 1A). To better understand the molecular architecture of the ESCRT-III complex, we first wanted to define architectural regions shared by its subunits that govern protein-protein and protein-endosome interactions.

To do this, we generated subunit truncations for each ESCRT-III subunit and asked if they retained endosomal localization and could interact with other ESCRT subunits. The N-terminal core domains (which lack their C-terminal regions and contain only alpha helices1-4) of Vps20, Snf7, Vps24, and Vps2 were fused to GFP and ectopically expressed in yeast lacking an endogenous copy of each subunit. Like their full-length counterparts, the core domains of all four ESCRT-III subunits localize to distinct intracellular punctae (Figure 1B-D and Figure S1A).

We hypothesized that these punctae were class E compartments, aberrant endosome-derived structures generated whenever the ESCRT pathway is blocked (Raymond, Howald-Stevenson et al. 1992). To confirm this, yeast were co-labeled

with the fluorescent membrane dye FM4-64, which accumulates in class E compartments. Vps20core, Snf7core, Vps24core, and Vps2core-GFP all co-localize with FM4-64, confirming their endosomal localization.

We next asked if each ESCRT-III core domain was sufficient to recruit a downstream ESCRT-III subunit to endosomal membranes. To test this, we took advantage of the observation that Snf7-GFP normally localizes to the class E compartment, but is redistributed into the cytoplasm in vps20Δ cells (Figure 1E). Ectopic expression of Vps20core rescues Snf7-GFP endosomal localization, confirming Vps20core is sufficient to recruit Snf7 (Figure 1E). Similar experiments in snf7Δ and vps24Δ yeast confirm that both Snf7core and Vps24core are sufficient to recruit their respective downstream subunits (Vps24 and Vps2, respectively) to endosomal membranes (Figure 1F&G). Further truncation of Snf7 to helices1-3 proved insufficient to recruit Vps24-GFP to class E compartments, although this truncation was sufficient to localize to class E compartments (Figure S1B, and unpublished observations). This suggests the need for an intact Snf7 core domain for Vps24 recruitment. Altogether, this indicates that the molecular architecture of the ESCRT-III complex relies primarily on core-core interactions between its subunits and the endosome.

Figure 1- N-terminal core domains mediate ESCRT-III assembly.

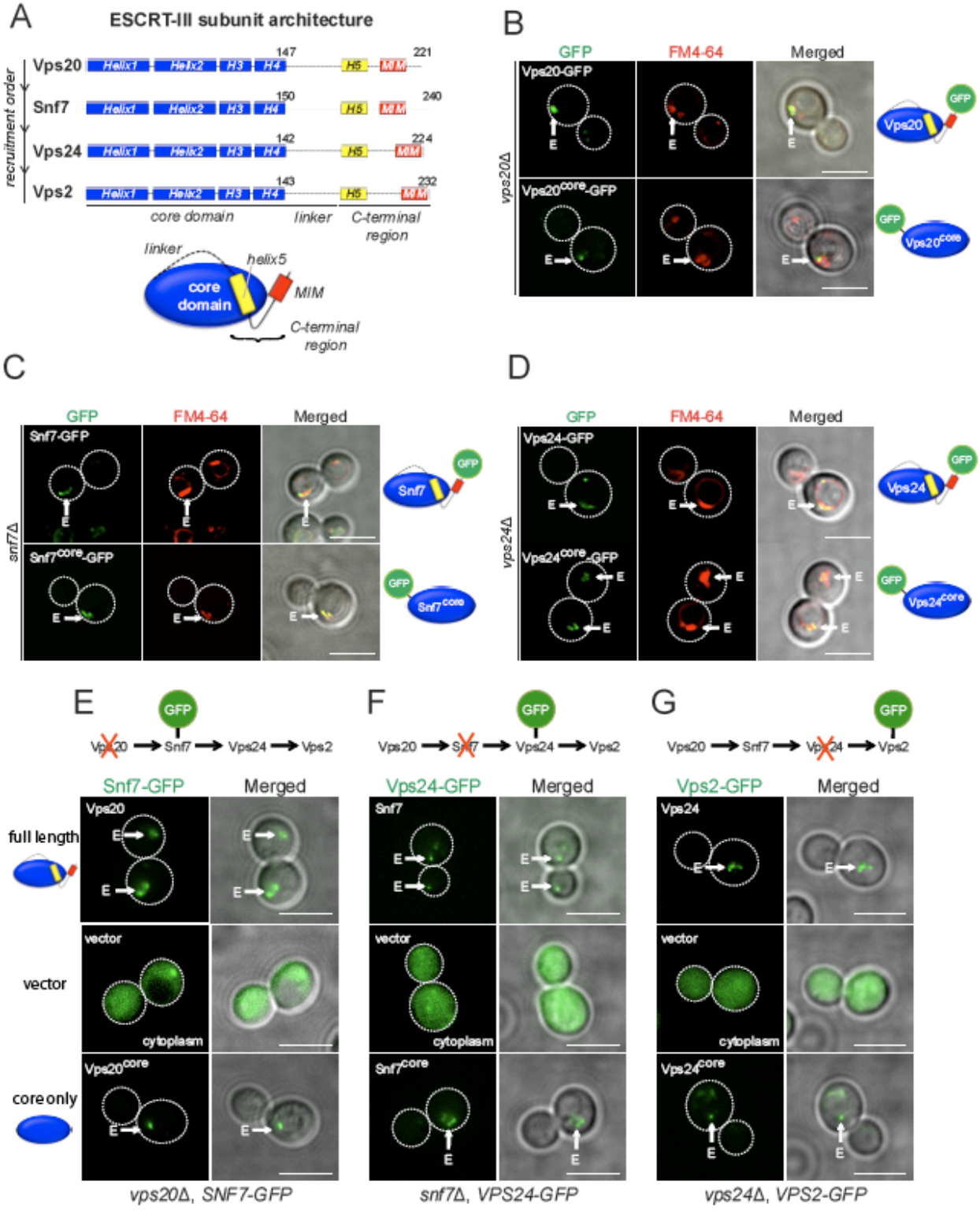

Figure 1- N-terminal core domains mediate ESCRT-III assembly.

(A) Schematic of ESCRT-III subunit architectures. Helices are denoted as boxes. The MIT interacting motif (MIM) is red.

(B-D) Representative images of vps20Δ, snf7Δ, or vps24Δ yeast expressing GFP-tagged full length or core domains of ESCRT-III subunits (green). Class E compartments are labeled with FM4-64 (red). Merged panels include GFP, FM4-64, and DIC images.

(E-G) Yeast lacking an ESCRT-III subunit and stably expressing a GFP-tagged downstream subunit are ectopically expressing either full length (top), vector (middle), or core domains (bottom). E: class E compartment. Scale bar: 5μm.

Figure 1S

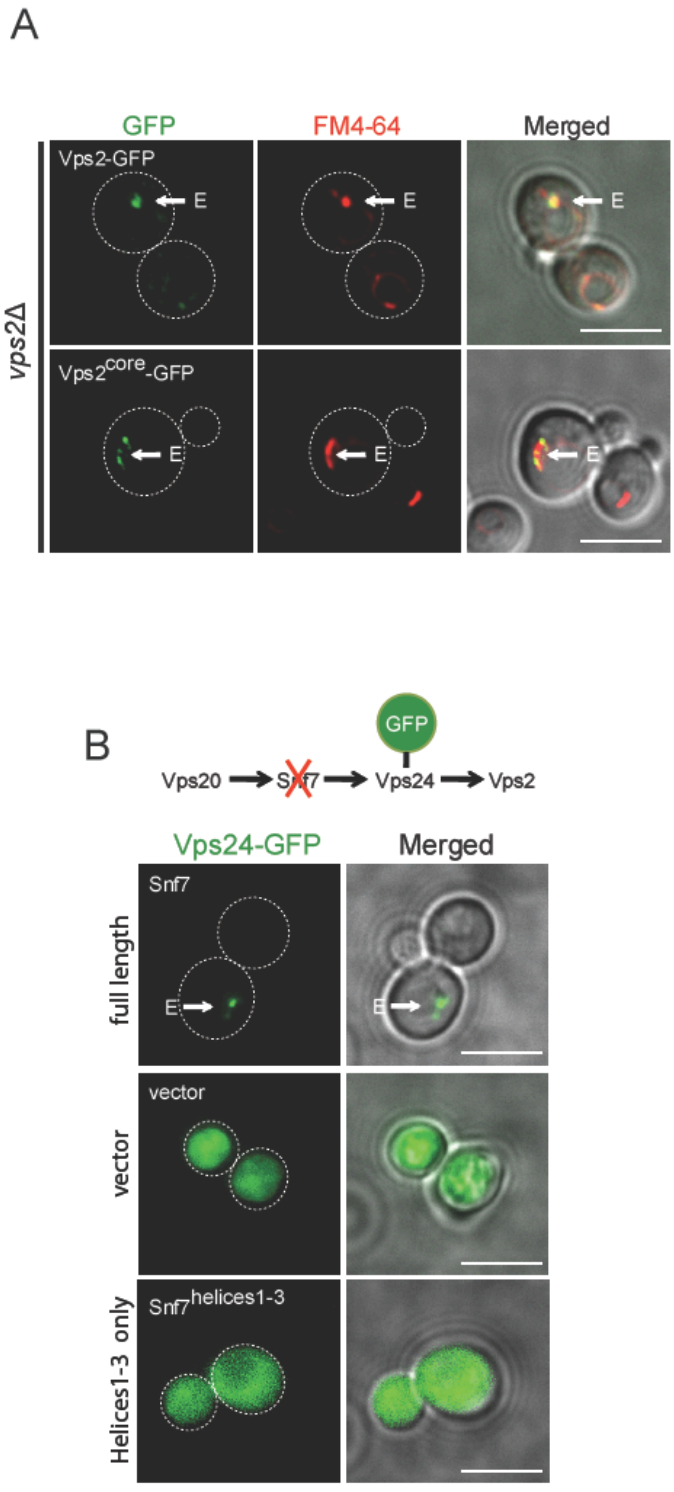
A
GFP
FM4-64
Merged
Vps2-GFP
vps2Δ
Vps2core-GFP
E
B
GFP
Vps20
Snf7
Vps24
Vps2
Vps24-GFP
Merged
full length
vector
Snf7helices1-3
Helices1-3 only

Figure 1S

A) Representative images localizing GFP-tagged Vps2 and Vps2^{core} (green) to endosomal membrane. FM4-64 is red.

B) Snf7$^{helices1\text{-}3}$ cannot recruit Vps24-GFP (green) to the class E compartment. Scale bars: 5μm.

Snf7 is activated by displacement of helix5 away from the core

Since all ESCRT-III N-terminal core domains are sufficient to localize to endosomal membrane and recruit other subunits of the ESCRT-III complex, we reasoned that conformational changes displacing the auto-inhibitory C-terminus promote ESCRT-III assembly by exposing core contacts. We wanted to understand these conformational changes, and chose to focus our investigation on Snf7, the most abundant ESCRT-III subunit. Using crystal structures of hVps24 (CHMP3), we generated a three-dimensional model of Snf7 in its "closed" conformation using the comparative protein structure modeling program Modeller (Eswar, Webb et al. 2006) (Figure 2A). The Snf7 model adopts the same overall fold as hVps24 and has four discernable alpha helices composing its core domain with a helix5 forming intramolecular contacts with the core.

We hypothesized that Snf7 activation involves the conformational displacement of helix5 away from its core contacts, allowing the core domain to be accessible for potential protein and membrane interactions. To investigate this conformational change, we developed a cysteine-based cross-linking assay that directly monitors the conformational state of Snf7. We first selected residues on both helix5 (T179) and the core region closely juxtaposed to helix5 (A51) (Figure S2A). Taking advantage of the fact that endogenous Snf7 contains no cysteines, we converted these residues to cysteines and purified Snf7T179C, Snf7A51C, and the dicysteine mutant (Snf7redox) from E.coli.

In the presence of the reducing agent dithiothreitol (DTT), all Snf7 cysteine mutants migrated to ~37kDa on SDS-PAGE gels, consistent with cysteineless Snf7 (Figure 2B and Figure S2B). We next oxidized the cysteine-containing Snf7 mutants by adding the chemical oxidant copper(II) 1,10-phenathroline (Cu2+Phen), and ran these samples on non-reducing SDS-PAGE gels. Strikingly, Snf7redox underwent a migration shift from ~37kDa to ~30kDa in the presence of Cu2+Phen, suggesting intramolecular disulfide bond formation (Figure 2B). Snf7A51C and Snf7T179C did not shift their migrations upon oxidization. The Snf7redox migration shift indicates the di-sulfide cross-linking of Snf7redox into an inactive "closed" conformation.

Since the Snf7redox migration shift may be correlated to its "open" and "closed" conformational states, we next asked if ESCRT subunits that initiate Snf7 activation promote Snf7redox "opening". Snf7 is activated by Vps20, which is itself activated by the ESCRT-II subunit Vps25 (Saksena, Wahlman et al. 2009). Thus, Vps25, Vps20, and liposomes were incubated with Snf7redox in mildly reducing conditions to allow conformational changes within Snf7redox. The samples were then oxidized with Cu2+Phen and run on non-reducing SDS-PAGE gels.

The separate incubation of Snf7 with either large unilamellar vesicles (LUVs, ~1micron) or small unilamellar vesicles (SUVs, <1 micron) failed to "open" Snf7redox (Figure 2C). Similarly, experiments adding SUVs together with either Vps20 or Vps25 separately, or adding Vps25 and Vps20 together but without SUVs, all failed to "open" Snf7redox (Figure S2C). However, the complete addition of SUVs,

Vps25, and Vps20 caused a dramatic shift of Snf7redox from its “closed” to “open” conformational state (Figure 2C). This effect was dose dependent, with increasing concentrations of Vps20 and Vps25 inducing more Snf7redox to an “open” conformation. This indicates that Vps25 and Vps20 promote the conformational “opening” of Snf7 on membrane by displacement of helix5 away from the core domain.

Figure 2- Snf7 is activated by displacement of helix5 from intra-molecular core contacts

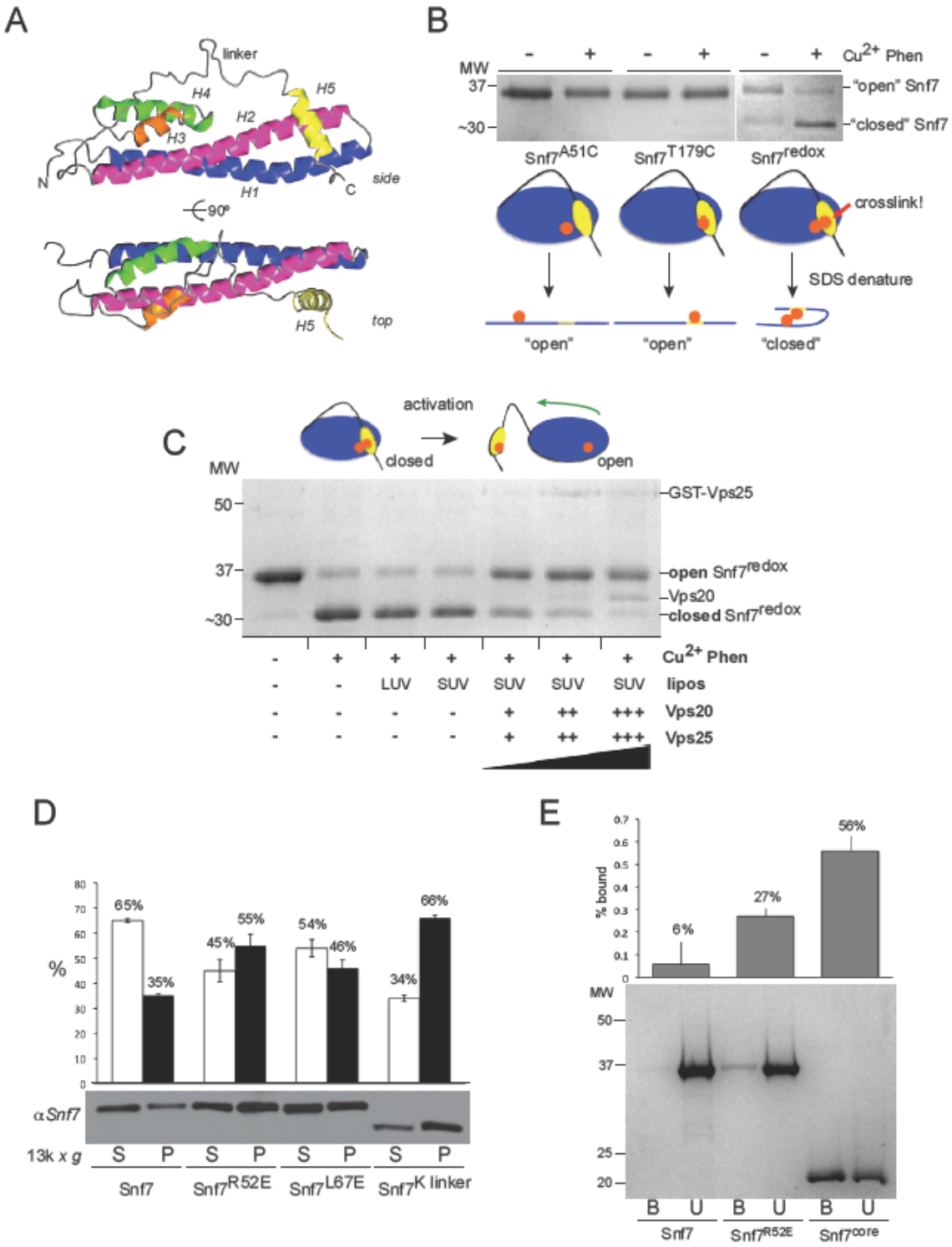

Figure 2- Snf7 is activated by displacement of helix5 from intra-molecular core contacts

(A) Ribbon diagrams (side and top) of modeled Snf7 (residues 10-183).

(B) Coomassie-stained non-reducing SDS-PAGE gels of Snf7 cysteine mutants. Cu2+Phen denotes copper(II) phenathroline. The cartoons are "closed" Snf7 with cysteines (orange).

(C) Snf7redox is conformationally "opened" by addition of Vps25, Vps20, and liposomes. LUV: large unilamallar liposomes, SUV: small unilamallar liposomes. Gels are non-reducing.

(D) Sub-cellular fractionations of snf7Δ yeast ectopically expressing Snf7 mutants. Histograms represent averages of three independent experiments. Standard deviations shown.

(E) Liposome flotation assays of reconstituted Snf7, Snf7R52E, and Snf7core. Liposome bound (B) and unbound (U) fractions are denoted. Histograms represent % Snf7 bound to liposomes as B/(B+U) (error bars denote standard deviation).

Figure S2

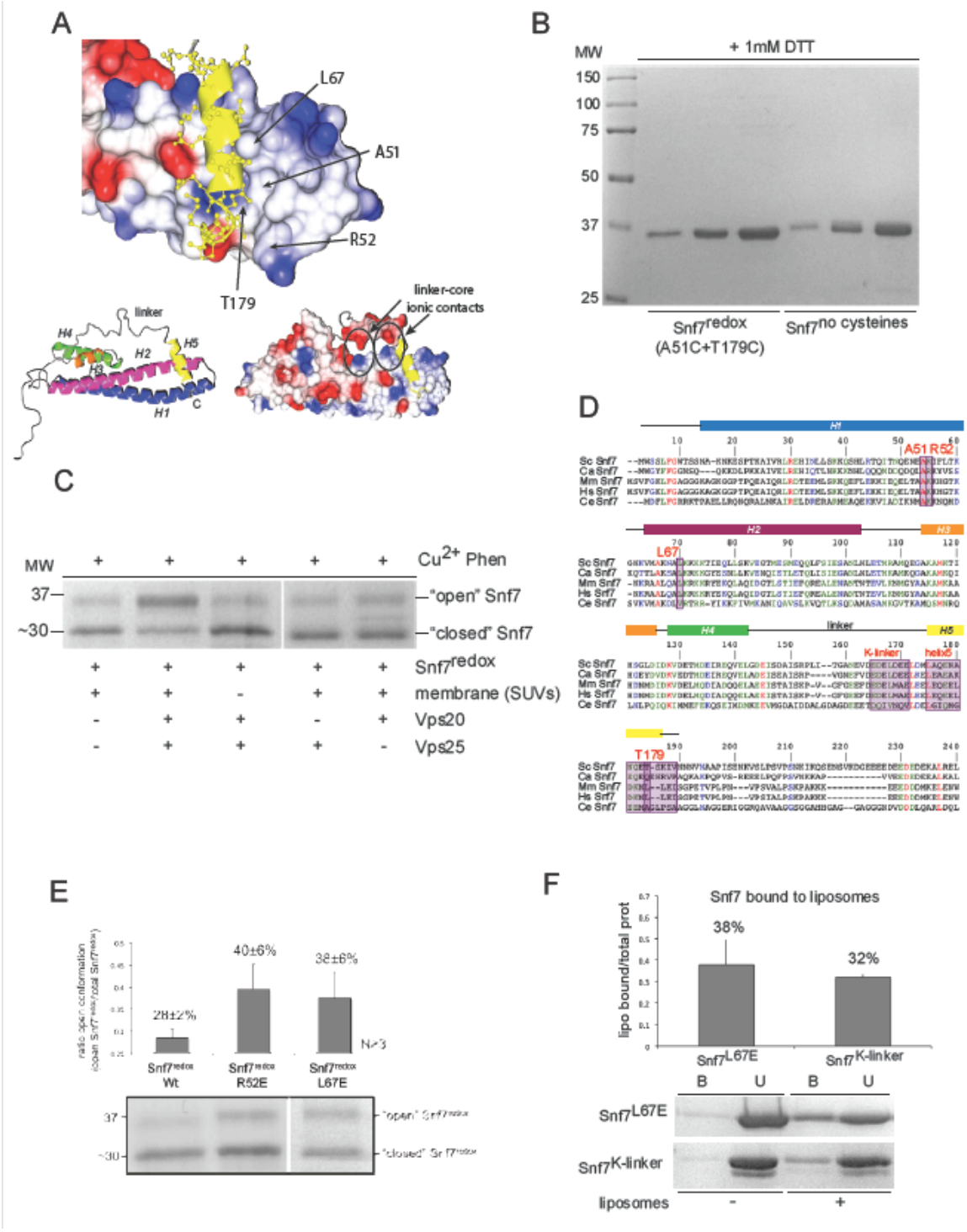
A
L67
A51
R52
T179
linker
H4
H2
H5
H3
H1
C
linker-core
ionic contacts
B
MW
+ 1mM DTT
150
100
75
50
37
25
Snf7redox
(A51C+T179C)
Snf7no cysteines
C
MW
Cu2+ Phen
37
~30
"open" Snf7
"closed" Snf7
Snf7redox
membrane (SUVs)
Vps20
Vps25
D
H1
H2
H3
H4
linker
H5
A51 R52
L67
K-linker
helix5
T179
Sc Snf7
Ca Snf7
Mm Snf7
Hs Snf7
Ce Snf7
E
radio open conformation
(open Snf7redox/total Snf7redox)
28±2%
40±6%
38±6%
N=3
Snf7redox Wt
Snf7redox R52E
Snf7redox L67E
37
~30
"open" Snf7redox
"closed" Snf7redox
F
Snf7 bound to liposomes
lipo bound/total prot
38%
32%
Snf7L67E
Snf7K-linker
B
U
B
U
Snf7L67E
Snf7K-linker
liposomes
-
+

Figure S2

A) Surface model of Snf7 *helix5*-core contacts with residues-of-interest labeled. Below the main image are two models in ribbon (*left*) and electrostatic surface (right) formats of modeled Snf7. The linker-core contacts mutated in $Snf7^{K\text{-}linker}$ are circled (*blue*: + charge, *red*: -charge).

B) DTT-treated $Snf7^{redox}$ and Snf7 containing no cysteines at 75μmol, 225μmol, and 375μmol amounts.

C) Control $Snf7^{redox}$ experiments on non-reducing gels. $Snf7^{redox}$ is primarily "closed" when incubated separately with only membranes (SUVs), membranes+Vps20, membranes+Vps25, or Vps20 and Vps25 without membrane. The addition of all three components promotes "opening". All samples contain Cu^{2+}Phen.

D) Snf7 orthologues from budding yeast (Sc), *Candida albicans* (Ca), mouse CHMP4B (Mm), human CHMP4B (Hs), and *C. elegans* (Ce). Predicted alpha-helices are boxed above the alignment. Residues of interest are purple.

E) $Snf7^{R52E+redox}$ and $Snf7^{L67E+redox}$ proteins are more "open" in solution without the addition of membranes or activating proteins (non-reducing gel). Standard deviations given.

F) Liposome flotation assays of $Snf7^{L67E}$ and $Snf7^{K\text{-}linker}$. B=bound, U=unbound. Standard deviations given.

Structure-based mutations promote Snf7 "opening"

Since Snf7 activation involves helix5 displacement, we reasoned that mutations disrupting helix5-core contacts would promote Snf7 activation, and consequently drive Snf7 to endosomes. Using site-directed mutagenesis, we substituted residues R52 and L67 on the Snf7 core domain with glutamates, which would disrupt helix5-core contacts, but not add additional positive-charge to Snf7 that may inadvertently promote membrane binding (Figure S2A&D). To test if these substitutions promoted Snf7 activation, we first examined the endosomal localization of the mutant proteins by sub-cellular fractionation. Normally, ~65% of Snf7 molecules localize to the cytoplasmic supernatant fraction (S13) after a 13,000x centrifugation spin (Babst, Katzmann et al. 2002). The remaining ~35% resides in the membrane-enriched pellet fraction (P13). Snf7R52E and Snf7L67E displayed enhanced P13 fractionation (~55% for Snf7R52E and ~46% for Snf7L67E, respectively) (Figure 2D), consistent with enhanced Snf7 activation.

We hypothesized that the R52E and L67E substitutions would promote Snf7redox "opening" independent of the presence of active Vps20 and membranes. To test this, we introduced the R52E and L67E mutations into Snf7redox constructs and oxidized the purified proteins with Cu2+Phen. As predicted, the R52E and L67E substitutions enhanced the percentage of Snf7redox remaining in an "open" state after their oxidation by Cu2+Phen (R52E: ~40% open, L67E: ~38% open, versus redox alone: ~28% open) (Figure S2E). This suggests that these mutations are

disrupting the Snf7 closed conformation by increasing the physical separation between the core and helix5.

We next attempted to "open" Snf7 by mutating residues on or near helix5 that make contact with the core domain. While helix5 primarily interacts with the core via weak hydrophobic contacts, we noticed a highly conserved acidic patch in the linker region immediately preceding helix5. This patch contains the sequence motif EDEL(D/M)EE and is almost completely conserved between yeast and man (Figure S2D). Several negatively-charged residues within this motif form electrostatic contacts with positively-charged residues along the core domain (Figure S2A). Inversion of these negatively-charged residues to positively-charged lysines (Snf7K-linker) significantly enhanced Snf7 P13 fractionation (66% P13), suggesting these mutations may drive Snf7 "opening" by displacing the linker and helix5 from contacting the core (Figure 2D). Snf7K-linker also changed its migration pattern, likely due to a net change in protein charge on SDS-PAGE gels.

Since our Snf7 mutants displayed enhanced P13 localization, we wanted to directly assay their ability to interact with lipid membranes. To do this, we next performed liposomes flotation experiments with purified Snf7 mutants to confirm they interacted with membranes better than "closed" wildtype Snf7. Whereas wildtype Snf7 displayed very low liposome binding (~6%), Snf7R52E, Snf7L67E, and Snf7K-linker showed enhanced liposome binding (27%, 38%, and 32%, respectively)

(Figure 2E and Figure S2F). As a positive control, the Snf7core domain alone was purified and displayed the most robust membrane binding (~56%).

Taken together these observations indicate that Snf7 exists in an inactive "closed" conformation that involves intramolecular contacts between the core domain and the linker-helix5 region. We propose that when Vps20 is activated, it recruits Snf7 and induces conformational changes within Snf7 that promote the movement of the linker and helix5 away from the core. This exposes regions of the core that were buried, allowing them to interact with the endosome and other ESCRT-III subunits. Several highly-conserved lysines line the core domain and form electrostatic contacts with the linker (Figure S2A). Once exposed by conformational opening they could potentially mediate Snf7 membrane binding (unpublished observations).

Activated Snf7 assembles into protofilaments

Once activated, Snf7 homo-oligomerizes forming the most abundant portion of the ESCRT-III complex (Teis, Saksena et al. 2008). Since Snf7R52E appeared to be auto-activated, we hypothesized that it would readily form higher-order structures visible by negative stain transmission electron microscopy (TEM). Whereas wildtype Snf7 does not assemble into ordered structures (Figure 3A), we observed the robust assembly of Snf7R52E into long protofilaments 14.5±3.7nm in diameter (Figure 3B&C).

Protofilament abundance and length were dependent on the period of time samples incubated on TEM grids prior to negative staining, suggesting the Formvar grid was the site of protofilament formation (Figure S3A&C). Protofilament formation was also protein concentration dependent, with robust formation at 34.5μM, reduced protofilament formation at 12.5μM, and no visible protofilaments under 5μM concentration (Figure S3B). The protofilaments were often "capped" by rings or spirals at one or both ends (Figure 3B-F, and red arrows). Longer incubation times led to more abundant ring/spiral "caps" on protofilaments (see Figure S3D for quantification).

To further examine the molecular architecture of Snf7 protofilaments, we used 2% ammonium molybdate as a negative stain. Ammonium molybdate forms a fine microcrystalline coat on biological samples, preserving their ultrastructural detail at the cost of electron density. It had the general affect of sharpening the resolution of

Snf7 protofilaments, and revealed that they are composed of two intertwining sub-filaments with a diameter of 4.1±0.6nm (Figure 3G-K). Using ammonium molybdate, the Snf7 protofilament diameter decreased to 9.0±1.3nm (Figure 3L). In rare samples single sub-filaments could be observed, but were generally short and broken (Figure 3I).

These observations indicate that the R52E mutation promotes the assembly of Snf7 into homo-oligomeric protofilaments. The basic unit of this oligomer is the ~4nm diameter sub-filament. Since the width of Snf7 monomers is ~3-4nm, we hypothesize that this sub-filament is composed of "open" Snf7 monomers arranged head-to-tail with one another (Figure 3K). Two sub-filaments then associate in parallel forming a more stable ~9nm protofilament.

Figure 3- Snf7 assembles into protofilaments.

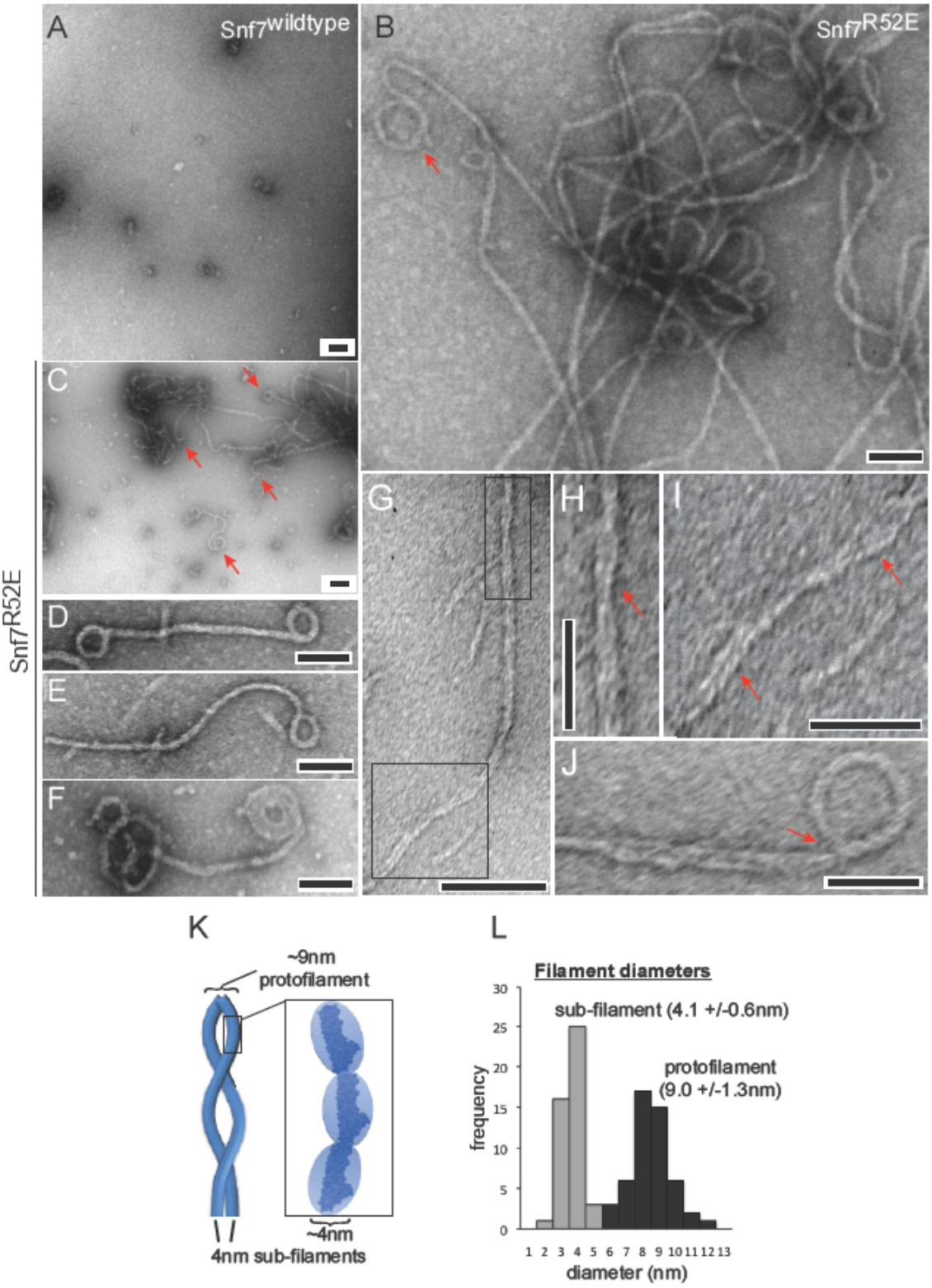

Figure 3- Snf7 assembles into protofilaments.

A) TEM micrograph showing Snf7 (wt) does not oligomerize.

(B-F) Snf7R52E assembles into long protofilaments that terminate in rings (red arrows).

(G) Snf7R52E protofilaments are composed of intertwining sub-filaments.

(H&I) Zoom-ins of the Snf7R52E protofilament in panel G showing sub-filament intertwining.

(J) Snf7R52E protofilament terminating in a ring. The red arrow denotes sub-filament hyper-coiling in the ring.

(K) Model of sub-filament packing in the Snf7 protofilament.

(L) Quantitation of Snf7 filament diameters. Scale bars are 100nm (Panels A-G) and 50nm (Panels H-J).

Figure S3

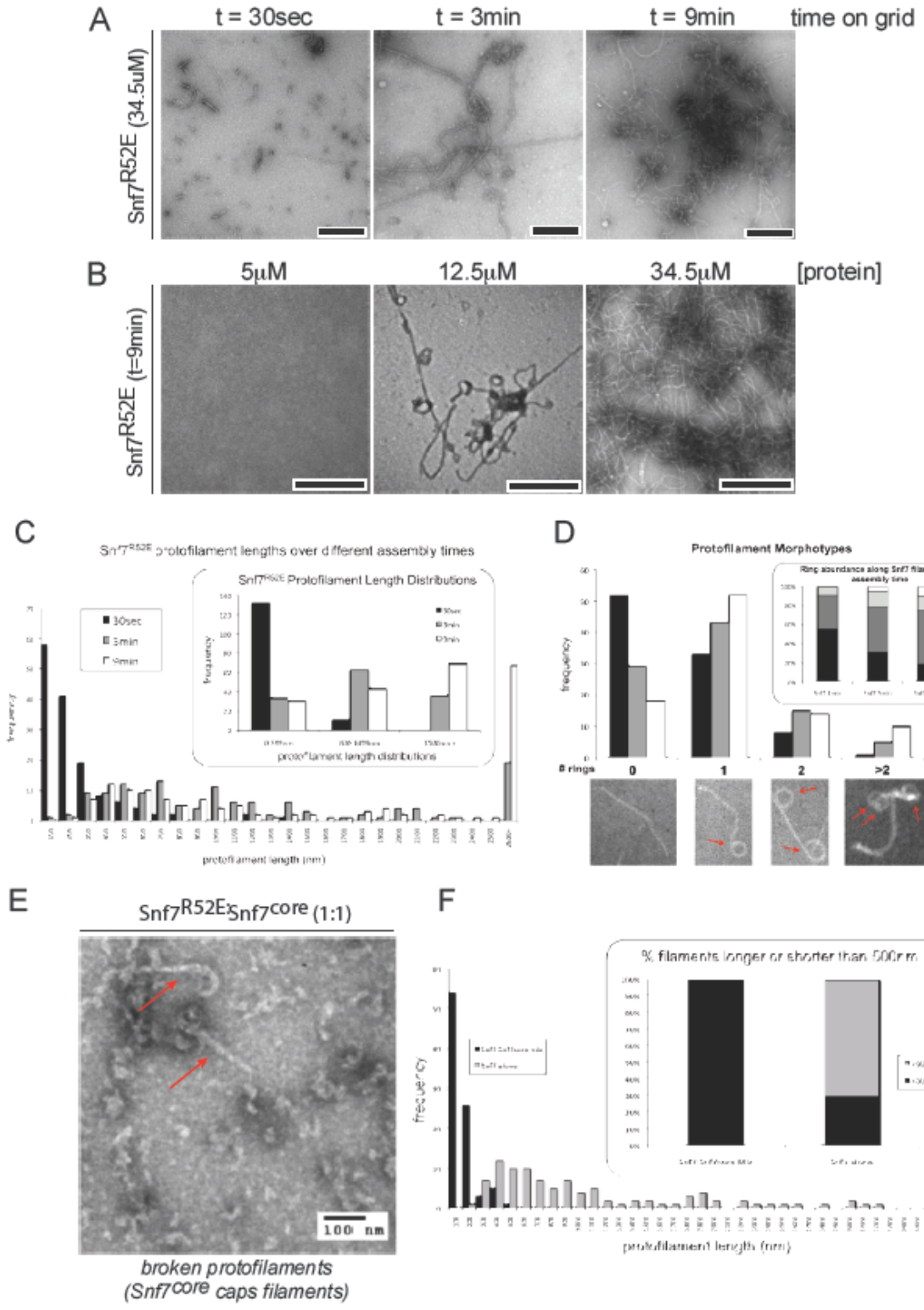
A
t = 30sec
t = 3min
t = 9min
time on grid
Snf7R52E (34.5uM)
B
5μM
12.5μM
34.5μM
[protein]
Snf7R52E (t=9min)
C
Snf7R52E protofilament lengths over different assembly times
Snf7R52E Protofilament Length Distributions
30sec
3min
9min
protofilament length (nm)
D
Protofilament Morphotypes
Ring abundance along Snf7 filaments by assembly time
frequency
rings
0
1
2
>2
E
Snf7R52E:Snf7core (1:1)
100 nm
broken protofilaments
(Snf7core caps filaments)
F
% filaments longer or shorter than 500nm
protofilament length (nm)

Figure S3

A) Snf7^{R52E} protofilament assembly across increasing grid incubation times.

B) Snf7^{R52E} protofilament formation is protein concentration dependent.

C) Quantification of Snf7^{R52E} protofilament length as a function of incubation time on TEM grids. All protein was added at 34.5μM.

D) Quantification of the number of rings formed along the length of Snf7^{R52E} protofilaments formed over different time periods. The number of rings decorating the protofilaments increases as incubation time increases.

E) TEM micrograph of Snf7^{core} mixed with Snf7^{R52E} (1:1).

F) Quantification of the length of Snf7^{R52E} protofilaments formed from Snf7^{R52E} alone or Snf7^{R52E}:Snf7^{core} (1:1) (9min incubation). Scale bar: Panels A&B-500nm, Panel E-100nm.

The Snf7 C-terminal region stabilizes protofilaments

Since the diameter of Snf7 sub-filaments suggested they were composed of Snf7 monomers packed head-to-tail into a chain, we hypothesized that Snf7core would be sufficient to form protofilaments in vitro. Surprisingly, Snf7core failed to assemble into protofilaments (Figure 4A&B). Consistent with this, when Snf7core and Snf7R52E were mixed at 1:1 stoichiometric ratios, protofilaments were formed, but their lengths were reduced dramatically (Figure S3E&F). This suggested that Snf7R52E was able to interact with Snf7core, but Snf7core negatively affected protofilament elongation.

Since Snf7core appeared unable to polymerize, we hypothesized that the Snf7 C-terminal region may play a role in Snf7 homo-oligomerization. To test this, we generated several mutants which perturb the C-terminal region and evaluated these mutations with three different assays to test: 1) if the mutants could assemble into protofilaments in vitro, 2) if they retained the ability to interact with endogenous Snf7 in vivo by co-immunoprecipitation, and 3) if the mutants were able to complement ESCRT pathway function when expressed in snf7Δ yeast.

We first investigated if helix5 was involved in Snf7 oligomerization. We deleted helix5 (residues 170-183) on the R52E background and found that purified Snf7R52E+Δhelix5 failed to form protofilaments (Figure 4D). To test if mutating helix5 affected Snf7 oligomerization in vivo, we next expressed Snf7Δhelix5 in yeast with a chromosomally integrated SNF7-3xFLAG gene and performed anti-FLAG

immunoprecipitations. Whereas wildtype Snf7 efficiently co-immunoprecipitated with Snf7-FLAG (Figure 4C), Snf7Δhelix5 failed to co-immunoprecipitate, indicating that the loss of helix5 attenuates Snf7 oligomerization (Figure 4D). This loss-of-function is not due to the non-specific deletion of residues within the C-terminal region, since deletion of residues immediately following helix5 (residues 185-195) did not affect ESCRT-III-dependent cargo sorting (Figure S4J). Importantly, Snf7R52E efficiently co-immunoprecipitated with Snf7-FLAG, consistent with the ability of Snf7R52E to assemble into protofilaments (Figure 4C).

If helix5 interacts in trans with neighboring Snf7 monomers, then the highly conserved linker region would also be critical for providing helix5 with the molecular "reach" necessary to interact with another Snf7 monomer. Consistent with this, we deleted the linker region (residues 151-170) and found that Snf7Δlinker failed to form protofilaments (Figure 4E). Snf7Δlinker also failed to co-immunoprecipitate with Snf7-FLAG in vivo, suggesting it is necessary for Snf7 oligomerization (Figure 4E).

Since we found that charge-inversion mutations within the linker region promote Snf7 activation, we examined Snf7K-linker and found that it formed short (98±73nm length) protofilaments (Figure 4F). In agreement, Snf7K-linker efficiently co-immunoprecipitated with Snf7-FLAG, again indicating that it was capable of oligomerizing (Figure 4F). Together, these observations suggest a role for the Snf7 C-terminal region in stabilizing Snf7 homo-oligomers.

Figure 4- The Snf7 C-terminal region stabilizes Snf7 homo-oligomers.

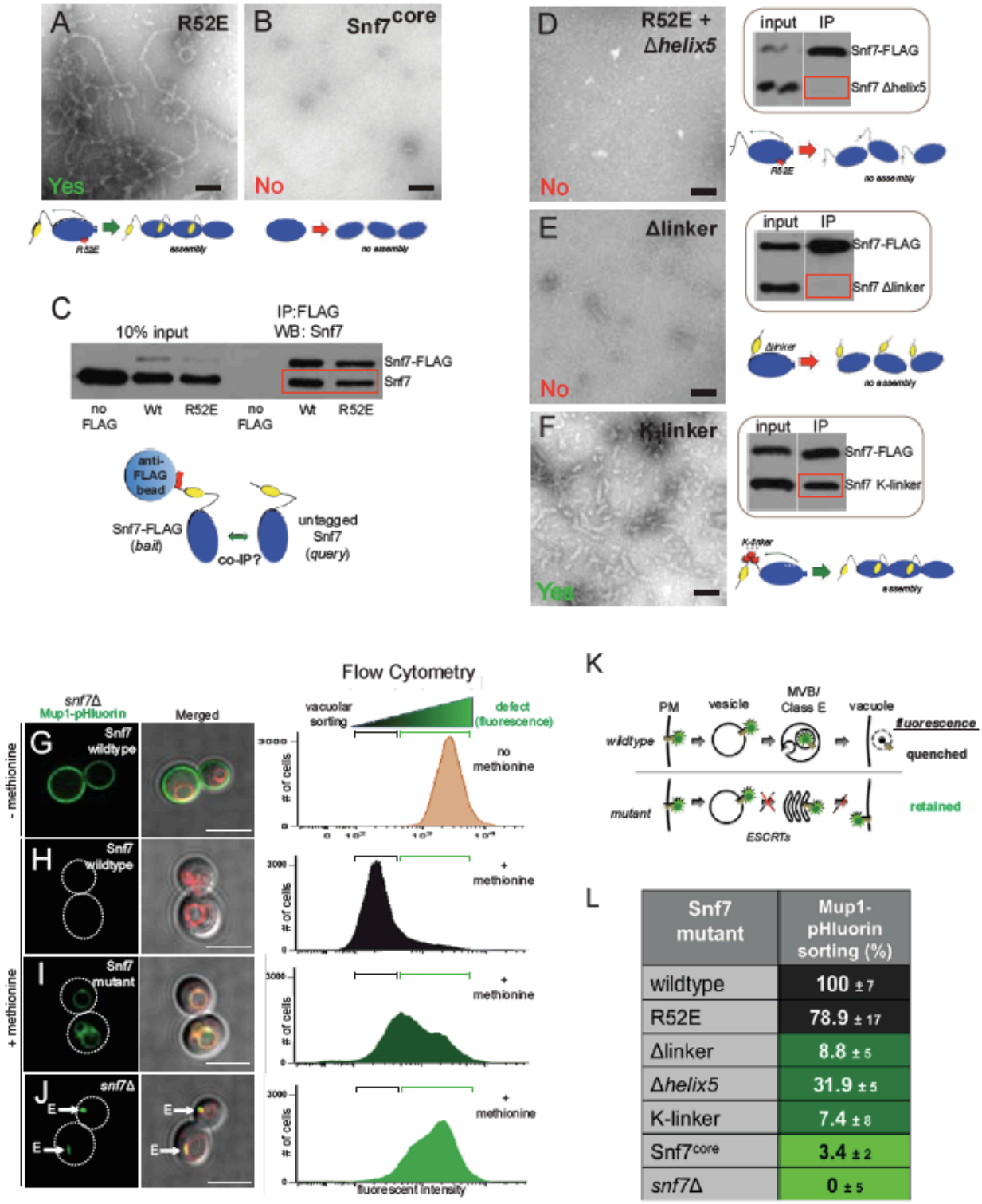

L

Snf7 mutant	Mup1-pHluorin sorting (%)
wildtype	100 ± 7
R52E	78.9 ± 17
Δlinker	8.8 ± 5
Δhelix5	31.9 ± 5
K-linker	7.4 ± 8
Snf7core	3.4 ± 2
snf7Δ	0 ± 5

Figure 4- The Snf7 C-terminal region stabilizes Snf7 homo-oligomers.

(A-B) TEM micrographs of Snf7R52E and Snf7core.

(C) Anti-FLAG co-immunoprecipitations to detect Snf7-Snf7 interaction. The schematic denotes the experimental design.

(D-F) TEM micrographs of Snf7 mutants with their corresponding co-immunoprecipitations and assembly model to their right.

(G-J) Representative images of yeast expressing Mup1-pHluorin (green) and Snf7 constructs (indicated) in the absence of methionine (G) and after methionine induction (H-J). FM4-64 is red. To the right of each image is the sorting profile of ~100,000 yeast plotted by FITC-channel intensity and cell number.

(K) Conceptual model for the pHluorin sorting assay.

(L) Table summarizing the effect of ESCRT mutations on Mup1 vacuole delivery. Standard deviation is reported. Scale bars: 100nm (Panels A-F), 5μm (Panels G-J).

Figure S4

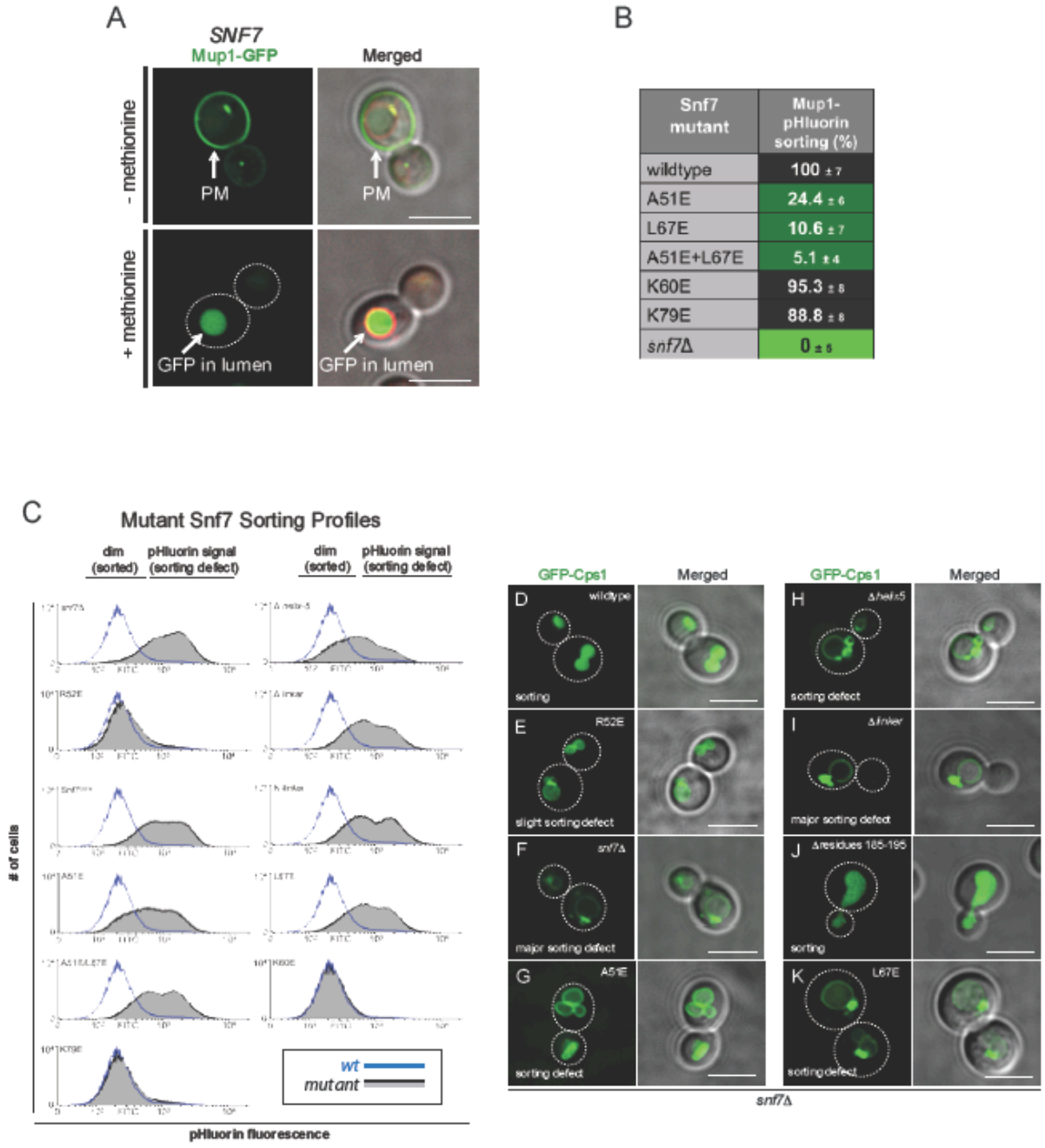
A
SNF7
Mup1-GFP
Merged
- methionine
+ methionine
PM
PM
GFP in lumen
GFP in lumen
B
Snf7 mutant
Mup1-pHluorin sorting (%)
wildtype
100 ± 7
A51E
24.4 ± 6
L67E
10.6 ± 7
A51E+L67E
5.1 ± 4
K60E
95.3 ± 8
K79E
88.8 ± 8
snf7Δ
0 ± 5
C
Mutant Snf7 Sorting Profiles
dim (sorted)
pHluorin signal (sorting defect)
dim (sorted)
pHluorin signal (sorting defect)
# of cells
wt
mutant
pHluorin fluorescence
GFP-Cps1
Merged
GFP-Cps1
Merged
D wildtype
sorting
H Δhelix5
sorting defect
E R52E
slight sorting defect
I Δlinker
major sorting defect
F snf7Δ
major sorting defect
J Δresidues 185-195
sorting
G A51E
sorting defect
K L67E
sorting defect
snf7Δ

Figure S4

A) Representative images of yeast expressing Mup1-GFP (green) +/- methionine. FM4-64 is red. 5μm scale bar.

B) Table summarizing several sorting profiles from Panel C.

C) Flow cytometry sorting profiles of FITC-excited yeast expressing vector or Snf7 mutants and Mup1-pHluorin. Profiles represent an average of three independent experiments and ~300,000 yeast. *y*-axis: cell number, *x*-axis: fluorescence.

D-K) Representative images of *snf7*Δ yeast co-expressing different Snf7 mutants and GFP-Cps1 (green). Scale bars: 5μm.

A pH-sensitive ESCRT cargo quantitatively scores Snf7 function

Previous studies have suggested that Snf7 homo-oligomerization promotes ILV formation, and thus the delivery of cargoes to the vacuole lumen (Teis, Saksena et al. 2008; Teis, Saksena et al. 2010). Since we characterized mutations that impaired Snf7 oligomerization, we next developed an assay to quantitatively access their effects of ESCRT pathway function. This assay utilizes a pH-sensitive GFP variant (pHluorin) fused to the plasma membrane methionine transporter Mup1 (Prosser, Whitworth et al. 2010) (see Figure 4K for conceptual model).

When extracellular methionine levels are low, Mup1-pHluorin localizes to the plasma membrane and fluoresces brightly when excited (Figure 4G). In response to increased extracellular methionine, Mup1 is rapidly endocytosed and delivered to the vacuole lumen in an ESCRT-dependent manner (Figure S4A) (Lin, MacGurn et al. 2008). At the vacuole, pHluorin fluorescence is quenched due to the acidity of the vacuole lumen (Figure 4H). Since ESCRT dysfunction results in a failure to sort Mup1-pHluorin into ILVs, we predicted that cells with a defective ESCRT-III would display persistent pHluorin fluorescence in the presence of methionine (Figure 4I&J). In this way, pHluorin fluorescence intensity is a quantifiable readout of the efficiency of ESCRT-III-mediated ILV formation.

To quantitatively score mutations that affect Snf7 oligomerization, we ectopically expressed Snf7 mutants in Mup1-pHluorin-expressing yeast lacking endogenous Snf7, and induced Mup1-pHluorin endocytic uptake by adding methionine. We then

used flow cytometry to quantify the pHluorin fluorescence intensities of at least 300,000 yeast expressing each mutant. When the fluorescence distribution of the population was plotted, each Snf7 mutant exhibited a unique and highly reproducible sorting profile (Figure S4C). We then calculated the percent deviation of each mutant from the wildtype profile to assign a "score" that reflects the severity of each mutation on ESCRT pathway function. The Table in Figure 4L summarizes these calculations.

Notably, ~79% of yeast expressing Snf7R52E sort Mup1-pHluorin as efficiently as wildtype cells, resulting in a sharply-peaked sorting profile that is only slightly brighter when compared to wildtype yeast (Figure S4C). This indicates that Snf7R52E retains functionality in vivo. Although the precise reason for the slight fluorescence shift is unclear, it may be attributed to perturbing the assembly:disassembly equilibrium of ESCRT-III, which may affect ILV formation. Consistent with this, mutations localized within the helix5-core contact site elicited Mup1-pHluorin sorting defects (L67E and A51E), whereas mutations outside this region had almost no effect on sorting (K60E and K79E) (Figure S4B&C).

Consistent with the need for helix5 to efficiently oligomerize in vitro, Snf7Δhelix5-expressing yeast displayed a significant Mup1-pHluorin sorting defect, resulting in only ~32% the sorting efficiency of wildtype cells (Figure 4L). Snf7Δlinker-expressing yeast also failed to efficiently sort Mup1-pHluorin, functioning at only ~9% of wildtype levels. This was similar to Snf7core alone, which had a sorting

phenotype similar to snf7Δ yeast. Surprisingly, Snf7K-linker also failed to sort Mup1-pHluorin efficiently (~7% sorting efficiency). The reason for this is unclear, but may be due to the inherent instability of the short (~100nm) filaments this mutant formed (Figure 4F).

To confirm that the sorting of Mup1 represents a general readout of ESCRT pathway function, we examined the sorting of another ESCRT-dependent cargo: the vacuolar protease Cps1. Snf7 mutants were co-expressed in yeast expressing GFP-Cps1, which is sorted from the Golgi to the vacuole in an ESCRT-dependent manner. The qualitatively scored ability of mutants to sort GFP-Cps1 closely matched the sorting profiles of Mup1-pHluorin (Figure S4D-K), suggesting that the Mup1-pHluorin sorting profile represent the general sorting capability of the ESCRT pathway.

Altogether, these data underscore the involvement of the Snf7 C-terminal region in stabilizing Snf7 homo-oligomers. It suggests that this region, following subunit "opening", may form contacts with a neighboring Snf7 monomer to promote oligomerization. Furthermore, the use of Mup1-pHluorin as a pH-sensitive cargo has allowed us for the first time, to our knowledge, to quantitatively access the effect of individual point mutations within the ESCRT pathway.

Snf7 assembles into spirals on lipid monolayers

Since we reconstituted Snf7 oligomerization and showed its importance in the sorting of cargoes to the vacuole, we next wanted to visualize Snf7 assembly directly on a lipid environment. To directly visualize ESCRT-III assembly on lipids and retain the high visual resolution of transmission electron microscopy, we generated supported lipid monolayers along the surface of Formvar coated TEM grids (Figure 5A&B). Monolayers of defined lipid composition (see Supplemental Methods) formed spontaneously across the surface of an aqueous buffer and were subsequently adhered to TEM grids. Proteins could then be injected, allowing the assembly of protein structures on the supported monolayer surface.

We first added purified Snf7R52E to lipid monolayers and observed the robust assembly of Snf7R52E into protofilament spirals across the monolayer surface (Figure 5C). Spirals were an average outer diameter of 50.4±9.8nm (Figure S5A). By examining regions of grids that were not coated with monolayer, we noted that Snf7 spirals closely resemble the more elongated Snf7 protofilaments formed on grids, but were more tightly coiled into spirals when assembled on a lipid environment (Figure 5C, top region).

We hypothesized that the negatively-charged phosphatidylserine (PS) and PtdIns(3)P lipids within the monolayer (30% PS, 10% PtdIns(3)P) mediated electrostatic interactions with Snf7 and promoted spiral assembly. To test this, we generated lipid monolayers with a reduced electrostatically-positive lipid

composition (now 5%PS, 1% PtdIns(3)P). As predicted, Snf7 failed to associate into tightly coiled spirals on this monolayer surface (Figure S5B).

Figure 5- Snf7 assembles into spirals on lipid monolayers and co-assembles with Vps24 and Vps2 into helices.

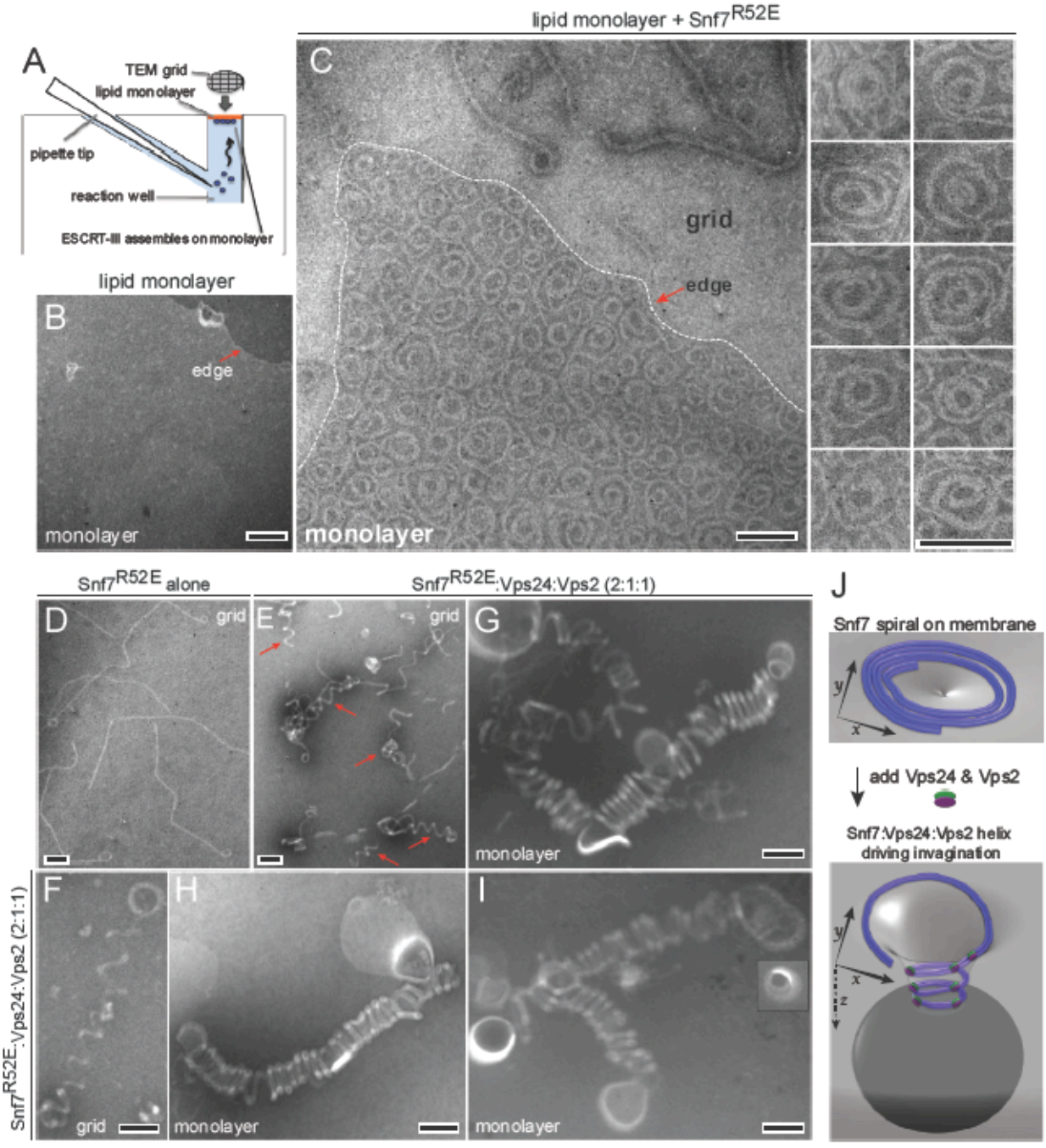

Figure 5- Snf7 assembles into spirals on lipid monolayers and co-assembles with Vps24 and Vps2 into helices.

(A) Schematic showing lipid monolayer creation.

(B) TEM micrograph of lipid monolayer. The monolayer "edge" is marked by an arrow.

(C) Snf7R52E protofilaments assembled directly on lipid monolayers. More linear protofilaments assembled on the "naked" grid (top region). The panels to the right are zoom-ins of several Snf7 spirals.

(D) Snf7R52E forming linear filaments on a grid.

(E&F) Snf7R52E, Vps24, and Vps2 co-assembling into helices (arrows) on a grid. G-I) Snf7R52E:Vps24:Vps2 helices assembled on lipid monolayers.

(J) Speculative model of a Snf7 spiral and Snf7:Vps24:Vps2 helix that may drive membrane invaginations. Scale Bars: 100nm.

Figure S5

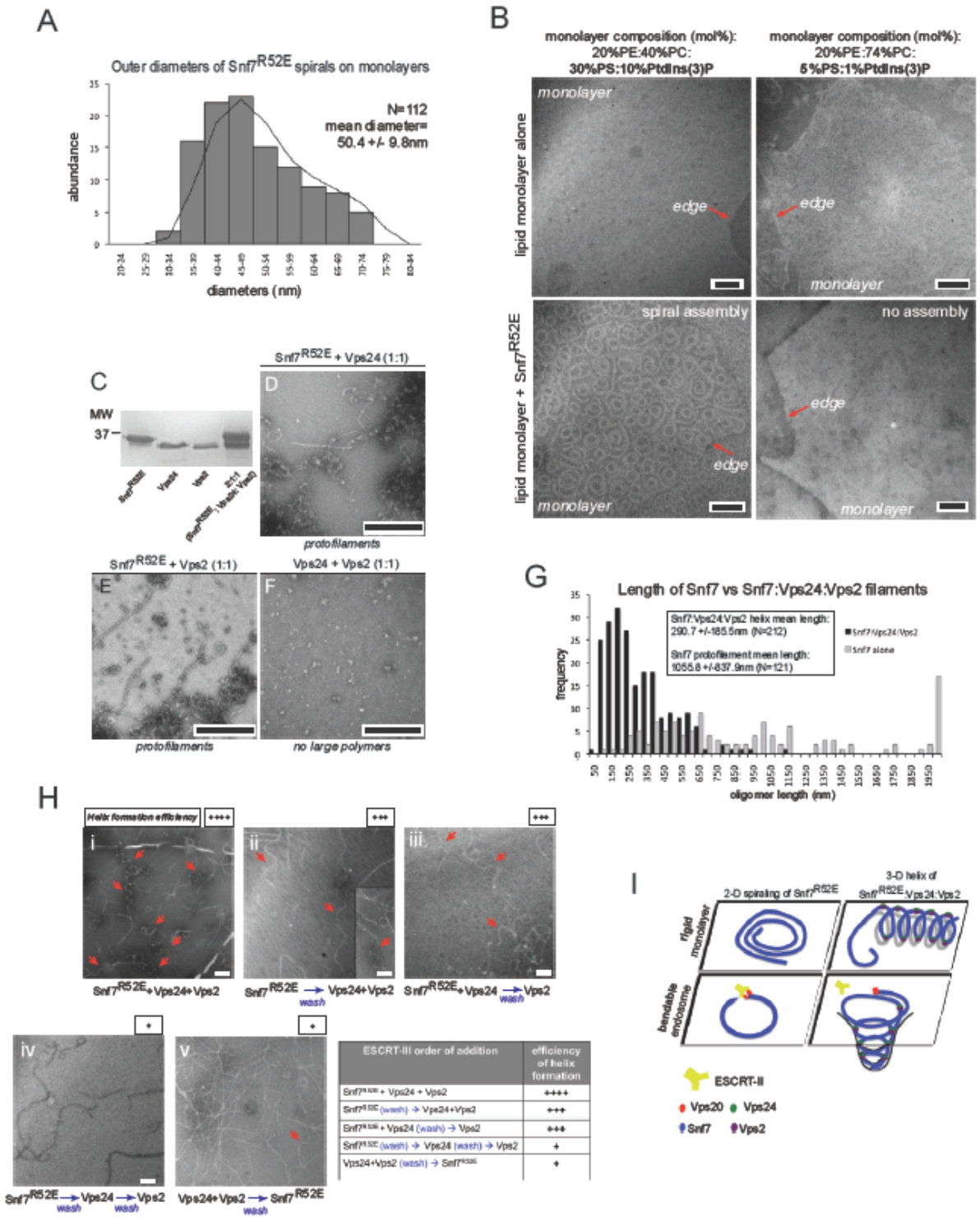
A
Outer diameters of Snf7R52E spirals on monolayers
N=112
mean diameter=
50.4 +/- 9.8nm
abundance
diameters (nm)
B
monolayer composition (mol%):
20%PE:40%PC:
30%PS:10%PtdIns(3)P
monolayer composition (mol%):
20%PE:74%PC:
5%PS:1%PtdIns(3)P
lipid monolayer alone
lipid monolayer + Snf7R52E
monolayer
edge
spiral assembly
no assembly
C
MW
37
D
Snf7R52E + Vps24 (1:1)
protofilaments
E
Snf7R52E + Vps2 (1:1)
protofilaments
F
Vps24 + Vps2 (1:1)
no large polymers
G
Length of Snf7 vs Snf7:Vps24:Vps2 filaments
Snf7:Vps24:Vps2 helix mean length:
290.7 +/-185.5nm (N=212)
Snf7 protofilament mean length:
1055.8 +/-837.9nm (N=121)
Snf7:Vps24:Vps2
Snf7 alone
frequency
oligomer length (nm)
H
Helix formation efficiency
i
ii
iii
iv
v
Snf7R52E+Vps24+Vps2
Snf7R52E → Vps24+Vps2
wash
Snf7R52E+Vps24 → Vps2
wash
Snf7R52E → Vps24 → Vps2
wash
wash
Vps24+Vps2 → Snf7R52E
wash
ESCRT-III order of addition
efficiency of helix formation
Snf7R52E + Vps24 + Vps2
++++
Snf7R52E (wash) → Vps24+Vps2
+++
Snf7R52E + Vps24 (wash) → Vps2
+++
Snf7R52E (wash) → Vps24 (wash) → Vps2
+
Vps24+Vps2 (wash) → Snf7R52E
+
I
2-D spiraling of Snf7R52E
3-D helix of
Snf7R52E:Vps24:Vps2
rigid monolayer
bendable endosome
ESCRT-II
Vps20
Vps24
Snf7
Vps2

Figure S5

A) Measured diameters of Snf7^{R52E} spirals.

B) Comparative micrographs of lipid monolayers of two different lipid compositions. Monolayers of high lipid acidity (*left column*) promote Snf7^{R52E} spiral assembly. Monolayers with lowered lipid acidity (*right column*) attenuate spiral formation. The monolayer edge is labeled in each micrograph.

C) Coomassie-stained gel of Snf7^{R52E}, Vps24, and Vps2. **D-F**) TEM micrographs of Snf7, Vps24, and Vps2 co-assembly reactions omitting Vps2 (**D**), Vps24 (**E**) or Snf7^{R52E} (**F**).

G) Quantification of the length of protofilaments formed from either Snf7^{R52E} alone or the co-assembly of Snf7^{R52E}, Vps24, and Vps2 (3min incubation).

H) Order-of-addition experiments showing Vps24 and Vps2 can induce helical architecture from pre-assembled Snf7 protofilaments. Protein was allowed to assemble on TEM grids for 3 minutes, followed by brief dehydration, a buffer wash step, and addition of the next protein. The table summarizes the efficiency of helix formation on a scale of four "+" marks. **I**) Speculative model of ESCRT-III helices on rigid supported monolayers *versus* a bendable endosome. Scale bars: Panels B&H- 100nm, Panels D-F- 500nm.

Snf7, Vps24, and Vps2 co-assemble into protein helices

Spirals are geometrically two-dimensional structures. In agreement with this, the Snf7 spirals we observed appeared "flat" and thus ostensibly incapable of mediating the drastic three-dimensional membrane remodeling necessary for ILV formation. Since Snf7 oligomerization recruits ESCRT-III subunits Vps24 and Vps2 to endosomes, we hypothesized that these proteins may modulate the molecular architecture of Snf7 polymers (Babst, Katzmann et al. 2002; Teis, Saksena et al. 2008). To test this, we reconstituted full length Vps24 and Vps2 from E.coli and incubated them with Snf7R52E at cellular abundance levels (~2:1:1 ratios; Snf7:Vps24:Vps2) (Figure S5C).

We first examined these co-assembly experiments on TEM grids. As before, Snf7R52E alone polymerized into long protofilaments capped with a ring or spiral (Figure 5D). Strikingly, the simultaneous addition of Snf7R52E, Vps24, and Vps2 generated coiled helices (a geometrically three-dimensional spiral) that extended across the grid surface (Figure 5E&F). The filaments composing these helices were identical in diameter to Snf7R52E protofilaments (~9nm), but generally shorter and of variable length (mean length: 290±185nm) (Figure S5G). These helical polymers are likely hetero-oligomers containing Snf7R52E, Vps24, and Vps2 because experiments including only two of the three subunits at 1:1 ratios did not produce helices (Figure S5D&E). Similarly, co-incubated Vps24 and Vps2 (1:1) failed to oligomerize, likely because there was no Snf7 present to induce Vps24/Vps2 activation (Figure S5F).

We next added Snf7R52E, Vps24, and Vps2 to lipid monolayers. The proteins again assembled into helices similar to those formed on TEM grids. High magnification of these helices indicated that they appeared to retain a three-dimensional coiling architecture indicative of protein helices like those formed by the membrane scission machine dynamin (Carr and Hinshaw 1997) (Figure 5G-I). These helices projected across the monolayer surface and were very distinct from the spirals Snf7R52E formed on its own. They displayed an average outer diameter of 85.4±6.5nm. Several were closely associated with liposomes that spontaneously form as a biproduct of monolayer biogenesis, suggesting the helices can readily interact with lipid membranes (Figure 5G-I).

Since Vps24 and Vps2 are recruited to endosomes after Snf7, we next asked if these proteins could remodel pre-existing Snf7 protofilaments into helices. To do this, we assembled Snf7 into protofilaments on TEM grids, washed unassembled protein away by droplet exchange, and added buffer containing Vps24 and Vps2 to the grids. We then examined the grids and qualitatively scored for the efficiency of helix formation relative to a control grid containing co-incubated Snf7:Vps24:Vps2. When Vps24 and Vps2 were added to pre-assembled Snf7 protofilaments, they were able to efficiently induce helix formation (Figure SH i&ii). Similarly, we also observed slightly less efficient helix formation when Snf7R52E and Vps24 were first added to grids, followed by a wash and Vps2 (Figure SH iii). In contrast, sequential addition of Snf7R52E, Vps24, and Vps2 in three stages, or the addition of Vps24 and Vps2 first,

followed by Snf7R52E led to drastically reduced helix formation (Figure SH iv & v). These experiments imply that Vps24 and Vps2 could potentially remodel pre-existing Snf7 polymers into helices during the ordered assembly of ESCRT-III (Figure 5J).

Vps24 and Vps2 promote ESCRT-III associated membrane invaginations on GUVs

Although TEM imaging of lipid monolayers provides high-resolution visualization of ESCRT-III assembly, the monolayers are adhered to a rigid grid support and thus cannot be deformed by ESCRT-III (Figure S5I). Since Snf7, Vps24, and Vps2 co-assembled into helices with implied membrane sculpting potential, we next wanted to investigate if these proteins could drive or be associated with membrane invaginations. To do this, we generated GUVs labeled with the lipophilic dye DiI. We noted that some GUVs could spontaneously deform in solution, so we wanted to ensure we could distinguish membrane invaginations that were specifically associated with ESCRT-III proteins. We fluorescently tagged Snf7R52E by engineering a cysteine into its C-terminus (V187C), to which we covalently attached a maleimide-conjugatable Alexa488 fluorophore (Figure S6A). Although Snf7R52E-A488 was able to interact with GUVs (Figure S6B), we wanted to reconstitute full ESCRT-III assembly, and so purified Vps20core, which was sufficient to recruit Snf7 to endosomal membranes (Figure 1E). GUVs treated with Vps20core and Snf7R52E-A488 displayed punctal Snf7R52E-A488 labeling across their surfaces, but were notably devoid of ESCRT-III-associated invaginations (Figure S6C&I).

In striking contrast, the addition of all four ESCRT-III subunits (now including Vps24 and Vps2) led to the formation of distinct membrane invaginations with which Snf7R52E-A488 punctae associated (Figure S6D-G). Snf7R52E punctae stably associated with these invaginations over time and several invaginations were

observed to form underneath sites of Snf7R52E enrichment, suggesting they may form as a consequence of ESCRT-III assembly (Figure S6H and SMovie 1). Interestingly, Snf7R52E–A488 remained at the top, neck region of these invaginations and was mostly excluded from the bud that protruded into the GUV interior. This may indicate that ESCRT-III assemblies containing Snf7R52E may have affinity for regions of high membrane curvature located at the necks of membrane invaginations.

Together with our TEM-based observations, we propose that Vps24 and Vps2 induce structural rearrangements in Snf7 polymers that create helices with potential membrane sculpting properties (Figure 5J). We speculate that because of the rigidity of TEM grid support, these helices cannot deform the lipid monolayer on which they assemble. Instead, they stably associate with the monolayer surface and extend across it (Figure S5I).

ESCRT-II regulates the assembly of Snf7 rings

We were intrigued by the architectural changes in Snf7 polymerization when we added downstream ESCRT-III subunits Vps24 and Vps2 to our reactions. Next, we wanted to investigate how upstream ESCRT machinery may affect Snf7 protofilament architecture. Prior to vesicle formation, ESCRT-II initiates the assembly of ESCRT-III at sites enriched with ubiquitinated cargo. We wanted to investigate the structural relationship between ESCRT-II and ESCRT-III, so we next attempted to reconstitute the co-assembly of complete ESCRT-II and ESCRT-III complexes.

ESCRT-II was purified as a complex by virtue of a hexahistidine (His6) tag on Vps36 (Figure 6A). ESCRT-II and Vps20 were then co-incubated with Snf7R52E at a ~1:2:10 ratio (ESCRT-II:Vps20:Snf7R52E) and examined by TEM. This reaction yielded TEM grids covered with small rings instead of the linear protofilaments normally observed when Snf7R52E was imaged alone (Figure 6B&C). Rings measured 65.1±22.1nm in diameter (Figure 6G&H), and many exhibited distinct globular densities at one point along their circumference. The rings were composed of highly curved ~9nm diameter protofilaments, suggesting they were composed of two Snf7 sub-filaments. Ring formation required the presence of ESCRT-II, Vps20, and Snf7R52E, as removal of either ESCRT-II or Vps20 drastically reduced ring formation in favor of linear protofilaments (Figure S7A-C).

Figure 6- ESCRT-II mediates ESCRT-III ring formation.

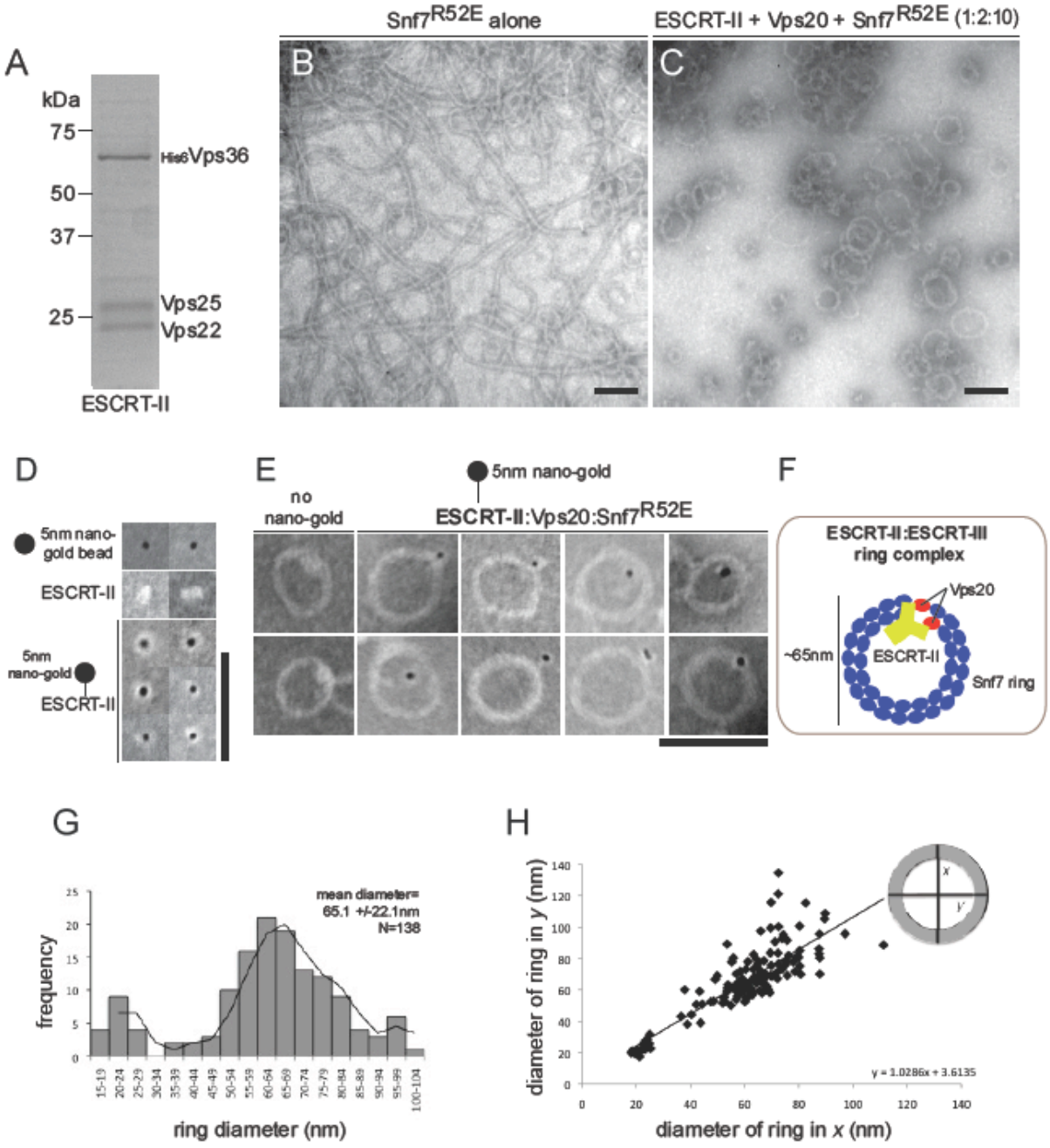

Figure 6- ESCRT-II mediates ESCRT-III ring formation.

(A) Coomassie-stained gel of reconstituted ESCRT-II.

(B) Snf7R52E protofilaments.

(C) ESCRT-II, Vps20, Snf7R52E (1:2:10 ratio) co-assemble into rings.

(D) Labeling of His6-ESCRT-II using 5nm Ni2+NTA nano-gold beads.

(E) ESCRT-II:ESCRT-III ring super-complexes with nano-gold labeled ESCRT-II.

(F) Model of ESCRT-II:Vps20:Snf7 ring complex.

(G) Histogram of ESCRT-II:Vps20:Snf7R52E ring diameters.

(H) Scatter plot of ring diameters measured in perpendicular x- and y- planes. Scale bars: 100nm.

Figure S6

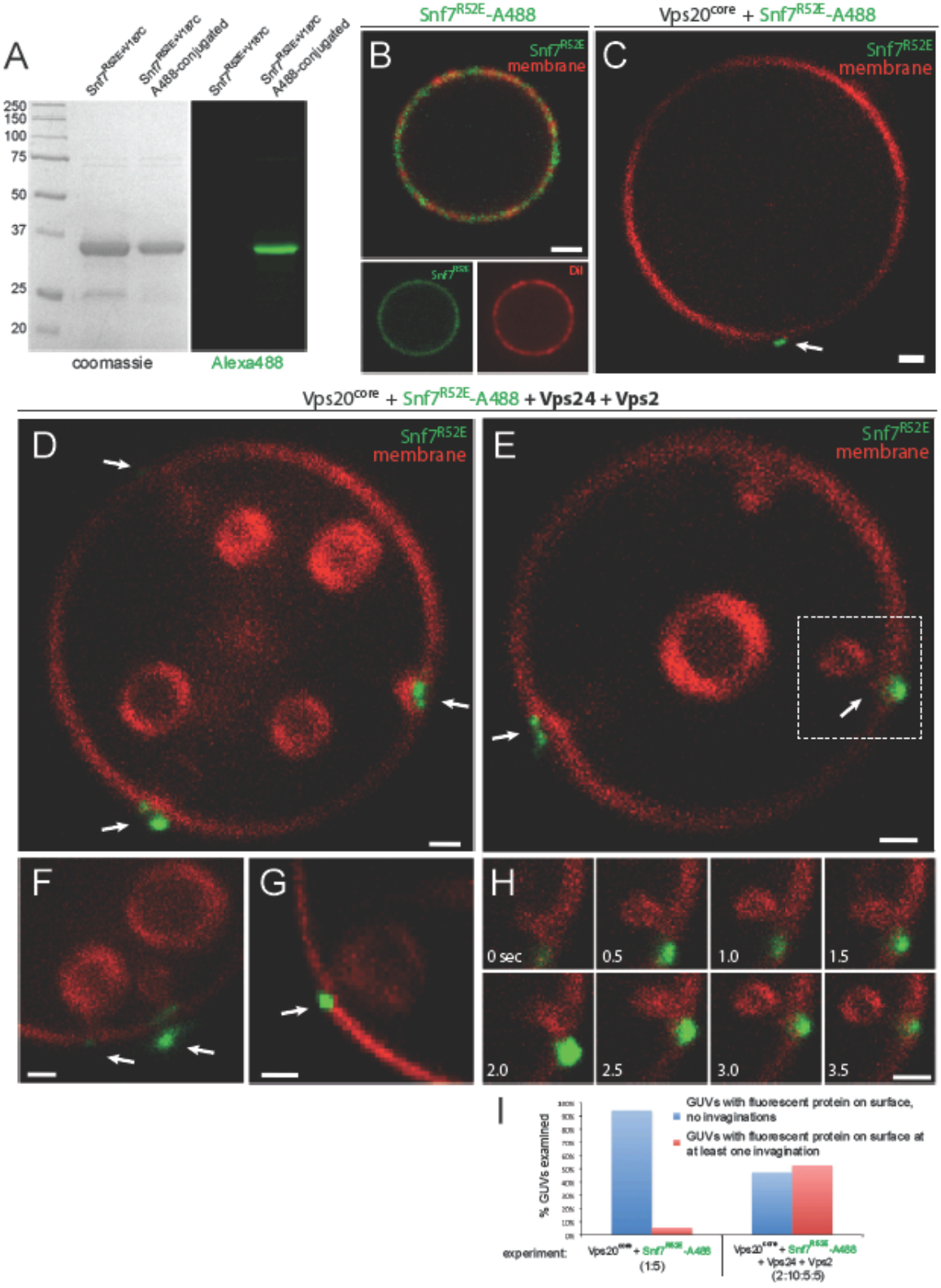
A
250
150
100
75
50
37
25
20
coomassie
Alexa488
B
Snf7R52E-A488
Snf7R52E membrane
DiI
C
Vps20core + Snf7R52E-A488
Snf7R52E membrane
D
Vps20core + Snf7R52E-A488 + Vps24 + Vps2
Snf7R52E membrane
E
Snf7R52E membrane
F
G
H
0 sec
0.5
1.0
1.5
2.0
2.5
3.0
3.5
I
% GUVs examined
GUVs with fluorescent protein on surface, no invaginations
GUVs with fluorescent protein on surface at least one invagination
experiment:
(1:5)
+ Vps24 + Vps2
(2:10:5:5)

Figure S6

A) Coomassie-stained and UV-excited gels of unlabelled Snf7$^{R52E+V187C}$ and Snf7$^{R52E+V187C}$ with covalently attached Alexa488 fluorophore (referred to as Snf7^{R52E}-A488).

B) Fluorescent DiI-labeled GUV displaying associated Snf7^{R52E}-A488 protein on its surface. Separate Alexa488 and DiI-channel images are shown below the merged panel.

C) Fluorescent GUV incubated with Vps20^{core} and Snf7^{R52E}–A488 (1:5 ratio). A Snf7^{R52E}-A488 punctae on the GUV surface is marked with an arrow.

D-G) Different fluorescent GUVs incubated with Vps20^{core}, Snf7^{R52E}–A488, Vps24, and Vps2 at a 2:10:5:5 ratio. Numerous Snf7^{R52E}-A488 punctae are present on the surface of these GUVs, and are associated with invaginations. **H**) Time-lapse frames of a membrane invagination forming that is associated with Snf7^{R52E}-A488. This invagination is boxed in Panel E.

Figure S7

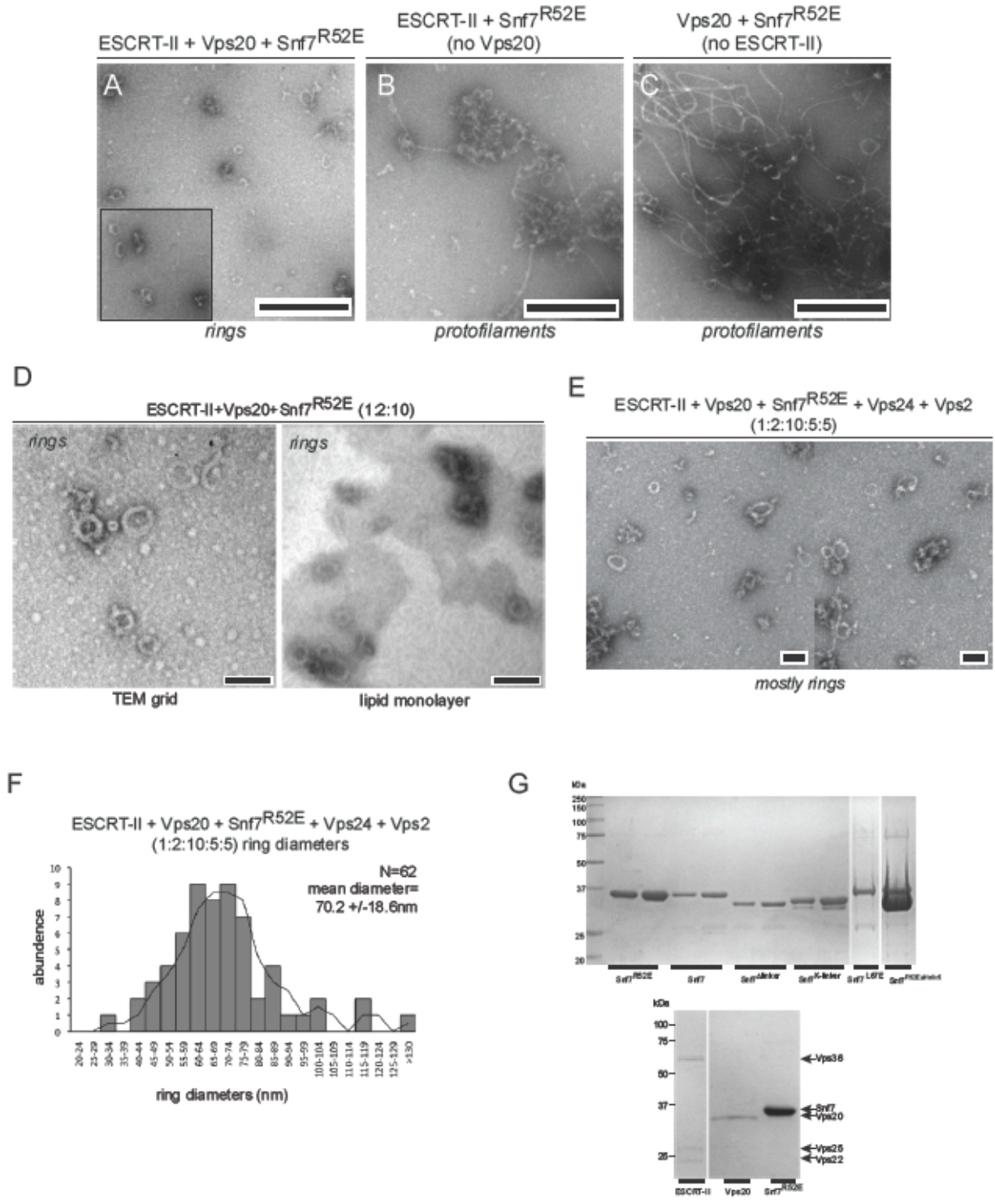
ESCRT-II + Vps20 + Snf7R52E
ESCRT-II + Snf7R52E (no Vps20)
Vps20 + Snf7R52E (no ESCRT-II)
A
B
C
rings
protofilaments
protofilaments
D
ESCRT-II+Vps20+Snf7R52E (1:2:10)
rings
rings
TEM grid
lipid monolayer
E
ESCRT-II + Vps20 + Snf7R52E + Vps24 + Vps2 (1:2:10:5:5)
mostly rings
F
ESCRT-II + Vps20 + Snf7R52E + Vps24 + Vps2 (1:2:10:5:5) ring diameters
N=62
mean diameter= 70.2 +/-18.6nm
abundance
ring diameters (nm)
G
kDa
Vps36
Snf7
Vps20
Vps25
Vps22
ESCRT-II
Vps20

Figure S7

A-C) TEM micrographs of ESCRT-II, Vps20, Snf7 co-assembly reactions containing all three components (**A**) or omitting Vps20 (**B**) or ESCRT-II (**C**).

D) Micrographs of ESCRT-II:Vps20:Snf7^{R52E} rings on TEM grids (*left*) or lipid monolayers (*right*).

E) ESCRT-II:Vps20:Snf7^{R52E}:Vps24:Vps2 (1:2:10:5:5) rings on TEM grids.

F) Measured ring diameters from Panel E.

G) Coomassie-stained gels of Snf7 mutant proteins used in this study. Coomassie-stained gels of ESCRT-II, Vps20, and Snf7^{R52E} used in the ESCRT-II:ESCRT-III co-assembly reactions. Scale bars: Panels A-C-500nm, Panels D&E-100nm.

We hypothesized that the globular densities associated with these rings represented ESCRT-II complexes that were potentially modulating ESCRT-III ring formation. When ESCRT-II was examined by TEM, globular protein densities 14.6±2.9nm in diameter were observed that appeared very similar to the densities associated with ESCRT-III rings (Figure 6D). Crystallographic studies suggest this diameter is consistent with the predicted size of negatively stained ESCRT-II complexes (Hierro, Sun et al. 2004). To confirm that these densities were indeed ESCRT-II, the complex was pre-incubated with 5nm Ni2+NTA-coated nano-gold beads, which can bind His6-tags with high affinity. Single 5nm nano-gold beads now decorated the protein densities, confirming they were ESCRT-II (Figure 6D).

We next added Vps20 and Snf7R52E with an ESCRT-II sample that was pre-incubated with 5nm nano-gold beads. We observed protein rings dotted by a single nano-gold labeled ESCRT-II (Figure 6E). These observations suggest that ESCRT-II and Vps20 may coordinate the polymerization of Snf7 polymers into highly curved ESCRT-II:ESCRT-III super-complexes (Figure 6F).

Interestingly, when ESCRT-II, Vps20, Snf7R52E, Vps24 and Vps2 were all co-incubated at a 1:2:10:5:5 ratio, almost no helical protofilaments were observed. Instead, we observed primarily rings with diameters 70.2±18.6nm similar to those formed by only ESCRT-II, Vps20, and Snf7R52E (Figure S7D-F).

Altogether, these data suggest that ESCRT-II and Vps20 may coordinate the architecture of Snf7 polymerization, favoring the formation of highly curved rings. These rings provide a possible structural explanation for the physical sequestration of transmembrane cargoes at distinct regions of the endosome surface prior to their packaging into vesicles.

Discussion

The ESCRT pathway mediates the capture, sequestration, and sorting of transmembrane proteins into multivesicular bodies that are ultimately delivered to the vacuole for degradation. The sequential assembly of distinct ESCRT complexes suggests an exquisite division of labor to achieve cargo sorting. Whereas ESCRTs-0,-I, and –II form stable hetero-oligomeric complexes, the dynamic cycling of ESCRT-III subunits from inactive monomers into active polymers drives the formation of cargo-laden vesicles. Here, we have reconstituted distinct stages of this dynamic ESCRT-III assembly that provide structural insights for how ESCRT-III achieves both cargo capture and vesicle formation.

Based on this work and the collective work of the ESCRT field, we propose a comprehensive model for ESCRT-mediated MVB biogenesis: 1) ESCRT-0,-I, and –II engage ubiquitinated cargo and concentrate this cargo into a patch on the endosome surface, 2) ESCRT-II initiates the assembly of an ESCRT-III ring-like polymer by directly binding Vps20, 3) ESCRT-III assembles by the sequential recruitment of its subunits, ultimately forming a helix, 4) the AAA ATPase Vps4 is recruited by ESCRT-III to recycle the ESCRT machinery off the MVB.

In our present work, we engineered precise residue substitutions that drive the robust oligomerization of Snf7. We then used a combination of TEM, biochemical, and cell biological techniques to elucidate the mechanism for Snf7 oligomeric assembly. Reconstituting Snf7 activation allowed us to characterize distinct sub-

reactions that occur during the ordered assembly of ESCRT-III. Ultimately, we propose that ESCRT-II and ESCRT-III co-assemble into cargo-capturing ring complexes that are transformed into membrane sculpting helices to drive ILV formation.

When assembled on an endosome, a ~65nm diameter protein ring would enclose approximately 3320nm2 of membrane surface. If this membrane area were remodeled into a sphere it would form a vesicle ~32nm in diameter, consistent with the observed size of ILVs in yeast MVBs (Wemmer, Azmi et al. 2011). Thus, we propose that an ESCRT-II:ESCRT-III ring super-complex assembles on the endosome surface and simultaneously mediates: 1) physical sequestration of transmembrane cargoes that will be packaged into the ILV, and 2) demarcation of the membrane surface area that is sculpted into the cargo-laden ILV (Figure 7A&B). Following Snf7 homo-oligomerization, Vps24 and Vps2 are recruited to the assembling ESCRT-III complex, potentially promoting the formation of an ESCRT-III helix with vesicle sculpting properties (Figure 7C&D).

Recent studies using giant unilamellar vesicles (GUVs) demonstrated that ESCRT-III constitutes the minimal machinery necessary to achieve ILV formation in vitro (Wollert and Hurley 2010). While these studies indeed highlighted the abilities of ESCRT-III to bind to and deform membranes, they were limited by the resolution of fluorescence microscopy and therefore provided little information as to the architecture ESCRT-III adopts during vesicle budding. Here, we have investigated

the underlying molecular mechanism of ESCRT-III-mediated membrane sculpting using the high visual resolution provided by TEM. Surprisingly, we find that specific ESCRT subunits modulate distinct architectural stages of ESCRT-III assembly. This is consistent with the fact that all core ESCRT proteins are essential to MVB cargo sorting; the loss of any subunit blocks cargo delivery to the vacuole.

ESCRT-II and Vps20 mediate Snf7 ring formation for cargo capture

ESCRT-II and Vps20, which physically links ESCRT-II to Snf7, appear to regulate both the size and shape of Snf7 oligomers. As such, ESCRT-II and Vps20 promote the formation of rings ~65nm in diameter that are ideal for physically capturing and sequestering ubiquitinated cargoes at the endosome. Since ESCRT-II contains two Vps25 subunits that each interact with a Vps20, a two-armed ESCRT-II may coordinate the formation of ESCRT-III rings by interacting with both Snf7 sub-filaments simultaneously. This is consistent with previous studies indicating that a two-armed ESCRT-II was necessary for ILV formation in yeast (Teis, Saksena et al. 2010).

Although ESCRT-II promotes the formation of highly curved ESCRT-III rings, it is notable that Snf7 protofilaments naturally spiral on lipid membranes. This intrinsic curvature is likely determined on the molecular level by specific interactions between Snf7 monomers that set the curvature pitch of the polymer. The flexibility of the Snf7 linker region, which has been shown in other ESCRT-III subunits to be

associated with conformational changes, may also provide flexibility that allows protofilament bending (Lata, Roessle et al. 2008).

Other protein polymers have been shown to undergo drastic changes in shape due to conformational changes within their monomers. FtsZ, a bacterial cytoskeletal protein, assembles into straight homo-oligomeric protofilaments that are converted into spirals and rings by conformational changes within their monomers (Lu, Reedy et al. 2000). Furthermore, these architectural dynamics can generate mechanical force that bends lipid membranes (Osawa, Anderson et al. 2009). FtsZ and ESCRT-III have both been proposed to play direct roles in the membrane remodeling necessary for cytokinesis, implying that there may be conceptual similarities shared between the dynamics of the protofilaments they form.

Vps24 and Vps2 promote ESCRT-III helix formation

Whereas ESCRT-II and Vps20 initiate ESCRT-III assembly that may promote capture cargo, we propose that Vps24 and Vps2 are recruited after cargo sequestration to transform ESCRT-III into a membrane deforming helix. They achieve this by directly modulating the three dimensional architecture of Snf7 filaments. By itself, Snf7 assembles into spirals that are ostensibly incapable of membrane deformation. The helices generated by the co-assembly of Snf7, Vps24, and Vps2 are architecturally distinct from these spirals and closely resemble protein helices formed by the membrane sculpting protein dynamin (Carr and Hinshaw 1997). One intriguing hypothesis is that the Snf7-dependent recruitment of Vps24 and Vps2 to endosomes

causes Snf7 spirals to reorganize into helices, thus driving membrane invaginations by a "molecular spring"-like mechanism. Protofilament remodeling may generate mechanical force that ultimately leads to membrane bending and the formation of a vesicle that buds into the endosomal interior (Figure 7C&D). The fact that Vps24 and Vps2 can remodel pre-existing Snf7 protofilaments into helices supports this model (Figure S5H). This is further supported by GUV-based experiments showing that Vps24 and Vps2 promote the association of fluorescent Snf7 with membrane invaginations (Figure S6D-H). This model also agrees with the proposed ordered assembly of ESCRT-III (Teis, Saksena et al. 2008).

Recent studies observed ~17nm diameter ESCRT-III-dependent helical filaments along the plasma membrane of cells undergoing cytokinetic abscission (Guizetti, Schermelleh et al. 2011). Human Snf7 and Vps2 localized along these filaments and were necessary for their assembly. One intriguing hypothesis is that the ESCRT-III helices presented here represent structural analogues of the filaments that purportedly drive mammalian cytokinetic abscission, suggesting structural conservation in ESCRT function between different biological processes.

Although we observed that Vps24 and Vps2 promoted the formation of protein helices, we did not detect Vps24/Vps2 "domes" in our assembly reactions, which have been previously implicated as mediators of ILV formation (Lata, Roessle et al. 2008). In these studies, "domes" formed in the absence of Snf7 and only through significant truncation of Vps24 and Vps2. The experiments presented here indicate

that Snf7, Vps24, and Vps2 may co-assemble into a hetero-oligomeric helix to achieve ILV budding.

The architecture of ESCRT-III is similar to other membrane sculpting oligomers

The ESCRT-III structures observed in this study are conceptually reminiscent of the membrane scission machines FtsZ and dynamin. Both these proteins oligomerize during membrane remodeling, as well as interact with other proteins that modulate their architectural dynamics. Intriguingly, FtsZ interacts with FzlA, a protein recently shown to transform linear FtsZ protofilaments into spiraling helices in vitro (Goley, Dye et al. 2011). Similarly, dynamin forms helices that work cooperatively with BAR and F-BAR proteins to mediate clathrin vesicle release.

One obvious difference between FtsZ, dynamin, and ESCRT-III is that FtsZ and dynamin directly hydrolyze GTP. This induces architectural changes that promote membrane scission. Although ESCRT-III subunits do not hydrolyze NTPs directly, they recruit the AAA ATPase Vps4 that provides energy via ATP hydrolysis. This energy may either be "stored" by ESCRT-III subunits in their "closed" conformations, or added directly to ESCRT-III through physical contact with ESCRT-III helices. Thus, the ~85nm diameter ESCRT-III helices presented here may represent a "relaxed" state that could be constricted or even broken by Vps4.

A working model: ESCRT-III adopts multiple architectures to achieve cargo sorting

The existence of distinct architectural forms to ESCRT-III suggests it matures through at least two stages during its ordered assembly:

1) "early" stage assembly that creates a cargo-sequestering ring of defined size, and

2) "late" stage assembly that generates a membrane-sculpting helix for ILV formation.

Several in vivo observations support the existence of distinct stages to ESCRT-III assembly. Vps24 and Vps2 constitute a sub-complex and are recruited during or after Snf7 polymerization, consistent with their role as "late" modulators of ESCRT-III architecture. Furthermore, deletion of either Vps24 or Vps2 blocks ILV formation, but not cargo sequestration at endosomes (Teis, Saksena et al. 2010). Consistent with this are studies showing that blockage of late stages of the ESCRT pathway lead to receptor enrichment at late endosomes and sustained EGF signaling (Babst, Odorizzi et al. 2000). These phenomena could be explained by the formation of ESCRT-II:ESCRT-III rings which sequester cargo, but fail execute vesicle formation.

Despite direct visualization of ESCRT-III oligomers, several key questions remain. The most pressing is the mechanism by which ESCRT-III mediates vesicle scission. The structures observed in this study indicate several possible mechanisms. Vps4 could engage the ESCRT-III helix and drive filament sliding or constriction. This

would narrow the ILV neck to a point of spontaneous collapse at the helix base, liberating the vesicle without consuming ESCRT-III itself (Figure 7D). Furthermore, the disassembly of ESCRT-III by Vps4 may destabilize the highly curved neck region, leading to membrane buckling and scission. In direct contrast to some previous studies, we noted that ESCRT-III often associates with membrane invaginations on GUVs for long periods of time (often several minutes). The presence of ESCRT-III proteins did not lead to "efficient" scission independent of Vps4 in these cases (Figure S6 and personal observations). As such, conclusions concerning Vps4-independent vesicle scission by ESCRT-III may need careful re-evaluation. No doubt future studies are needed to further reveal insights about the remarkable ESCRT-III pathway.

Figure 7- Proposed model for ESCRT-III-mediated MVB biogenesis.

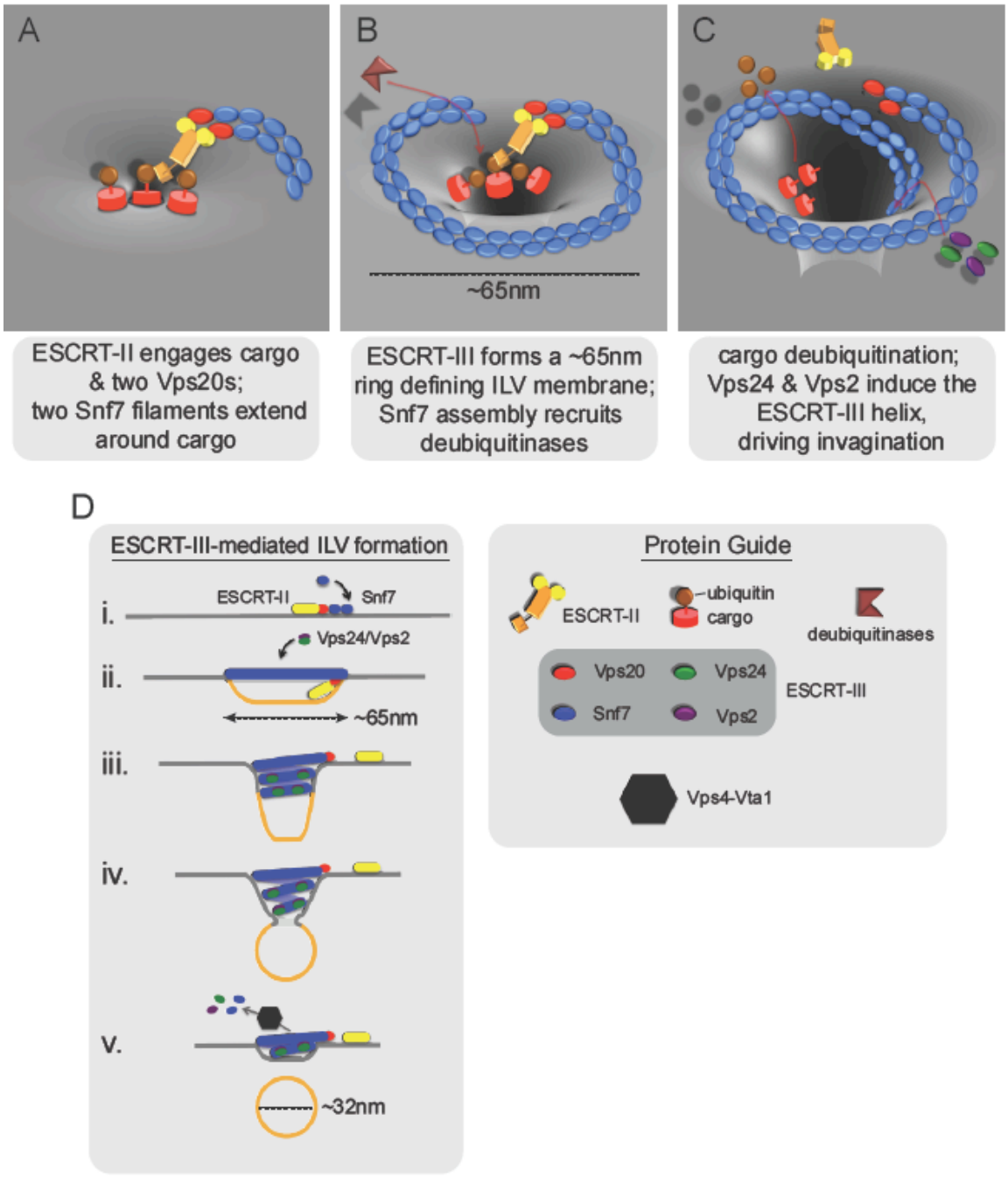

Figure 7- Proposed model for ESCRT-III-mediated MVB biogenesis.

Acknowledgements:

WMH is supported by a Sam and Nancy Fleming Research Fellowship. NJB is supported by an American Cancer Society Postdoctoral Fellowship (PF-12-062-01-DMC). We thank Beverly Wendland for the Mup1-pHluorin integration plasmid, and Roger Williams for the ESCRT-II expression construct. The authors particularly thank Neil Adige and Bret Judson for all technical expertise. We also thank Jeanne Quirit, Abbie Davies, Chris Stefan, Jason MacGurn, Tony Bretscher, Chris Fromme, David Teis, and Suraj Saksena for helpful discussions.

References

Aigelsreiter, A., E. Janig, et al. (2007). "How a cell deals with abnormal proteins. Pathogenetic mechanisms in protein aggregation diseases." Pathobiology **74**(3): 145-58.

Alberti, S., K. Bohse, et al. (2004). "The cochaperone HspBP1 inhibits the CHIP ubiquitin ligase and stimulates the maturation of the cystic fibrosis transmembrane conductance regulator." Mol Biol Cell **15**(9): 4003-10.

Apaja, P. M., H. Xu, et al. "Quality control for unfolded proteins at the plasma membrane." J Cell Biol **191**(3): 553-70.

Babst, M. (2011). "MVB vesicle formation: ESCRT-dependent, ESCRT-independent and everything in between." Curr Opin Cell Biol **23**(4): 452-7.

Babst, M., D. J. Katzmann, et al. (2002). "Escrt-III: an endosome-associated heterooligomeric protein complex required for mvb sorting." Dev Cell **3**(2): 271-82.

Babst, M., G. Odorizzi, et al. (2000). "Mammalian tumor susceptibility gene 101 (TSG101) and the yeast homologue, Vps23p, both function in late endosomal trafficking." Traffic **1**(3): 248-58.

Babst, M., B. Wendland, et al. (1998). "The Vps4p AAA ATPase regulates membrane association of a Vps protein complex required for normal endosome function." EMBO J **17**(11): 2982-93.

Bajorek, M., H. L. Schubert, et al. (2009). "Structural basis for ESCRT-III protein autoinhibition." Nat Struct Mol Biol **16**(7): 754-62.

Barral, J. M., S. A. Broadley, et al. (2004). "Roles of molecular chaperones in protein misfolding diseases." Semin Cell Dev Biol **15**(1): 17-29.

Becuwe, M., N. Vieira, et al. "A molecular switch on an arrestin-like protein relays glucose signaling to transporter endocytosis." J Cell Biol **196**(2): 247-59.

Blobel, G. (1980). "Intracellular protein topogenesis." Proc Natl Acad Sci U S A **77**(3): 1496-500.

Bolen, D. W. and I. V. Baskakov (2001). "The osmophobic effect: natural selection of a thermodynamic force in protein folding." J Mol Biol **310**(5): 955-63.

Bowie, J. U. (2005). "Solving the membrane protein folding problem." Nature **438**(7068): 581-9.

Brown, C. R., L. Q. Hong-Brown, et al. (1996). "Chemical chaperones correct the mutant phenotype of the delta F508 cystic fibrosis transmembrane conductance regulator protein." Cell Stress Chaperones **1**(2): 117-25.

Carr, J. F. and J. E. Hinshaw (1997). "Dynamin assembles into spirals under physiological salt conditions upon the addition of GDP and gamma-phosphate analogues." J Biol Chem **272**(44): 28030-5.

Choo-Kang, L. R. and P. L. Zeitlin (2001). "Induction of HSP70 promotes DeltaF508 CFTR trafficking." Am J Physiol Lung Cell Mol Physiol **281**(1): L58-68.

Cohen, M., F. Stutz, et al. (2003). "Ubp3 requires a cofactor, Bre5, to specifically de-ubiquitinate the COPII protein, Sec23." Nat Cell Biol **5**(7): 661-7.

Connell, P., C. A. Ballinger, et al. (2001). "The co-chaperone CHIP regulates protein triage decisions mediated by heat-shock proteins." Nat Cell Biol **3**(1): 93-6.

Demmel, L., M. Beck, et al. (2008). "Nucleocytoplasmic shuttling of the Golgi phosphatidylinositol 4-kinase Pik1 is regulated by 14-3-3 proteins and coordinates Golgi function with cell growth." Mol Biol Cell **19**(3): 1046-61.
Doherty, G. J. and H. T. McMahon (2009). "Mechanisms of endocytosis." Annu Rev Biochem **78**: 857-902.
Eccles, S. A., A. Massey, et al. (2008). "NVP-AUY922: a novel heat shock protein 90 inhibitor active against xenograft tumor growth, angiogenesis, and metastasis." Cancer Res **68**(8): 2850-60.
Egan, M. E., J. Glockner-Pagel, et al. (2002). "Calcium-pump inhibitors induce functional surface expression of Delta F508-CFTR protein in cystic fibrosis epithelial cells." Nat Med **8**(5): 485-92.
Egner, R. and K. Kuchler (1996). "The yeast multidrug transporter Pdr5 of the plasma membrane is ubiquitinated prior to endocytosis and degradation in the vacuole." FEBS Lett **378**(2): 177-81.
Ellis, J. (1987). "Proteins as molecular chaperones." Nature **328**(6129): 378-9.
Eswar, N., B. Webb, et al. (2006). "Comparative protein structure modeling using Modeller." Curr Protoc Bioinformatics **Chapter 5**: Unit 5 6.
Eswar, N., B. Webb, et al. (2007). "Comparative protein structure modeling using MODELLER." Curr Protoc Protein Sci **Chapter 2**: Unit 2 9.
Finley, D. (2009). "Recognition and processing of ubiquitin-protein conjugates by the proteasome." Annu Rev Biochem **78**: 477-513.
Garcia-Mata, R., Y. S. Gao, et al. (2002). "Hassles with taking out the garbage: aggravating aggresomes." Traffic **3**(6): 388-96.
Gardner, R. G., Z. W. Nelson, et al. (2005). "Degradation-mediated protein quality control in the nucleus." Cell **120**(6): 803-15.
Gekko, K. and S. N. Timasheff (1981). "Mechanism of protein stabilization by glycerol: preferential hydration in glycerol-water mixtures." Biochemistry **20**(16): 4667-76.
Glover, J. R. and S. Lindquist (1998). "Hsp104, Hsp70, and Hsp40: a novel chaperone system that rescues previously aggregated proteins." Cell **94**(1): 73-82.
Glozman, R., T. Okiyoneda, et al. (2009). "N-glycans are direct determinants of CFTR folding and stability in secretory and endocytic membrane traffic." J Cell Biol **184**(6): 847-62.
Goley, E. D., N. A. Dye, et al. (2011). "Imaging-based identification of a critical regulator of FtsZ protofilament curvature in Caulobacter." Mol Cell **39**(6): 975-87.
Gong, X. and A. Chang (2001). "A mutant plasma membrane ATPase, Pma1-10, is defective in stability at the yeast cell surface." Proc Natl Acad Sci U S A **98**(16): 9104-9.
Guizetti, J., L. Schermelleh, et al. (2011). "Cortical Constriction During Abscission Involves Helices of ESCRT-III-Dependent Filaments." Science.
Haglund, K., S. Sigismund, et al. (2003). "Multiple monoubiquitination of RTKs is sufficient for their endocytosis and degradation." Nat Cell Biol **5**(5): 461-6.
Hanna, J., N. A. Hathaway, et al. (2006). "Deubiquitinating enzyme Ubp6 functions noncatalytically to delay proteasomal degradation." Cell **127**(1): 99-111.

Hanson, P. I., R. Roth, et al. (2008). "Plasma membrane deformation by circular arrays of ESCRT-III protein filaments." J Cell Biol **180**(2): 389-402.
Harada, K., T. Okiyoneda, et al. (2006). "Calreticulin negatively regulates the cell surface expression of cystic fibrosis transmembrane conductance regulator." J Biol Chem **281**(18): 12841-8.
Hardesty, B. and G. Kramer (2001). "Folding of a nascent peptide on the ribosome." Prog Nucleic Acid Res Mol Biol **66**: 41-66.
Hatakeyama, R., M. Kamiya, et al. "Endocytosis of the aspartic acid/glutamic acid transporter Dip5 is triggered by substrate-dependent recruitment of the Rsp5 ubiquitin ligase via the arrestin-like protein Aly2." Mol Cell Biol **30**(24): 5598-607.
Heck, J. W., S. K. Cheung, et al. (2010). "Cytoplasmic protein quality control degradation mediated by parallel actions of the E3 ubiquitin ligases Ubr1 and San1." Proc Natl Acad Sci U S A **107**(3): 1106-11.
Henne, W. M., N. J. Buchkovich, et al. (2011). "The ESCRT pathway." Dev Cell **21**(1): 77-91.
Heo, J. M., N. Livnat-Levanon, et al. "A stress-responsive system for mitochondrial protein degradation." Mol Cell **40**(3): 465-80.
Hicke, L. and H. Riezman (1996). "Ubiquitination of a yeast plasma membrane receptor signals its ligand-stimulated endocytosis." Cell **84**(2): 277-87.
Hierro, A., J. Sun, et al. (2004). "Structure of the ESCRT-II endosomal trafficking complex." Nature **431**(7005): 221-5.
Hirano, S., N. Suzuki, et al. (2006). "Structural basis of ubiquitin recognition by mammalian Eap45 GLUE domain." Nat Struct Mol Biol **13**(11): 1031-2.
Hochstrasser, M. (2009). "Origin and function of ubiquitin-like proteins." Nature **458**(7237): 422-9.
Horwich, A. (2004). "Cell biology: sight at the end of the tunnel." Nature **431**(7008): 520-2.
Hu, Y. and N. F. Mivechi (2003). "HSF-1 interacts with Ral-binding protein 1 in a stress-responsive, multiprotein complex with HSP90 in vivo." J Biol Chem **278**(19): 17299-306.
Iwai, K. and F. Tokunaga (2009). "Linear polyubiquitination: a new regulator of NF-kappaB activation." EMBO Rep **10**(7): 706-13.
Jacobson, A. D., N. Y. Zhang, et al. (2009). "The lysine 48 and lysine 63 ubiquitin conjugates are processed differently by the 26 s proteasome." J Biol Chem **284**(51): 35485-94.
Jenness, D. D., Y. Li, et al. (1997). "Elimination of defective alpha-factor pheromone receptors." Mol Cell Biol **17**(11): 6236-45.
Jensen, M. R., J. Schoepfer, et al. (2008). "NVP-AUY922: a small molecule HSP90 inhibitor with potent antitumor activity in preclinical breast cancer models." Breast Cancer Res **10**(2): R33.
Katzmann, D. J., M. Babst, et al. (2001). "Ubiquitin-dependent sorting into the multivesicular body pathway requires the function of a conserved endosomal protein sorting complex, ESCRT-I." Cell **106**(2): 145-55.

Katzmann, D. J., S. Sarkar, et al. (2004). "Multivesicular body sorting: ubiquitin ligase Rsp5 is required for the modification and sorting of carboxypeptidase S." Mol Biol Cell **15**(2): 468-80.
Kee, Y., W. Munoz, et al. (2006). "The deubiquitinating enzyme Ubp2 modulates Rsp5-dependent Lys63-linked polyubiquitin conjugates in Saccharomyces cerevisiae." J Biol Chem **281**(48): 36724-31.
Kolling, R. and C. P. Hollenberg (1994). "The ABC-transporter Ste6 accumulates in the plasma membrane in a ubiquitinated form in endocytosis mutants." EMBO J **13**(14): 3261-71.
Kopito, R. R. (2000). "Aggresomes, inclusion bodies and protein aggregation." Trends Cell Biol **10**(12): 524-30.
Lam, M. H., D. Urban-Grimal, et al. (2009). "Interaction of the deubiquitinating enzyme Ubp2 and the e3 ligase Rsp5 is required for transporter/receptor sorting in the multivesicular body pathway." PLoS One **4**(1): e4259.
Lansbury, P. T. and H. A. Lashuel (2006). "A century-old debate on protein aggregation and neurodegeneration enters the clinic." Nature **443**(7113): 774-9.
Lata, S., M. Roessle, et al. (2008). "Structural basis for autoinhibition of ESCRT-III CHMP3." J Mol Biol **378**(4): 818-27.
Lauwers, E., G. Grossmann, et al. (2007). "Evidence for coupled biogenesis of yeast Gap1 permease and sphingolipids: essential role in transport activity and normal control by ubiquitination." Mol Biol Cell **18**(8): 3068-80.
Lee, B. H., M. J. Lee, et al. "Enhancement of proteasome activity by a small-molecule inhibitor of USP14." Nature **467**(7312): 179-84.
Leggett, D. S., J. Hanna, et al. (2002). "Multiple associated proteins regulate proteasome structure and function." Mol Cell **10**(3): 495-507.
Lennox, G., J. Lowe, et al. (1988). "Ubiquitin is a component of neurofibrillary tangles in a variety of neurodegenerative diseases." Neurosci Lett **94**(1-2): 211-7.
Lewis, M. J. and H. R. Pelham (2009). "Inefficient quality control of thermosensitive proteins on the plasma membrane." PLoS One **4**(4): e5038.
Li, Y., T. Kane, et al. (1999). "Yeast mutants affecting possible quality control of plasma membrane proteins." Mol Cell Biol **19**(5): 3588-99.
Lin, C. H., J. A. MacGurn, et al. (2008). "Arrestin-related ubiquitin-ligase adaptors regulate endocytosis and protein turnover at the cell surface." Cell **135**(4): 714-25.
Lowe, J., G. Lennox, et al. (1988). "A filamentous inclusion body within anterior horn neurones in motor neurone disease defined by immunocytochemical localisation of ubiquitin." Neurosci Lett **94**(1-2): 203-10.
Lu, C., M. Reedy, et al. (2000). "Straight and curved conformations of FtsZ are regulated by GTP hydrolysis." J Bacteriol **182**(1): 164-70.
Lukacs, G. L., X. B. Chang, et al. (1993). "The delta F508 mutation decreases the stability of cystic fibrosis transmembrane conductance regulator in the plasma membrane. Determination of functional half-lives on transfected cells." J Biol Chem **268**(29): 21592-8.

Lukacs, G. L., A. Mohamed, et al. (1994). "Conformational maturation of CFTR but not its mutant counterpart (delta F508) occurs in the endoplasmic reticulum and requires ATP." EMBO J **13**(24): 6076-86.
Macgurn, J. A., P. C. Hsu, et al. "Ubiquitin and membrane protein turnover: from cradle to grave." Annu Rev Biochem **81**: 231-59.
Macgurn, J. A., P. C. Hsu, et al. (2012). "Ubiquitin and membrane protein turnover: from cradle to grave." Annu Rev Biochem **81**: 231-59.
Magby, J. P., A. P. Neal, et al. "Channelopathies: summary of the hot topic keynotes session." Neurotoxicology **32**(5): 661-5.
Marcusson, E. G., B. F. Horazdovsky, et al. (1994). "The sorting receptor for yeast vacuolar carboxypeptidase Y is encoded by the VPS10 gene." Cell **77**(4): 579-86.
McNicholas, S., E. Potterton, et al. (2011). "Presenting your structures: the CCP4mg molecular-graphics software." Acta Crystallogr D Biol Crystallogr **67**(Pt 4): 386-94.
Melnikova, I. (2007). "Therapies for Alzheimer's disease." Nat Rev Drug Discov **6**(5): 341-2.
Meng, F. G., Y. K. Hong, et al. (2004). "Osmophobic effect of glycerol on irreversible thermal denaturation of rabbit creatine kinase." Biophys J **87**(4): 2247-54.
Meusser, B., C. Hirsch, et al. (2005). "ERAD: the long road to destruction." Nat Cell Biol **7**(8): 766-72.
Mori, H., J. Kondo, et al. (1987). "Ubiquitin is a component of paired helical filaments in Alzheimer's disease." Science **235**(4796): 1641-4.
Murata, S., Y. Minami, et al. (2001). "CHIP is a chaperone-dependent E3 ligase that ubiquitylates unfolded protein." EMBO Rep **2**(12): 1133-8.
Murata, S., H. Udono, et al. (2001). "Immunoproteasome assembly and antigen presentation in mice lacking both PA28alpha and PA28beta." EMBO J **20**(21): 5898-907.
Muziol, T., E. Pineda-Molina, et al. (2006). "Structural basis for budding by the ESCRT-III factor CHMP3." Dev Cell **10**(6): 821-30.
Nikko, E. and H. R. Pelham (2009). "Arrestin-mediated endocytosis of yeast plasma membrane transporters." Traffic **10**(12): 1856-67.
Nillegoda, N. B., M. A. Theodoraki, et al. (2010). "Ubr1 and Ubr2 function in a quality control pathway for degradation of unfolded cytosolic proteins." Mol Biol Cell **21**(13): 2102-16.
Nunes, S. L. and S. K. Calderwood (1995). "Heat shock factor-1 and the heat shock cognate 70 protein associate in high molecular weight complexes in the cytoplasm of NIH-3T3 cells." Biochem Biophys Res Commun **213**(1): 1-6.
Okiyoneda, T., H. Barriere, et al. "Peripheral protein quality control removes unfolded CFTR from the plasma membrane." Science **329**(5993): 805-10.
Osawa, M., D. E. Anderson, et al. (2009). "Curved FtsZ protofilaments generate bending forces on liposome membranes." EMBO J **28**(22): 3476-84.
Papa, F. R., A. Y. Amerik, et al. (1999). "Interaction of the Doa4 deubiquitinating enzyme with the yeast 26S proteasome." Mol Biol Cell **10**(3): 741-56.
Parsell, D. A., A. S. Kowal, et al. (1994). "Protein disaggregation mediated by heat-shock protein Hsp104." Nature **372**(6505): 475-8.

Paulson, G. W. and T. W. Prior (1997). "Issues related to DNA testing for Huntington's disease in symptomatic patients." Semin Neurol **17**(3): 235-8.
Pind, S., J. R. Riordan, et al. (1994). "Participation of the endoplasmic reticulum chaperone calnexin (p88, IP90) in the biogenesis of the cystic fibrosis transmembrane conductance regulator." J Biol Chem **269**(17): 12784-8.
Pizzirusso, M. and A. Chang (2004). "Ubiquitin-mediated targeting of a mutant plasma membrane ATPase, Pma1-7, to the endosomal/vacuolar system in yeast." Mol Biol Cell **15**(5): 2401-9.
Prosser, D. C., K. Whitworth, et al. (2010). "Quantitative analysis of endocytosis with cytoplasmic pHluorin chimeras." Traffic **11**(9): 1141-50.
Puertollano, R. and J. S. Bonifacino (2004). "Interactions of GGA3 with the ubiquitin sorting machinery." Nat Cell Biol **6**(3): 244-51.
Qian, S. B., X. Zhang, et al. (2010). "mTORC1 links protein quality and quantity control by sensing chaperone availability." J Biol Chem **285**(35): 27385-95.
Raymond, C. K., I. Howald-Stevenson, et al. (1992). "Morphological classification of the yeast vacuolar protein sorting mutants: evidence for a prevacuolar compartment in class E vps mutants." Mol Biol Cell **3**(12): 1389-402.
Ren, X. and J. H. Hurley "VHS domains of ESCRT-0 cooperate in high-avidity binding to polyubiquitinated cargo." EMBO J **29**(6): 1045-54.
Risinger, A. L. and C. A. Kaiser (2008). "Different ubiquitin signals act at the Golgi and plasma membrane to direct GAP1 trafficking." Mol Biol Cell **19**(7): 2962-72.
Roberson, E. D. and L. Mucke (2006). "100 years and counting: prospects for defeating Alzheimer's disease." Science **314**(5800): 781-4.
Robinson, J. S., D. J. Klionsky, et al. (1988). "Protein sorting in Saccharomyces cerevisiae: isolation of mutants defective in the delivery and processing of multiple vacuolar hydrolases." Mol Cell Biol **8**(11): 4936-48.
Rosser, M. F., D. E. Grove, et al. (2008). "Assembly and misassembly of cystic fibrosis transmembrane conductance regulator: folding defects caused by deletion of F508 occur before and after the calnexin-dependent association of membrane spanning domain (MSD) 1 and MSD2." Mol Biol Cell **19**(11): 4570-9.
Rubenstein, R. C., M. E. Egan, et al. (1997). "In vitro pharmacologic restoration of CFTR-mediated chloride transport with sodium 4-phenylbutyrate in cystic fibrosis epithelial cells containing delta F508-CFTR." J Clin Invest **100**(10): 2457-65.
Rubenstein, R. C. and B. M. Lyons (2001). "Sodium 4-phenylbutyrate downregulates HSC70 expression by facilitating mRNA degradation." Am J Physiol Lung Cell Mol Physiol **281**(1): L43-51.
Rubenstein, R. C. and P. L. Zeitlin (2000). "Sodium 4-phenylbutyrate downregulates Hsc70: implications for intracellular trafficking of DeltaF508-CFTR." Am J Physiol Cell Physiol **278**(2): C259-67.
Rubio-Texeira, M. and C. A. Kaiser (2006). "Amino acids regulate retrieval of the yeast general amino acid permease from the vacuolar targeting pathway." Mol Biol Cell **17**(7): 3031-50.

Saksena, S. and S. D. Emr (2009). "ESCRTs and human disease." Biochem Soc Trans **37**(Pt 1): 167-72.
Saksena, S., J. Wahlman, et al. (2009). "Functional reconstitution of ESCRT-III assembly and disassembly." Cell **136**(1): 97-109.
Scaglione, K. M., E. Zavodszky, et al. (2011). "Ube2w and ataxin-3 coordinately regulate the ubiquitin ligase CHIP." Mol Cell **43**(4): 599-612.
Sharma, M., F. Pampinella, et al. (2004). "Misfolding diverts CFTR from recycling to degradation: quality control at early endosomes." J Cell Biol **164**(6): 923-33.
Shearer, A. G. and R. Y. Hampton (2004). "Structural control of endoplasmic reticulum-associated degradation: effect of chemical chaperones on 3-hydroxy-3-methylglutaryl-CoA reductase." J Biol Chem **279**(1): 188-96.
Shenoy, S. K. and R. J. Lefkowitz (2005). "Receptor-specific ubiquitination of beta-arrestin directs assembly and targeting of seven-transmembrane receptor signalosomes." J Biol Chem **280**(15): 15315-24.
Shenoy, S. K., P. H. McDonald, et al. (2001). "Regulation of receptor fate by ubiquitination of activated beta 2-adrenergic receptor and beta-arrestin." Science **294**(5545): 1307-13.
Sheppard, D. N. and M. J. Welsh (1999). "Structure and function of the CFTR chloride channel." Physiol Rev **79**(1 Suppl): S23-45.
Shi, Y., D. D. Mosser, et al. (1998). "Molecular chaperones as HSF1-specific transcriptional repressors." Genes Dev **12**(5): 654-66.
Shim, S., L. A. Kimpler, et al. (2007). "Structure/function analysis of four core ESCRT-III proteins reveals common regulatory role for extreme C-terminal domain." Traffic **8**(8): 1068-79.
Sigismund, S., T. Woelk, et al. (2005). "Clathrin-independent endocytosis of ubiquitinated cargos." Proc Natl Acad Sci U S A **102**(8): 2760-5.
Sipos, L. and G. von Heijne (1993). "Predicting the topology of eukaryotic membrane proteins." Eur J Biochem **213**(3): 1333-40.
Slagsvold, T., R. Aasland, et al. (2005). "Eap45 in mammalian ESCRT-II binds ubiquitin via a phosphoinositide-interacting GLUE domain." J Biol Chem **280**(20): 19600-6.
Sokolov, M. V., I. V. Panyutin, et al. "Dynamics of the transcriptome response of cultured human embryonic stem cells to ionizing radiation exposure." Mutat Res **709-710**: 40-8.
Stringer, D. K. and R. C. Piper "A single ubiquitin is sufficient for cargo protein entry into MVBs in the absence of ESCRT ubiquitination." J Cell Biol **192**(2): 229-42.
Sun, F., Z. Mi, et al. (2008). "Chaperone displacement from mutant cystic fibrosis transmembrane conductance regulator restores its function in human airway epithelia." FASEB J **22**(9): 3255-63.
Taylor, J. P., J. Hardy, et al. (2002). "Toxic proteins in neurodegenerative disease." Science **296**(5575): 1991-5.
Teis, D., S. Saksena, et al. (2008). "Ordered assembly of the ESCRT-III complex on endosomes is required to sequester cargo during MVB formation." Dev Cell **15**(4): 578-89.

Teis, D., S. Saksena, et al. (2010). "ESCRT-II coordinates the assembly of ESCRT-III filaments for cargo sorting and multivesicular body vesicle formation." EMBO J **29**(5): 871-83.
Teo, H., O. Perisic, et al. (2004). "ESCRT-II, an endosome-associated complex required for protein sorting: crystal structure and interactions with ESCRT-III and membranes." Dev Cell **7**(4): 559-69.
Tokunaga, F., S. Sakata, et al. (2009). "Involvement of linear polyubiquitylation of NEMO in NF-kappaB activation." Nat Cell Biol **11**(2): 123-32.
Vashist, S., M. Cushman, et al. "Applying Hsp104 to protein-misfolding disorders." Biochem Cell Biol **88**(1): 1-13.
Vishnivetskiy, S. A., M. M. Hosey, et al. (2004). "Mapping the arrestin-receptor interface. Structural elements responsible for receptor specificity of arrestin proteins." J Biol Chem **279**(2): 1262-8.
Wang, J., H. Q. Sun, et al. (2007). "PI4P promotes the recruitment of the GGA adaptor proteins to the trans-Golgi network and regulates their recognition of the ubiquitin sorting signal." Mol Biol Cell **18**(7): 2646-55.
Wang, X., J. Venable, et al. (2006). "Hsp90 cochaperone Aha1 downregulation rescues misfolding of CFTR in cystic fibrosis." Cell **127**(4): 803-15.
Ward, C. L. and R. R. Kopito (1994). "Intracellular turnover of cystic fibrosis transmembrane conductance regulator. Inefficient processing and rapid degradation of wild-type and mutant proteins." J Biol Chem **269**(41): 25710-8.
Wemmer, M., I. Azmi, et al. (2011). "Bro1 binding to Snf7 regulates ESCRT-III membrane scission activity in yeast." J Cell Biol **192**(2): 295-306.
Winklhofer, K. F., J. Tatzelt, et al. (2008). "The two faces of protein misfolding: gain- and loss-of-function in neurodegenerative diseases." EMBO J **27**(2): 336-49.
Wollert, T. and J. H. Hurley (2010). "Molecular mechanism of multivesicular body biogenesis by ESCRT complexes." Nature **464**(7290): 864-9.
Wooten, M. W. and T. Geetha (2006). "The role of ubiquitin in neurotrophin receptor signalling and sorting." Biochem Soc Trans **34**(Pt 5): 757-60.
Yang, Y., S. Janich, et al. (1993). "The common variant of cystic fibrosis transmembrane conductance regulator is recognized by hsp70 and degraded in a pre-Golgi nonlysosomal compartment." Proc Natl Acad Sci U S A **90**(20): 9480-4.
Yao, X. L. and M. Hong (2001). "Dipolar filtered 1H-13C heteronuclear correlation spectroscopy for resonance assignment of proteins." J Biomol NMR **20**(3): 263-74.
Zamborlini, A., Y. Usami, et al. (2006). "Release of autoinhibition converts ESCRT-III components into potent inhibitors of HIV-1 budding." Proc Natl Acad Sci U S A **103**(50): 19140-5.

Table 2 Summarizes of strains used in the Chapter II, III, IV

Strain	Genotype	Source
SEY6210	*MATα leu2-3, 112 ura3-52 his3- Δ 200 trp1-Δ901 lys2-801 suc2- Δ9*	Robinson et al., 1988
SEY6210.1	*MATa leu2-3, 112 ura3-52 his3- Δ 200 trp1-Δ901 lys2-801 suc2- Δ9*	Robinson et al., 1988
BY4741	*MATa ura3-Δ0 his3-Δ1 leu2-Δ0 met15-Δ0*	ResGen™ Collection
CLY461	*Δart1*::HIS3MX6 (SEY6210.1)	Lin et al., 2008
CLY378	*Δart2*::HIS3MX6 (SEY6210.1)	Lin et al., 2008
CLY383	*Δart3*::HIS3MX6 (SEY6210.1)	Lin et al., 2008
CLY385	*Δart4*::HIS3MX6 (SEY6210.1)	Lin et al., 2008
CLY386	*Δart5*::HIS3MX6 (SEY6210.1)	Lin et al., 2008
CLY387	*Δart6*::HIS3MX6 (SEY6210.1)	Lin et al., 2008
CLY388	*Δart7*::HIS3MX6 (SEY6210.1)	Lin et al., 2008
CLY389	*Δart8*::HIS3MX6 (SEY6210.1)	Lin et al., 2008
CLY390	*Δart9*::HIS3MX6 (SEY6210.1)	Lin et al., 2008
YYZ9	*Δart1*::HIS3MX6*, Δart2*::TRP (SEY6210.1)	This study
MLY143	*Δart1*::HIS *Δart4*::KAN *Δart5*::KAN(SEY6210.1*)*	This study
MLY142	*Δart1*::HIS *Δart2::TRP Δart7*::KAN *Δart9*::KAN(SEY6210*)*	This study
MLY137	*Δart1*::HIS *Δart2::TRP Δart3*::KAN *Δart4*::KAN Δart5::KAN Δart6::KAN Δart9::KAN(SEY6210.1*)*	This study
TCY60	*SEY6210 rsp5 ::HIS3 pRS416-pRSP5-3xHA-RSP5*	This study
JMY1085	*SEY6210 rsp5 ::HIS3 pRS415-pRSP5-3xHA-rsp5ww1*	This study
JMY1086	*SEY6210 rsp5 ::HIS3 pRS415-pRSP5-3xHA-rsp5ww2*	This study
JMY1087	*SEY6210 rsp5 ::HIS3 pRS415-pRSP5-3xHA-rsp5ww3*	This study
JMY78	Mup1-HTF::TRP1MX6 (SEY6210)	
YYZ72	Pdr5-HTF::TRP1MX6 (SEY6210)	Lin et al., 2008
YYZ74	Hxt3-HTF::TRP1MX6 (SEY6210)	This study
YYZ73	*Aqr1-HTF::TRP1MX6 (SEY6210)*	This study
YYZ79	Ste3-HTF::TRP1MX6 (SEY6210)	This study
YYZ77	*Δart1*::HIS3MX6 LYP1-HTF::TRP1MX6 (SEY6210)	
SRY76	*Δend3*::HIS3MX6 (SEY6210)	This study
HDY371	*Δrvs163*::TRP (SEY6210)	This study
YYZ12	*Δlyp1::HIS3MX6 (SEY6210)*	This study
YYZ15	*Δart1::HIS3MX6 Δlyp1::TRP* (SEY6210.1)	This study

Table 3 Summarizes of plasmids used in the Chapter II, III, IV

Strain	Description	Source
pCHL677	pRS416-P_{LYP1}-*LYP1*-GFP	Lin et al., 2008
pCHL571	pRS416-P_{CAN1}-*CAN1*-GFP	Lin et al., 2008
pCHL642	pRS416-P_{MUP1}-*MUP1*-GFP	Lin et al., 2008
pSR21	pRS416-P_{FUR4}-*FUR4*-GFP	Lin et al., 2008
pEAE64	pRS416-P_{YOR1}-*YOR1*-GFP	This study
pEAE83	pRS416-P_{YOR1}-*YOR1*-3XHA	This study
pJAM367	pRS415-P_{ART1}-*ART1*-3xFLAG	This study
pJAM518	pRS415-P_{CPY}-*3xFLAG-ART1*	This study
pJAM519	pRS415-P_{ADH1}-*3xFLAG-ART1*	This study
pJAM520	pRS415-P_{TDH3}-*3xFLAG-ART1*	This study
pCHL641	pRS416-P_{ART1}-*ART1*-3xHA	This study
pJAM601	pRS416-P_{LYP1}-*LYP1*-3xFLAG	This study
pJAM603	pRS416-P_{CPY}-*3xFLAG-LYP1*	This study
pJAM604	pRS416-P_{ADH1}-*3xFLAG-LYP1*	This study
pJAM605	pRS416-P_{TDH3}-*3xFLAG-LYP1*	This study
pJAM643	pRS416-P_{LYP1}-*Lyp1 10XR*-3xFLAG	This study
pJAM684	pRS416-P_{CPY}-*3xFLAG-Lyp1 10XR*	This study
pJAM685	pRS416-P_{ADH1}-*3xFLAG-Lyp1 10XR*	This study
pJAM686	pRS416-P_{TDH3}-*3xFLAG-Lyp1 10XR*	This study
pJAM687	pRS416-P_{CPY}-*Lyp1 10XR GFP*	This study
pJAM688	pRS416-P_{ADH1}-*Lyp1 10XR GFP*	This study
pJAM689	pRS416-P_{TDH3}-*Lyp1 10XR GFP*	This study
pCHL639	pRS416-P_{ART1}-*ART1*-GFP	Lin et al., 2008

Table 4 Expression conditions for reconstituted ESCRT-II and –III complexes used in Chapter V

protein	*E.coli*	[IPTG]	expression conditions
His_6-Vps20	C41(DE3)	0.4mM	overnight (16-20 hours) at 20°C
His_6-Snf7 FL & mutants	BL21	1mM	4 hours at 37°C
His_6-Vps24	C41(DE3)	1mM	overnight at 25°C
His_6-Vps2	BL21	1mM	overnight at 25°C
His_6-ESCRT-II	C41(DE3)	0.3mM	15 hours at 16°C
GST-Vps25 & GST-$Vps20^{core}$	BL21	1mM	overnight at 25°C

Table 5 The following Table summarizes plasmids used in Chapter V for *in vitro* reconstitution of ESCRTs-II and –III:

Supplemental Table 4: Plasmids for Bacterial Expression of ESCRTs-II & -III			
vector	***name***	***description***	***reference/source***
pET23d	Snf7 (wildtype)	full length (fl), N-His_6	(Teis, Saksena et al. 2008)
pET23d	$Snf7^{R52E}$	full length, R52E, N-His_6	this study
pET23d	$Snf7^{L67E}$	full length, L67E, N-His_6	this study
pET23d	$Snf7^{K\text{-}linker}$	Snf7 160-KAAKKAK-166	this study
pET23d	$Snf7^{core}$	Snf7 1-150, N-His_6	this study
pET23d	$Snf7^{A51C}$	full length, A51C, N-His_6	this study
pET23d	$Snf7^{T179C}$	full length, T179C, N-His_6	this study
pET23d	$Snf7^{redox}$	fl, A51C+T179C, N-His_6	this study
pET23d	$Snf7^{R52E+redox}$	fl, A51C+R52E+T179C	this study
pET23d	$Snf7^{L67E+redox}$	fl, A51C+L67E+T179C	this study
pET23d	$Snf7^{\Delta linker}$	fl, Snf7 Δ151-170	this study
pET23d	$Snf7^{R52E+\Delta helix5}$	fl, $Snf7^{R52E}$ + Δ170-183	this study
pET23d	$Snf7^{R52E+V187C}$	fl, R52E+V187C, N- His_6	this study
pOP185	ESCRT-II	Vps22, His6-Vps36, Vps25	(Teo, Perisic et al. 2004)
pGEX6P1	GST-Vps25	full length Vps25, N-GST	this study
pET23d	Vps20	full length, N-His_6	this study
pGEX6P1	GST-$Vps20^{core}$	Vps20 1-147, N-GST	this study
pET23d	Vps24	full length, N-His_6	this study
pET23d	Vps2	full length, N-His_6	this study

Table 6 Protein samples used in TEM Experiments in Chapter V

Proteins (Panel) [negative stain: UA or AM]	**Concentrations (μM)**
Figure 3	
Snf7 wildtype (Panel A) [UA]	25
$Snf7^{R52E}$ (Panels B-J) [B-F:UA, G-J:AM]	25
Figure 4	
$Snf7^{R52E}$ (Panel A) [UA]	15
$Snf7^{core}$ (Panel B) [UA]	25
$Snf7^{R52E+\Delta helix5}$ (Panel D) [UA]	15
$Snf7^{\Delta linker}$ (Panel E) [UA]	15
$Snf7^{K^-linker}$ (Panel F) [UA]	15
Figure 5	
$Snf7^{R52E}$ on monolayer (ML) (Panel C) [AM]	6
$Snf7^{R52E}$ (Panel D) [AM]	34.5
$Snf7^{R52E}$:Vps24:Vps2 (Panels E&F) [AM]	17, 7, 7
$Snf7^{R52E}$:Vps24:Vps2 on ML (Panels G,H, I) [AM]	6, 2.5, 2.5
Figure 6	
$Snf7^{R52E}$ (Panel B) [AM]	25
ESCRT-II:Vps20:$Snf7^{R52E}$ (Panels C&E) [AM]	1.8, 4, 25
ESCRT-II (Panel D) [AM]	4
Supplemental Figure 3	
$Snf7^{R52E}$ (Panel A) [UA]	34.5
$Snf7^{R52E}$ (Panel B) [UA]	5, 12.5, 34.5
$Snf7^{core}$:$Snf7^{R52E}$ mix (Panel E) [UA]	15,15
Supplemental Figure 5	
$Snf7^{R52E}$ on lipid monolayers (Panel B) [AM]	6
$Snf7^{R52E}$:Vps24 (Panel D) [UA]	11.25, 9
$Snf7^{R52E}$:Vps2 (Panel E) [UA]	11.25, 8
Vps24:Vps2 (Panel F) [UA]	13.5, 12
$Snf7^{R52E}$:Vps24: Vps2 (Panel H) [AM]	17, 7, 7
Supplemental Figure 7	
ESCRT-II:Vps20:$Snf7^{R52E}$ (Panel A) [UA]	1.8, 4, 25
ESCRT-II:$Snf7^{R52E}$ (Panel B) [UA]	1.8, 25
Vps20:$Snf7^{R52E}$ (Panel C) [UA]	4, 25
ESCRT-II:Vps20:$Snf7^{R52E}$ (Panel D) [UA]	0.5, 1, 6
ESCRT-II:Vps20:$Snf7^{R52E}$:Vps24:Vps2 (Panel E) [UA]	1.0, 2.2, 8, 4, 4

Table 7 The following Table summarizes yeast strains and pRS plasmids used in Chapter V

S. cerevisiae strains			
strain	***name***	***genotype***	***reference/source***
SEY6210	*wild type*	*Matα, leu1-3, 112 ura3-52 his3-Δ200, trp1-Δ901 lys2-801 suc2-D9*	(Robinson, Klionsky et al. 1988)
MBY25	*vps20*Δ	6210; *VPS20::HIS3*	(Babst, Katzmann et al. 2002)
MBY24	*snf7*Δ	6210; *SNF7::HIS3*	(Babst, Katzmann et al. 2002)
BWY102	*vps24*Δ	6210; *VPS24::HIS3*	(Babst, Wendland et al. 1998)
MBY28	*vps2*Δ	6210; *VPS2::HIS3*	(Babst, Katzmann et al. 2002)
DTY36	*vps20*Δ, SNF7-GFP	6210.1; *VPS20::HIS3 SNF7-GFP::HIS3MX6*	(Teis, Saksena et al. 2008)
DTY25	*snf7*Δ, VPS24-GFP	6210; *SNF7::HIS3 VPS24-GFP::HIS3MX6*	(Teis, Saksena et al. 2008)
DTY235	VPS2-GFP	6210*; VPS2-GFP::HIS3MX6*	(Teis, Saksena et al. 2008)
DTY229	*vps24*Δ, VPS2-GFP	6210.1; *VPS24::HIS3 VPS2-GFP::HIS3MX6*	(Teis, Saksena et al. 2008)
DTY11	*SNF7-3xFLAG*	6210.1; *SNF7-Flag::HIS3MX6*	(Teis, Saksena et al. 2008)
NBY44	*snf7*Δ, MUP1-pHluorin	6210; *SNF7::HIS3 MUP1-pHluorin::KAN*	this study
NBY39	MUP1-pHluorin	6210; *MUP1-pHluorin::KAN*	this study

S. cerevisiae expression and integration plasmids			
vector	***name***	***description***	***reference/ source***
pRS415	Vps20-GFP	full length, C-term GFP	this study
pRS415	Vps20^{core}-GFP	Snf7 1-147, C-term GFP	this study
pRS416	Snf7-GFP	full length, C-term GFP	this study
pRS416	Snf7 ^{core}-GFP	Snf7 1-150, C-term GFP	this study
pRS414	Vps24-GFP	full length, C-term GFP	this study
pRS414	Vps24^{core}-GFP	Snf7 1-142, C-term GFP	this study
pRS415	Vps2^{core}-GFP	Snf7 1-143, C-term GFP	this study
pRS416	Snf7 wildtype	full length	this study
pRS416	Snf7^{R52E}	R52E	this study
pRS416	Snf7^{L67E}	L67E	this study
pRS416	Snf7$^{K\text{-}linker}$	Snf7 160-KAAKKAK-166	this study

pRS416	Snf7$^{\Delta_{linker}}$	Snf7 Δ151-170	this study
pRS416	Snf7$^{\Delta_{helix5}}$	Snf7 Δ170-183	this study
pRS416	Snf7$^{\Delta_{res.\ 185\text{-}195}}$	Snf7 Δ185-195	this study
pRS416	Snf7^{core}	Snf7 1-150	this study
pBW1571	Mup1-pHluorin	Mup1-pHluorin::KAN genomic integration plasmid	(Prosser, Whitworth et al. 2010)